UNIVERSITÉ DE SHERBROOKE
Faculté de Génie
Département de génie chimique et biotechnologique

# ÉTUDE DE L'IMPACT DE LA NUANCE DE CARBONE CATHODIQUE SUR LA FORMATION DE DÉPÔTS À L'INTERFACE BLOC CATHODIQUE-ALUMINIUM DANS UNE CELLULE HALL-HÉROULT

Mémoire de maîtrise
Spécialité : génie chimique

Jean-René LANDRY

Sherbrooke (Québec) Canada
Juillet 2018

# MEMBRES DU JURY

Gervais SOUCY
Directeur

Véronique DASSYLVA-RAYMOND
Évaluatrice

Joël SIROIS
Rapporteur

# RÉSUMÉ

L'aluminium est issu du procédé Hall-Héroult, seul procédé industriel permettant la formation d'aluminium primaire. De nos jours, plus de la moitié de la production mondiale provient de la Chine. Afin de rester compétitifs, les plus petits producteurs, tels que le Canada, doivent réduire constamment leurs coûts de production. Sachant que ce procédé d'électrolyse en sels fondus est énergivore (12 à 14 kWh/kg Al), il convient aux petits producteurs de chercher des routes pour réduire autant que possible cette demande énergétique. La présence de dépôts résistifs entre la nappe d'aluminium et le bloc cathodique augmente la résistance au passage du courant et du coup, contribue à augmenter les pertes de potentiel au niveau du bloc cathodique et les coûts de production.

Les cellules modernes d'électrolyse d'aluminium emploient des blocs cathodiques de types graphitisés à haute conductivité électrique et thermique afin de minimiser les pertes de potentiel et maximiser la production. Cependant ces types de cellules ont une durée de vie écourtée et ont des tendances divergentes en termes d'embourbement.

L'objectif de ce projet de recherche est de déterminer en quoi les nuances de blocs cathodiques peuvent influencer la formation des boues dans les cellules Hall-Héroult par le biais de leurs propriétés physico-chimiques. Avec une compréhension plus détaillée des mécanismes de formation des boues, il est possible de saisir l'influence de chaque propriété des blocs cathodiques sur la formation des boues. Par la minimisation de l'embourbement des cellules, les pertes de potentiel peuvent être diminuées, ce qui contribuerait à réduire les coûts de production de l'aluminium.

Dans ce projet de recherche, des nuances de bloc cathodique de calibre industriel ont été employées pour des expériences d'électrolyse en laboratoire. Celles-ci ont démontré des comportements différents en termes d'embourbement et de pertes de potentiel. Le taux d'embourbement a été mis en relation avec les pertes de chaleur des différentes nuances et la chimie du bain. De plus, cette étude a poussé plus loin la compréhension des mécanismes menant à la formation et la dissolution des boues à l'interface carbone-aluminium.

**Mots-clés** : Aluminium, nuance de bloc cathodique, boue, chute de voltage cathodique.

# REMERCIEMENTS

L'auteur aimerait remercier l'Université de Sherbrooke, Rio Tinto et Carbone Savoie pour leur contribution qui ont rendu possible ce projet de recherche. L'auteur aimerait remercier particulièrement Pr Gervais Soucy de l'Université de Sherbrooke pour son support durant ce projet. Des remerciements particuliers sont aussi accordés à M. Mojtaba Fallah Fini, collègue de groupe de recherche, pour le partage des connaissances, la synergie de groupe, l'aide et la révision des travaux présentés dans ce mémoire.

L'auteur aimerait aussi remercier M. Martin Brassard pour l'entrainement sur le banc d'essai au début du projet, M. André Bilodeau et M. Serge Gagnon pour leur support technique en laboratoires et Pr Martin Désilets pour son apport de connaissance durant les maintes discussions. Des remerciements vont aussi aux employés du Centre de Caractérisation des Matériaux (CCM) de l'Université de Sherbrooke pour leur assistance dans la caractérisation des résultats de cette étude. Plus particulièrement M. Carl St-Louis, M. Charles Bertrand, Mme Sonia Blais et M. Stéphane Gutierrez.

L'auteur souhaite aussi remercier les intervenants provenant de l'externe. À cet effet, les contributions de Pr Patrice Chartrand (École Polytechnique de Montréal), M. Patrick Pelletier (Rio Tinto Canada), M. Jean-François Bilodeau (Rio Tinto Canada), M. Didier Lombard (Rio Tinto France) et M. Loig Rivoaland (Carbone Savoie) sont grandement appréciées.

Finalement, l'auteur remercie spécialement le Conseil de Recherche en Sciences Naturelles et en Génie du Canada (CRSNG), Rio Tinto et Carbone Savoie pour le financement tout au long du projet de recherche.

# TABLE DES MATIÈRES

# LISTE DES FIGURES

# LISTE DES TABLEAUX

# LISTE DES ACRONYMES

ACD Distance anode-cathode (*anode to cathode distance*)

CVD Chute de voltage cathodique (*cathode voltage drop*)

CR Ratio de cryolite, ratio molaire (*cryolite ratio*)

BR Ratio de bain, ratio massique (*bath ratio*)

IFT Tension interfaciale (*interfacial tension*)

MHD Magnétohydrodynamique

# CHAPITRE 1 INTRODUCTION

## 1.1 Mise en contexte et problématique

### 1.1.1 Le marché mondial de l'aluminium

L'aluminium est un des métaux les plus abondants sur Terre et l'un des plus utilisés au quotidien. Ces propriétés métalliques liées à sa légèreté le rendent un matériau indispensable pour les industries automobile, aéronautique ou même de l'emballage. L'accroissement de ces secteurs tend à faire augmenter la demande en aluminium dont la production mondiale annuelle frôle 60 millions de tonnes aujourd'hui [Aluminium, 2018]. La Chine contribue à plus de 60 % de cette production. La particularité du marché de l'aluminium vient de la forte demande énergétique que requiert le procédé Hall-Héroult. Ce procédé est basé sur la réduction électrochimique de l'alumine en sel fondu, selon l'équation 1.1.

$$2Al_2O_{3(diss.)} + 3C_{(solide)} \rightarrow 4Al_{(liquide)} + 3CO_{2(gaz)} \quad (1.1)$$

La quantité d'énergie théorique requise pour produire l'aluminium selon cette réaction est 6.34 kWh/kg à 977 °C [Grjotheim, 2010]. La plupart des cellules modernes opèrent autour de 14.5 kWh/kg. À ce jour, les usines les plus performantes rapportées dans la littérature opèrent entre 12 et 12.7 kWh/kg dont la technologie AP60 de Rio Tinto au Québec [Chai *et coll.*, 2018, Coursol *et coll.*, 2012]. L'efficacité énergétique moyenne actuelle est donc près de 50 % au mieux. En raison des conditions nécessaires pour produire l'aluminium, l'industrie de la production primaire a été intégralement basée sur ce procédé depuis sa découverte.

Pour une cellule Hall-Héroult, le bilan d'énergie peut être simplifié selon l'équation 1.2.

$$W_{el} = n\Delta H_{tot} + q \quad (1.2)$$

L'énergie électrique fournie ($W_{el}$) est balancée par le changement d'enthalpie pour la complétion de la réaction 1.1 et par les pertes de chaleur occasionnées durant l'opération. L'augmentation de l'efficacité énergétique passe ainsi par la minimisation des pertes ohmiques de voltage et par l'optimisation du bilan de chaleur des cellules. La compétition engendrée par la performance de la Chine sur le marché mondial de l'aluminium oblige les producteurs à

trouver des routes pour réduire la consommation énergétique globale du procédé, ainsi les coûts de production.

### 1.1.2 Le procédé Hall-Héroult

Le procédé Hall-Héroult fut inventé par les scientifiques Paul Héroult et Charles Martin Hall à la fin du 19$^{e}$ siècle. Il s'agit du seul procédé industriel commercial de production d'aluminium. Le principe repose sur l'électrolyse de l'oxyde d'aluminium dissout en sels fondus. L'oxyde d'aluminium ($Al_2O_3$), aussi appelé « alumine », provient du procédé Bayer, étape antérieure au procédé Hall-Héroult. Ce dernier consiste en l'extraction et la purification de l'alumine à partir de la bauxite, un minerai abondant riche en alumine.

L'électrolyte, ou « bain électrolytique » utilisé est composé essentiellement de cryolite liquide, $Na_3AlF_6$, dont le point de fusion est 1011 °C [Holm, 1962]. Le bain typique contient 9 à 11 % de $AlF_3$, 4 à 6 % de $CaF_2$, 1.5 à 4 % d'alumine ainsi que 2 à 4 % de $MgF_2$ et LiF [Tabereaux et Peterson, 2014]. Les additifs permettent d'abaisser le point de fusion du bain et sa résistivité électrique, diminuant du fait même les coûts d'opération. La Figure 1.1 illustre le schéma d'une cellule industrielle Hall-Héroult typique.

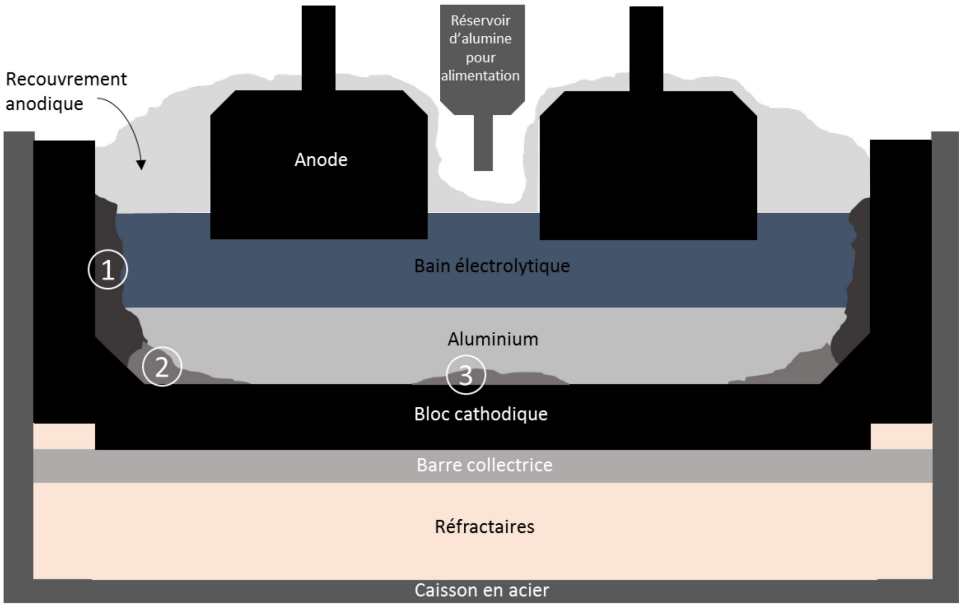


**Figure 1.1 Schéma simplifié d'une cellule Hall-Héroult et ses composantes principales. Talus protecteur (1); pied de talus (2); Boue (3)**

Dans le procédé Hall-Héroult, l'alumine est dissoute dans de la cryolite ($Na_3AlF_6$). L'ajout de sels tels que les fluorures d'aluminium et de calcium, $AlF_3$ et $CaF_2$ respectivement, aident la diminution du point de fusion du mélange électrolytique entre 950 et 1000°C. L'électrolyte est contenu dans un caisson avec un revêtement en carbone qui joue également le rôle de bloc cathodique. Les anodes suspendues sont aussi faites de carbone et sont consommées durant l'opération. Le bain électrolytique est un conducteur électrique qui possède une densité moins élevée que celle de l'aluminium, permettant une séparation naturelle des phases à l'intérieur de la cellule.

Les réactions principales ont lieu aux interfaces entre le bain et les électrodes. La réduction de l'alumine a lieu à la cathode électrochimique, qui est l'interface entre le bain et l'aluminium liquide selon les équations 1.3 et 1.4. L'alumine est dissociée dans la cryolite et est réduite à l'interface aluminium-électrolyte selon les réactions suivantes [Yurkov, 2015]:

$$Al_2O_3 \rightarrow 2Al^{3+} + 3O^{2-} \tag{1.3}$$

$$Al^{3+} + 3e^- \rightarrow Al \downarrow \tag{1.4}$$

Les anodes sont consommées et du gaz carbonique est généré selon la réaction suivante :

$$2O^{2-} + C \rightarrow CO_2 + 4e^- \tag{1.5}$$

La plupart des usines opèrent avec des anodes dites « précuites ». Celles-ci doivent être remplacées périodiquement durant l'opération de changement d'anodes, contrairement à des anodes de types Soderberg. La production d'aluminium génère de grandes quantités de gaz carbonique et de fluors. Des systèmes de captage des gaz fluorés sont mis en place pour réduire l'impact environnemental et pour fins de récupération. Durant l'opération des cellules, lorsque la concentration en alumine dans le bain d'une cellule est trop basse, il se produit un effet anodique, qui est marqué par la production de CO, $CF_4$ et $C_2F_6$ et une augmentation du voltage de la cellule. Pour maintenir une opération normale, l'alumine est alimentée en petite quantité périodiquement par un alimenteur qui casse la croute de recouvrement et injecte la quantité appropriée.

### 1.1.3 L'opération et le défi lié aux dépôts

Afin d'éviter que le bain chaud très corrosif pénètre le revêtement en carbone et le détériore, des pertes de chaleur sur les côtés sont nécessaires afin de permettre à une couche de bain de se solidifier et ainsi créer une barrière entre le bain liquide et le carbone. Cette couche de bain solidifié est appelée « talus protecteur » en anglais *side ledge*. L'épaisseur du talus protecteur dépend de la quantité de chaleur qui est transférée aux parois durant l'opération. Le prolongement du talus sur la surface horizontale du revêtement cathodique est appelé pied de talus ou *ledge toe*. Le bilan de chaleur de la cellule est d'une grande importance par rapport à la formation de dépôts. Environ 20 % de la chaleur produite (par réaction exothermique) est en fait utilisée pour la production d'aluminium [Grjotheim, 2010]. Une partie de la chaleur a une contribution utile au procédé en maintenant l'électrolyte et le métal liquide, en chauffant les réactifs et servant à la dissolution de l'alumine. Le reste de la chaleur est perdue en raison de la géométrie des cuves d'électrolyse. L'optimisation de la conductivité thermique du bloc cathodique (côtés et dessous) permettrait de sauver de l'énergie. La conception des cellules devrait être faite de manière à garder la température du bain constante et les flux de chaleurs devraient être suffisants pour maintenir un talus protecteur assez épais, empêchant ainsi les attaques de bain dans le bloc cathodique et la mort de la cellule [Grjotheim, 2010]. Si les pertes de chaleur par le dessous sont trop importantes, il en résulte une croute de bain sur le plancher cathodique, ce qui perturbe la MHD, mais aussi augmente le voltage. À l'opposé, des pertes de chaleurs trop faibles empêcheraient la formation du talus protecteur dans certaines zones, résultant en l'érosion et la dégradation du revêtement en carbone par contact direct avec le bain électrolytique corrosif [Grjotheim, 2010]. Malgré la grande quantité de pertes de chaleur durant l'opération des cellules industrielles, l'option de récupérer la chaleur pour l'utiliser ailleurs s'avère difficile en raison de la basse qualité de cette énergie (faible température) et de complexités pratiques [Barzi et Assadi, 2013]. Plusieurs brevets de systèmes d'échangeurs de chaleurs à cet effet ont été publiés dans la littérature.

Durant l'opération d'une cellule, le bain est agité par les bulles de gaz formées au bout des anodes durant les réactions. Aussi, la nappe d'aluminium a un mouvement magnétohydrodynamique (MHD) entrainé par le champ magnétique existant autour du courant alimentant les cuves. Ce mouvement de MHD entraine l'instabilité de la surface de la nappe de

métal, ce qui a pour conséquence entre autres d'augmenter la solubilité de l'aluminium dans le bain (perte d'efficacité de courant) et de rendre difficile la diminution de la distance anode-cathode (ACD). Le courant circule par plusieurs régions qui tendent à augmenter la résistance à son passage, ce qui occasionne des pertes de voltage dans le système. Les points de plus haute résistance au courant sont les interfaces, notamment entre l'aluminium et le bloc cathodique. Les pertes de voltage à l'interface carbone-aluminium peuvent être accentuées considérablement lorsque des dépôts de boues (*sludge*) se forment entre le bloc de carbone et le métal. La boue peut se solidifier et entrainer l'augmentation des composantes horizontales de courant électrique, occasionnant une hausse de la chute de voltage cathodique. Dans les cellules Hall-Héroult, la boue est un mélange de bain électrolytique saturé en alumine et de particules d'alumine solide non dissoutes. Ce mélange a une densité de plus élevée que le métal et donc lorsque formé, se retrouve coincé sous la nappe de métal durant l'opération. La boue peut aussi provenir de débris tombant durant les opérations comme les changements d'anodes ou l'alimentation d'alumine. En raison de la complexité du système, une multitude de facteurs ont une influence sur la formation des boues tels que la température du bain, la chimie du bain ou encore la dynamique du système. Le choix des matériaux des composantes impliquées dans un tel système est donc crucial, particulièrement pour le bloc cathodique, car celui-ci est la première couche solide en contact avec l'aluminium et le liquide électrolytique. L'importance du bloc cathodique provient aussi du fait que d'inévitables flux de masse, de chaleur et d'électricité le traversent. Les blocs cathodiques en carbone peuvent varier d'une usine à l'autre selon la nuance de carbone. Les nuances de carbone diffèrent de par leur structure cristalline et leur procédé de fabrication. Ces différences permettent de faire varier les propriétés physico-chimiques des cathodes en carbone et ainsi créer des technologies d'électrodes répondant aux besoins des différentes usines de production d'aluminium primaire. Les mécanismes de formation des boues seront détaillés dans la revue de la littérature.

### 1.1.4 Les nuances de carbone

Il existe plusieurs formes cristallines allotropiques pour le carbone. Les plus connues sont le diamant et le graphite, qui sont les seules formes allotropies retrouvées dans la nature. D'autres formes se sont ajoutées telles que les nanotubes et fullerènes [Donnet, 2006]. Le graphite a une structure lamellaire (plane) avec une série de cycles aromatiques appelés graphènes

[Kroschwitz, 2004]. Les plans sont retenus par des liaisons faibles de Van der Walls, ce qui explique que le graphite soit tendre [Charette, 2012].

Les carbones industriels suivent des traitements leur donnant une structure et des propriétés désirées. Les substances obtenues ont une structure qui dépend du mode de préparation, principalement de la plus haute température de traitement (HTT). Les précurseurs des produits industriels de carbone peuvent être des substances naturelles (pétrole, charbons) ou des dérivés (produits de la pétrochimie, coke, goudron ou brai issu des charbons). L'industrie de l'aluminium utilise beaucoup le coke comme précurseur pour les électrodes. Le coke est un solide à teneur élevée en l'élément carbone d'origine variée (coke calciné, coke de pétrole, etc.). Le traitement thermique de graphitisation sur ces substances permet d'augmenter leur aromaticité et de tendre vers le graphite qui est thermodynamiquement plus stable, tel qu'illustré sur la Figure 1.2, [Burchell, 1999].

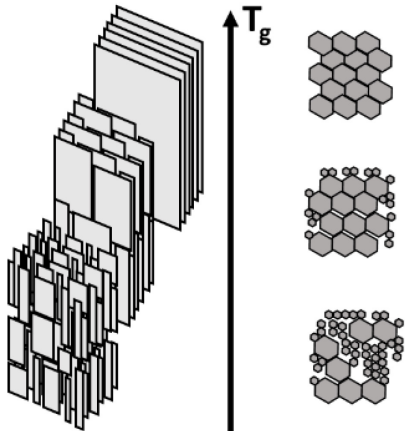


**Figure 1.2 Schématisation qualitative de la graphitisation du carbone en fonction de la température de graphitisation ($T_g$), adapté de [Sorlie et Oye, 2010]**

Il est donc possible pour les producteurs de cathodes industrielles d'innover dans les étapes de préparation des blocs afin de leur donner des propriétés désirées. L'optimisation des blocs cathodiques implique une haute conductivité thermique, une faible résistivité électrique ainsi qu'une faible tendance au gonflement sodique. Ceci leur permet de tolérer une plus haute intensité de courant, donc d'augmenter la production journalière [Charette, 2012].

Les familles de blocs cathodiques sont : amorphe, semi-graphitique ou graphitique et graphitisé. Les blocs de type semi-graphitique sont faits d'un mélange d'agrégats de graphite et d'anthracite de proportions variées cuits autour de 1200 °C, alors que les blocs graphitiques sont faits à 100

% d'agrégats de graphite cuits sans graphitisation. Les blocs graphitisés sont faits d'un mélange de coke de pétrole et de brai cuit autour de 800 °C avant d'être soumis à l'étape de graphitisation à des températures dépassant 2500 °C [Charette, 2012]. Certains blocs graphitisés sont imprégnés avec du brai liquide et recuits à 1000 °C afin d'abaisser davantage la résistivité du bloc et de prolonger sa durée de vie [Schnittker et Nawrocki, 2003]. Le Tableau 1.1 compare les différentes propriétés des familles de cathodes.

Tableau 1.1 : Comparaison qualitative de quelques propriétés des trois grandes familles de technologies de cathodes [Sorlie et Oye, 2010]

| Propriété | Amorphe | Graphitique | Graphitisé |
|---|---|---|---|
| Prix | faible | moyen | élevé |
| Résistance à l'abrasion | excellente | bonne | faible |
| Résistance aux chocs thermiques | acceptable | bonne | excellente |
| Conductivité thermique | acceptable | élevée | très élevée |
| Résistance électrique (à température d'électrolyse) | moyenne | basse | très basse |
| Gonflement sodique* | acceptable | faible | très faible |

*Gonflement sodique : pénétration de sodium dans le bloc cathodique menant à son gonflement pouvant engendrer des fissures se produisant sous conditions d'électrolyse.

Traditionnellement, les usines de production d'aluminium primaire utilisent des blocs cathodiques de type amorphe ou graphitique [Mirchi *et coll.*, 2003]. Durant les dernières décennies, les producteurs se tournent vers les cathodes de type graphitisées afin de réduire les pertes de voltage cathodiques (du même coup la consommation énergétique) et d'adapter les cellules à des intensités de courant électrique plus élevées [Larsen *et coll.*, 2010, Reny et Wilkening, 2000]. Cependant les blocs graphitisés ont une faible résistance à l'abrasion. Ceci, combiné aux hautes de courant des cuves modernes et de la chimie acide du bain, les rendent plus fragiles à l'usure [Charette, 2012].

### 1.1.5 Distribution du voltage dans les cellules Hall-Héroult

En raison de la nature électrochimique du procédé Hall-Héroult, le coût d'opération est directement lié à la facilité avec laquelle le courant peut être fourni au système pour la formation d'aluminium, c'est-à-dire le voltage du système. En industrie, le voltage appliqué dans les cellules Hall-Héroult est généralement situé entre 4 et 5 V. Les variations de voltage proviennent des différents types de cellules et des conditions d'opération utilisées dans l'industrie. La distribution du voltage nécessaire pour la production d'aluminium compte pour la résistance ohmique au passage du courant et aux différents phénomènes électrochimiques dans la cellule. Le Tableau 1.2 résume la distribution de voltage typique d'une cellule Hall-Héroult.

Tableau 1.2 : Distribution du voltage dans une cellule Hall-Héroult [Grjotheim, 2010]

| Demande | Voltage (V) |
|---|---|
| Décomposition de l'alumine | 2,21 |
| Décomposition de l'alumine avec le carbone | 1,18 |
| Dépolarisation du carbone | 1,03 |
| Surtension anodique et cathodique | 0,6 |
| Force contre-électromotrice | 1,7 |
| Perte de voltage dans l'électrolyte et aux bulles | 1,85 |
| Pertes de voltage anodique et externe | 0,5 |
| **Pertes de voltage cathodiques (CVD)** | **0,5** |

Tel qu'indiqué, les pertes de voltage cathodiques sont du même ordre que les pertes de voltage anodiques et externes mises ensemble. La CVD inclut les pertes de voltage dans chaque partie du bloc cathodique. Le Tableau 1.3 décrit les contributions à la CVD dans le bloc cathodique.

Tableau 1.3 : Contributions moyennes à la CVD de multiples phases de matériaux dans le bloc cathodique [Singh *et coll.*, 2017a]

| Phases des matériaux | Contribution à la CVD (%) |
|---|---|
| Carbone | 26 |
| Interface carbone-aluminium | 25 |
| Métal interne (sous le bloc de carbone) | 18 |
| Barre de métal externe | 31 |

Il en résulte que près de la moitié de la CVD provient du bloc de carbone et de l'interface carbone-aluminium, donc près de 0,25 V d'après le Tableau 1.2. Comme il a été mentionné précédemment, cette contribution à la CVD peut croître lorsque la résistance à l'interface carbone-aluminium est augmentée par la présence excessive de dépôts de boue. Bien qu'une perte de voltage minimale est inévitable au niveau du bloc cathodique, la diminution de l'embourbement des cellules permettrait ainsi de réduire sous 25 % la contribution à la CVD de l'interface carbone-aluminium.

De nos jours, la recherche et le développement des cuves industrielles à haute intensité passent par la réduction de la distance anode-cathode (ACD), la stabilité de la nappe de métal, les procédures d'assemblage des anodes et cathodes (pour la minimisation des pertes de voltage extérieures) et la modélisation du bilan de chaleur [Coursol *et coll.*, 2012]. Cependant, l'optimisation doit aussi prendre en compte la minimisation de la tendance des cellules à produire des boues. Or, la nuance de cathode peut avoir une influence sur les facteurs affectant la formation de boues. Donc, il est important de se pencher davantage sur l'optimisation des propriétés de matériaux cathodiques afin de contribuer à réduire les boues et ainsi ralentir la hausse de la CVD.

### 1.1.6 Problématique

L'efficacité des cellules d'électrolyse est réduite par l'augmentation de la chute de voltage cathodique (CVD). Ces pertes de potentiel sont principalement associées à la résistance au niveau des interfaces que traverse le courant électrique, notamment entre l'aluminium et le bloc

cathodique. La présence de dépôts de boues à l'interface carbone-aluminium favorise l'augmentation de la CVD en raison de leur forte résistance au courant électrique. L'embourbement excessif des cellules industrielles diminue leur efficacité énergétique ainsi que leur durée de vie. La recherche portant sur les dépôts vise à cerner les facteurs régissant leur comportement dans le but de cerner des conditions optimales minimisant la CVD. L'objectif est de réduire les coûts de production d'aluminium des cellules industrielles en minimisant la CVD. L'amélioration de l'efficacité énergétique des cellules Hall-Héroult est particulièrement importante pour les compagnies à plus faibles taux de production afin de rester compétitives face aux gros producteurs tels que la Chine.

Comme mentionné plus haut, le matériau utilisé pour le revêtement carboné de la cathode est particulièrement important, car il est directement en contact avec le bain et l'aluminium et voit des flux de masse (liquide et gazeux), de chaleurs et d'électricité. Il a donc intuitivement un impact sur la formation des boues. Les compagnies se spécialisant dans la production de cathodes pour électrolyse de l'aluminium développent des matériaux carbonés nuancés. Les différentes méthodes de préparation de ces technologies permettent de faire varier leur structure cristalline et donc leurs propriétés physico-chimiques.

Ce projet de recherche consiste à étudier l'impact de la nuance de carbone cathodique sur la formation de dépôts à l'interface carbone-aluminium. Les analyses de dépôts précédemment faites par Marc-André Coulombe et François Allard à l'Université de Sherbrooke ont permis de caractériser et de différencier les dépôts selon leur composition, mécanisme de formation et emplacement dans la cellule. Dans ce projet de recherche, on tente de déterminer en laboratoire quelle est l'influence des différentes propriétés des blocs cathodiques sur la formation des boues à l'interface carbone-aluminium. Il s'agit donc d'aider à éclairer l'industrie sur les propriétés optimales à viser lors de la conception de matériaux de blocs cathodiques.

## 1.2 Question de recherche

Ce projet de recherche traitant de la formation des boues est élaboré dans le but de réduire le coût associé à la production d'aluminium. La minimisation de la formation de boues entre la nappe d'aluminium et la cathode contribuerait à baisser la résistance totale du système et réduire la CVD. Sachant que la formation de boues est affectée par plusieurs paramètres (température,

chimie de bain, etc.), la question de recherche de cette étude vise à mieux comprendre comment les propriétés des différentes nuances de blocs cathodiques peuvent influer sur la formation des boues qui se retrouvent à l'interface carbone-aluminium. Il convient alors de mieux comprendre les mécanismes de formation et de dissolution des boues et de mettre en relief le rôle des propriétés du bloc cathodique lors de ces phénomènes.

Les études sur les nuances de cathode sont nombreuses, mais très peu traitent de leur influence sur le phénomène de formation de boues (*sludge*). En effet, le problème concernant la formation des boues est reconnu dans l'industrie, mais l'observation de différents comportements de cellules amène à croire que ce phénomène est plus complexe que l'on pense. L'intérêt de ce travail est de pouvoir comparer différentes nuances de bloc cathodiques industrielles et de mettre en évidence l'impact de leurs propriétés sur les mécanismes de formation des boues. De plus, la nature expérimentale de ce projet permet une approche ouverte face à la compréhension des phénomènes.

## 1.3 Objectifs du projet de recherche

### 1.3.1 Objectif principal

- Déterminer l'influence des différentes propriétés physico-chimiques des blocs cathodiques sur les mécanismes de formation des boues à l'interface carbone-aluminium.

### 1.3.2 Objectifs secondaires

- Mesurer le niveau d'embourbement des cellules (position et épaisseur des boues, du pied de talus) sur un montage expérimental.
- Déterminer la composition chimique des dépôts situés à l'interface carbone-aluminium des cellules expérimentales.
- Étudier l'état de l'interface carbone-aluminium (présence de film de bain, marques d'érosion dans le bloc cathodique) des cellules expérimentales.
- Étudier le comportement des différents paramètres des cellules expérimentales (température, voltage, fuites de bain, usure).

## 1.4 Contributions originales

### 1.4.1 Contributions à l'industrie de l'aluminium

La présence de dépôts résistifs à la surface du bloc cathodique est souvent associée à des opérations de routines telles que les changements d'anode ou l'alimentation d'alumine. Il est aussi reconnu qu'une alimentation optimale en alumine est de mise pour limiter la formation de boues. La réduction des boues est souvent liée à la méthode d'alimentation d'alumine, mais peu d'attention est mise sur à quel point la formation des boues peut être gouvernée par les propriétés du bloc cathodique. Les recherches visent à procurer de nouvelles connaissances scientifiques en ce qui a trait aux mécanismes de formation des boues et le rôle de la nuance de cathode. Les contributions originales effectuées dans le cadre de ce projet de recherche sont présentées dans les paragraphes suivants.

### 1.4.2 Revue de la littérature sur la formation des boues

Aucune revue de la littérature n'existe à propos de la formation des boues dans les cellules d'électrolyse de l'aluminium, malgré son existence centenaire. La formation des boues est reconnue comme résultant d'opérations routinières, mais beaucoup d'articles parlent aussi de mécanismes plus complexes menant à la formation de boues (phénomène d'interfaces, température du bain, hydrodynamique). La revue de littérature présentée dans le chapitre 2 est la première revue de littérature comprenant tous les facteurs influant sur la formation ou la dissolution des boues. Ce document a été écrit avec Mojtaba Fallah Fini, qui quantifie les facteurs menant à la formation des boues par un plan d'expérience dans le cadre de son projet de doctorat à l'Université de Sherbrooke. L'un des facteurs majeurs présentés dans cette revue est l'impact du bloc cathodique. Les brevets de cathodes sont aussi présentés dans cette section. Cette revue de littérature, acceptée dans le journal *Mineral Processing and Extractive Metallurgy Review*, permet de rassembler toute l'information concernant les boues dans l'industrie de l'aluminium et de guider l'industrie dans l'optimisation des cellules d'électrolyse d'aluminium.

### 1.4.3 Impact de la nuance de cathode sur la formation de boues et de carbures d'aluminium

Les résultats préliminaires de la présente étude expérimentale sont présentés dans le cadre de la conférence annuelle TMS 2018 en Arizona. Le montage expérimental utilisé a permis de générer des dépôts de boues et de pied de talus. De plus, une couche de carbure d'aluminium présente à l'interface carbone-aluminium est aussi analysée. Cette couche a été reconnue comme responsable de l'érosion de la surface des blocs cathodiques. Dans les résultats présentés à cette conférence, l'accent est mis sur le dimensionnement des dépôts de boues et de pied de talus en plus des mesures de l'épaisseur de la couche de carbures d'aluminium. Cette publication apporte une meilleure compréhension du rôle des propriétés de bloc sur la croissance de la couche de carbures d'aluminium et prouve que l'embourbement varie selon la nuance de cathode.

La suite des résultats est présentée dans un article englobant la totalité des expériences réalisées dans le cadre de cette étude et soumis au journal *Metallurgical and Materials Transactions B*. L'accent est davantage mis sur l'influence des propriétés des nuances de cathode sur les mécanismes d'embourbement. De plus, les observations faites permettent un meilleur saisi des phénomènes de formation et de dissolution des boues en l'absence de point d'alimentation d'alumine. Les connaissances scientifiques émanant de cet article peuvent aider l'industrie à peaufiner le contrôle des cuves d'électrolyse et de ce fait même réduire l'embourbement et la CVD.

## 1.5 Plan du document

Ce mémoire par article est divisé en 6 chapitres. Le chapitre 1 est l'introduction, mettant en contexte le projet de recherche. Le chapitre 2 est la revue de la littérature par article sur la formation des boues. Dans le chapitre 3, la méthodologie pour les expériences et analyses de cette étude est décrite. Le chapitre 4 est l'article présenté à la conférence TMS 2018 et le chapitre 5 est l'article soumis au journal *Metallurgical and Materials Transactions B*. Le chapitre 6 résume les travaux effectués dans cette étude et discute des différentes avenues de recherches potentiel dans le futur.

# CHAPITRE 2 REVUE DE LA LITTÉRATURE

## 2.1 Avant-propos

**Auteurs et affiliations :**

**Mojtaba Fallah Fini** : Département de génie chimique et biotechnologique, Université de Sherbrooke, Québec, Canada.

**Jean-René Landry** : Département de génie chimique et biotechnologique, Université de Sherbrooke, Québec, Canada.

**Gervais Soucy** : Département de génie chimique et biotechnologique, Université de Sherbrooke, Québec, Canada.

**Martin Désilets** : Département de génie chimique et biotechnologique, Université de Sherbrooke, Québec, Canada.

**Patrick Pelletier** : Rio Tinto, Centre de Recherche et Développement Arvida, Saguenay, Québec, Canada.

**Loig Rivoaland** : Carbone Savoie, Vénissieux, France.

**Didier Lombard** : Rio Tinto, St-Jean-de-Maurienne, France.

**Date de soumission :** 13 juillet 2018

**État et date de l'acceptation :** accepté le 30 août 2018

**Journal :** Mineral Processing and Extractive Metallurgy Review

**Référence de l'article :** https://doi.org/10.1080/08827508.2018.1536658

**Contribution du document au mémoire :**

Ce document est la première revue de littérature sur la formation des boues dans les cellules Hall-Héroult. Les principaux facteurs affectant la formation ou la dissolution des boues sont énoncés et discutés, dont la nuance de cathode. Ma contribution à cet article consiste en la recherche dans la littérature sur les nuances de cathode et leur impact sur la formation des boues et en la rédaction de la section *Influence of cathode carbon materials*. Les matériaux utilisés

aujourd'hui, les différentes géométries et les brevets de cathode sont aussi présentés dans cette section. Ma contribution inclut aussi le travail en équipe avec le premier auteur pour la recherche de la littérature des autres sections ainsi que la révision de la totalité de la revue.

## 2.2 Titre et résumé français

**Titre :**

La formation des boues dans les cellules Hall-Héroult : conséquences et paramètres influents

**Résumé :**

Cette revue de littérature discute de la formation des boues dans les cellules Hall-Héroult. La formation de boue et sa transformation en dépôts résistifs est un des principaux problèmes pour les producteurs d'aluminium. Les boues interviennent dans la dynamique complexe des cellules d'électrolyse toute en augmentant la demande nécessaire en énergie et réduisant l'efficacité de courant. Les données se rapportant à un phénomène d'une aussi grande importance sont éparpillées dans les actes de conférences TMS Light Metals et dans les journaux scientifiques; d'où la nécessité d'une revue en profondeur comprenant les principaux facteurs tels que la température (surchauffe du bain), la chimie du bain, la nuance de cathode, l'alimentation d'alumine, l'hydrodynamique et les phénomènes d'interfaces.

## 2.3 Revue de littérature sur la formation des boues et l'impact de la nuance de cathode

### 2.3.1 Title

Sludge formation in Hall-Héroult Cells: drawbacks and significant parameters

**Keywords :** Sludge, bottom crust, muck, Hall-Héroult cells, resistive deposits.

### 2.3.2 Abstract

This literature review discusses the sludge formation in the Hall-Héroult process. Sludge formation and its transformation into resistive cathodic deposits is one of the focal concerns of the aluminum producers. Sludge formation interacts with the complex dynamics of the electrolysis cells while increasing the energy demand and decreasing the current efficiency. The data on such important phenomenon is scattered through years in proceedings of TMS Light Metals and journal articles; hence requiring an in-depth review including the influence of important parameters such as temperature (i.e. superheat), bath chemistry, cathode type, alumina feeding characteristics, hydrodynamics and interfacial phenomena.

### 2.3.3 Introduction

According to the world's annual production of aluminum and its trend in recent years [Bray, 2018], China has become a formidable producer of aluminum in the last couple of years and this has forced other producers to reduce their production costs. Besides, the Hall–Héroult process has gone through years of investigation and subtle modifications since its commercialization at the beginning of the 20$^{th}$ century [Grjotheim et Welch, 1989, Tarcy *et coll.*, 2011]. Looking at the trend of such developments reveals that the Achilles' heel of the aluminum electrolysis has always been its high consumption of electrical power and improvement of current efficiency (Figure 2.1).

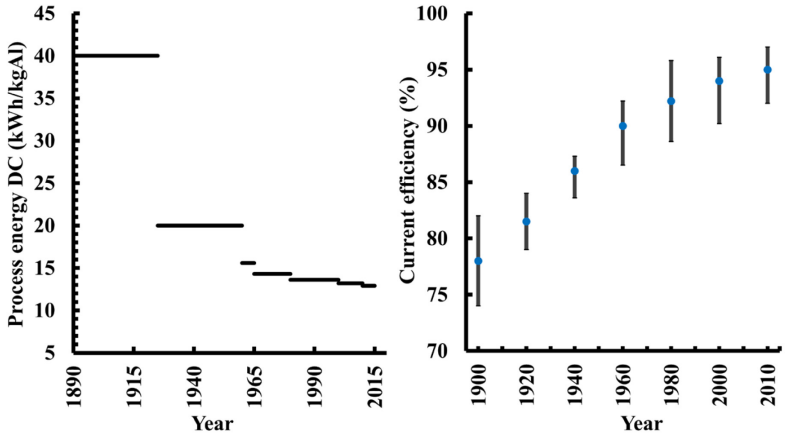


**Figure 2.1 DC electrical energy consumption in Hall-Héroult process [Welch et Kinery, 2000, World-Aluminium, 2017, Tabereaux et Peterson, 2014]**

In an ideal aluminum electrolysis process and according to Faraday law for 1 kAh of electrical current, 0.3356 kg of aluminum is produced [Grjotheim et Kvande, 1993b]. On top of that, at a typical temperature of 960 ºC, the ideal process energy for production of 1 kg of aluminum with a current efficiency of 100% is about 6.3 kWh [Thonstad *et coll.*, 2001a]. However, in reality (Figure 2.1), a current efficiency of ≈ 95% and a typical process energy of 13-15 kWh/kgAl is observed. Among other factors, two major phenomena decrease the current efficiency and increase the energy demand. The first phenomenon (which drastically reduces the current efficiency) is the back reaction of solubilized metallic species with $CO_2$ gas followed by production of CO gas and dissolved $Al_2O_3$. The second major phenomenon is the formation of resistive deposits on the surface of the cathode. Such deposits create more resistance and increase the required electrical energy. Figure 2.2 shows the different types of solid species found inside aluminum electrolysis cells.

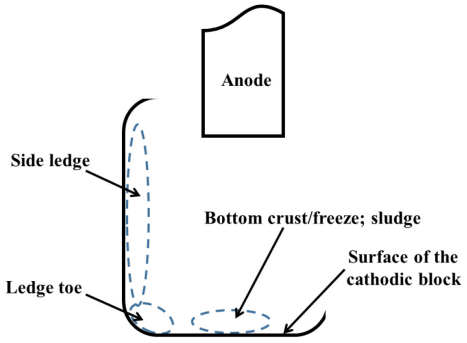


**Figure 2.2 Typical loci of common deposits within a typical aluminum electrolysis cells**

The side ledge is a beneficial layer because it not only protects the cell walls from the bath/aluminum corrosion but also prevents the infiltration of aluminum into the cell lining. Nevertheless, a proper heat balance is required to avoid the extensive elongation of the side ledge on the surface of cathodic block (i.e. extended ledge toe). The frozen side ledge mostly consists of cryolite and therefore its melting has an important effect on the chemistry of the bath. On the contrary, the detrimental solid deposits are the bottom deposits namely, bottom crust/freeze and sludge. The behavior of these solid deposits has been investigated for quite a while and it is one of the focal points of research on aluminum electrolysis [Gasik et Gasik, 2003]. In this literature review, first a general overview of the sludge formation and its drawbacks are presented, followed by the most important factors that could affect the formation or dissolution of such deposits.

### 2.3.4 Sludge formation and its drawbacks

According to Tabereaux et Peterson (2014), the following steps are followed upon addition of 1–2 kg of alumina particles onto the surface of the bath by point feeders. At first, the bath wets some of the particles and dissolves them immediately. However, some of the particles form agglomerates surrounded by a frozen bath layer. Later, the alumina particles absorb the sensible heat and their temperature increases from 100°C to 960°C. At this stage, the process is heat transfer controlled while the frozen bath layer around some of the agglomerates gradually disintegrates. Finally, alumina particles dissolve into the bath and distribute in the cell by the turbulent flow. Nevertheless, not all of the alumina particles dissolve and when undissolved clumps of alumina sink to the bottom of the cell, beneath the metal pad, a dense and viscous phase called sludge is formed. In addition, there are other probable scenarios for the formation of sludge, including the falling of anode cover materials and collapse of the top crust. For example, each anode change, including the removal of the anode butt and installation of new anodes, creates abundant opportunities for around 200 kg of anode cover materials to fall into the cell [Taylor et Welch, 2004]. Furthermore, during the anode change and feeding procedure, clumps of top crust are often introduced into the cell, leading to the formation of sludge. $AlF_3$ feeding may also affect sludge formation, although such possibility was much more significant in old technologies in which $AlF_3$ was added in sudden and huge quantities of about 50 kg. In

the latter case, the sludge contains an excessively high amount of $AlF_3$ and its dissolution will take a much longer time than the alumina-rich sludge [Utigard, 1987].

The other possible route for the formation of sludge is related to the influence of bath chemistry on the phase equilibria. A simple demonstration of such behavior is presented in Figure 2.3. As it is evident, in case of keeping the same operational temperature in the cell, upon the depletion of the alumina content in an unsaturated bath, a mixture of the bath and alumina is prone to be precipitated as is shown by the horizontal arrow in Figure 2.3. Such precipitates, upon accumulation on the bath-metal interface, may be able to penetrate through the metal pad or slip to the sides of the bath-metal interface and join the ledge toe. Furthermore, the sodium concentration polarization at the bath-metal interface also may help such deposits to solidify, by increasing the interfacial liquidus temperature (Figure 2.3).

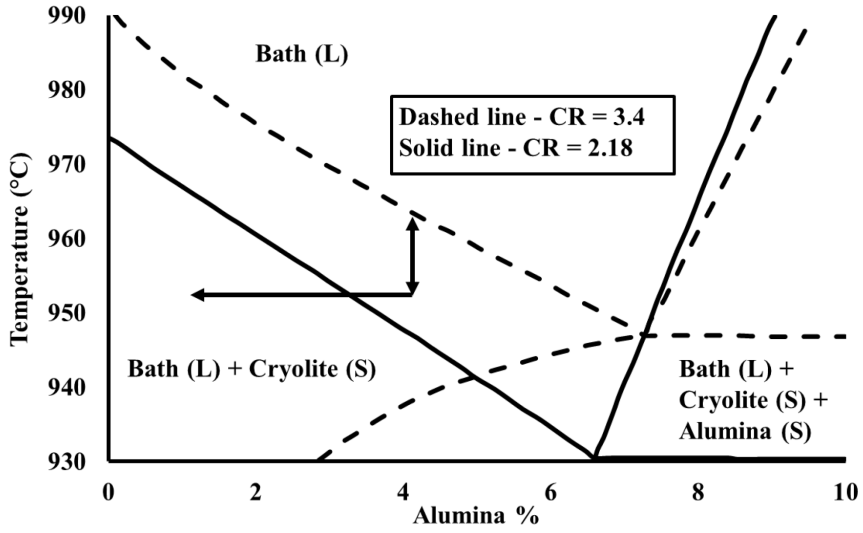


**Figure 2.3 The horizontal and vertical arrows show the formation of solid cryolitic species because of depletion of alumina and sodium concentration polarization at the bath-metal interface respectively**

Sludge, formed upon alumina agglomeration, is a viscous paste-like combination of alumina particles and alumina-saturated bath with a typical density of 2400 kg/m$^3$ [Grjotheim et Kvande, 1993b, Thonstad *et coll.*, 1980]. The acidity of the sludge is less than mother bath (typically 2-5% excess $AlF_3$ [Grjotheim et Kvande, 1993b] or cryolite ratio (CR) of 1.4-1.8 [Thonstad *et coll.*, 1972]). The lower acidity of sludge compared to the mother bath can be either attributed to its equilibrium with a metal pad that has a high sodium content [Keller *et coll.*, 1988] or precipitation of cryolite due to the higher interfacial liquidus temperature [Solheim, 2002]. As

Figure 2.3 depicts, the precipitation of cryolitic species not only dissolves the solid alumina content of the sludge but also increases the cryolite ratio of the sludge (i.e. less acidity). Dissolution of alumina in the precipitated cryolite, creates saturated bath with low density that may find its way to the mother bath by forming a film between aluminum and side ledge or through the aluminum pad [Solheim, 2002]. Such vertical gradient of CR has been noticed in laboratory experiments and industrial samples [Allard *et coll.*, 2014a, 2014c]. If the amount of heat loss from the bottom of the cell is enough (i.e. if it gets below the liquidus temperature of the sludge) and the sludge is not back-fed fast enough, such sludge can create a resistive deposit on the surface of the cathode usually called bottom crust. Bottom crust typically has a density of 3200-3700 kg/m$^3$, a porosity of 1-20 % and acts as an electrically resistive layer [Thonstad *et coll.*, 1982, Veneraki *et coll.*, 1973]. The size and shape of the alumina particles within the bottom crust is larger than and different from the size of the fed alumina because of the alumina phase transformation catalyzed by presence of an alumina-saturated bath [Kachanovskaya et Arakelyan, 1976, Landi *et coll.*, 1968]. Another type of bottom deposit that mostly consists of cryolite, is called bottom freeze (Table 2.1). Bottom freeze is generally created when the solidified bath close to the sidewalls extends on the surface of the cathode. The other possible path for creation of bottom freeze is the falling of the frozen bath around the newly installed anodes (i.e. anode freeze) [Utigard, 1999b].

Table 2.1 : Typical composition of different bottom solid phases found in industrial cells [Allard *et coll.*, 2015]

| Type | $AlF_3$ (%) | $CaF_2$ (%) | $Al_2O_3$ (%) |
|---|---|---|---|
| Bottom freeze | 2-13 | 4-6 | 2-10 |
| Sludge | 2-10 | 2-5 | 20-50 |
| Bottom crust | 2-5 | 2 | 65-85 |

Formation of sludge is not a desirable phenomenon because it affects significant operational factors including current efficiency, operational temperature, bath chemistry, current density and the stability of the metal-bath interface [Fallah Fini *et coll.*, 2017a, Welch, 1995]. A typical sludge phase has an electrical conductivity of 1.0 S/cm ± 0.2, which is about twice when compared to bath and 30,000 times when compared to molten aluminum [Keller, 2005b, Geay *et coll.*, 2013]. Such electrical resistivity diverts the local current density and creates areas with higher current density and consequently higher cathode wear [Liao et Øye, 2013]. Besides, Sludge formation consequently influences the carbide content in the bath, carbon particles

dispersion, bath superheat and loss of current efficiency [Thonstad et al., 2001a]. Extensive sludge formation increases the occurrence of anode effects, during which the anode is poorly wetted by the electrolyte resulting in an extensive carbon dusting. Presence of dispersed carbon particles in the bath not only increases the electrical resistivity of the bath (i.e. higher energy consumption) [Bugnion et Fischer, 2016], but also causes higher solubility of aluminum and loss of current efficiency by reaction with dissolved aluminum and formation of aluminum carbide [Ødegård *et coll.*, 2013b, Wang *et coll.*, 1994].

Moreover, sludge also tampers with the hydrodynamics of the cell. The higher electrical resistivity of the sludge-covered cathode area diverts the local current to flow horizontally towards the edges of the sludge. Such horizontal current flows perturb the dominant vertical current flows leading to additional instability of the metal-bath interface [Tarapore, 2013]. The oscillation of metal-bath interface has a dramatic effect on the optimum operation of the cell considering the large aspect ratio of the cell and higher resistivity of the bath compared to metal pad [Davidson et Lindsay, 1998]. Moreover, the shear amount of metal-bath interfacial stress leads to higher aluminum solubility (i.e. fogging effect), which consecutively accounts for higher back reaction and loss of current efficiency [Thonstad et al., 2001a]. In addition, such metal/bath instability results in change of anode-cathode distance (i.e. uneven ACD), cell voltage drop (CVD) and heat balance which dramatically affect the current efficiency and energy consumption [Welch et Kuschel, 2007].

As it was mentioned, there are various parameters involved in the formation or dissolution of the sludge; therefore, it is necessary to review the influence of important factors such as cathode grade, hydrodynamics, interfacial phenomena, temperature, bath chemistry, physicochemical characteristics of alumina and feeding strategy. Furthermore, considering the complex nature of alumina dissolution, which is strongly interlinked with the bath chemistry, level of superheat, alumina feeding strategy, etc., it is quite evident that the cycle of sludge formation and dissolution is a common phenomenon in the smelters around the world. However, before individual investigation of each parameter, it is helpful to review the previous studies on sludge formation in both laboratory and industrial scale (Table 2.2 and Table 2.3) and get a summary of the corresponding results.

Table 2.2 : Observations on central deposits from industrial electrolysis cells

| Observation | Average chemistry of the deposit | Reference |
|---|---|---|
| - Graphitic cathode<br>- Whitish rounded spots with thickness of 0.5-9 mm<br>- Under the feeder containing α-alumina platelets 50-700 µm<br>- Cathode surface coverage 3-9 % | $CaF_2$ ~ 5.2%; CR ~ 2.5; alumina ~ 18% | [Coulombe *et coll.*, 2016a] |
| - Graphitized cathode<br>- Dark stripes covered by whitish material with thickness of 3-50 mm<br>- Scattered on the bottom surface containing α-alumina platelets 5-80 µm<br>- Cathode surface overage 16% | $CaF_2$ ~ 4.1%; CR ~ 2.4; alumina ~ 44% | [Coulombe et al., 2016a] |
| - Black carbonaceous material surrounded by carbide<br>- Visible aluminum droplets and α-alumina platelets | $CaF_2$ ~ 2.8%; Excess AlF3 ~ 2.4%; alumina ~ 42%<br>Impurities (Si: 120, P: 40 ppm) | [Geay et al., 2013] |
| - Thickness few mm<br>- Under the feeder<br>- Just thin deposits on the middle of the cell | $CaF_2$ ~1.3%; CR ~2.5; alumina 21.8 % | [Allard et al., 2014c] |
| - Thickness few mm positioned under the feeder<br>- Spots of thin layer on the surface | $CaF_2$ ~ 5%; CR ~ 2.5; alumina ~ 26% | [Allard et al., 2014a] |
| - Bottom crust (65-85% alumina) formation requires enough ΔT (15-20 °C)<br>- Majority of α-alumina platelets were 10-400 µm, few 3-4 mm<br>- α-alumina platelets have a yellowish tint | 65-74% alumina | [Thonstad et al., 1982] |
| - The dissolution of the bottom crust is hindered due to its insulating effect.<br>- The difference in liquidus temperature of sludge (950-964 °C) is mostly due to the $CaF_2$ content. | 1-5% $AlF_3$; 1.6-3.5% $CaF_2$; 35-60% alumina; 40-60% cryolite | [Liu, 1995] |

| Observation | Average chemistry of the deposit | Reference |
|---|---|---|
| - Viscosity of the sludge increases dramatically at 25% alumina<br>- As bottom crust grows the size of the alumina particles increase | Alumina 23-53% (60-90% α-alumina); Higher CR than the bath (1.4-1.7); 0.3% $Al_4C_3$; 0.03% Al | [Thonstad et al., 1972] |
| - There is a fairly rapid mass exchange between the sludge and the bath<br>- The mass transfer is likely due to the thin film between side ledge and metal | - | [Thonstad et al., 1980] |
| - Alumina content of the sludge is dependent on feeding strategy<br>- Upon hardening, the sludge rejects $AlF_3$ | Soft sludge: Excess $AlF_3$ ~ 3%, alumina 42%<br>Bottom crust: Excess $AlF_3$ ~ 0.7%, alumina 69% | [Taylor *et coll.*, 1990] |
| - The alumina particles are relatively large and thick irrespective to the feed's degree of calcination. | - | [Abd El All *et coll.*, 1980] |

Table 2.3 : Experimental laboratory scale investigations of central deposits

| Bath composition | Operational characteristics | Central deposit characteristics and remarks | Reference |
|---|---|---|---|
| 74% cryolite, 11% $AlF_3$, 5% $CaF_2$, 9% α-alumina, 1% γ-alumina, CR = 2.2, 3.0 and 4.0 | Graphitized cathode, 960 °C, electrolysis at 0.7 A/cm$^2$ for 6 h; with two conditions of alumina underfeeding and overfeeding | - Surface deposit: 21% alumina, CR ~ 2.3<br>- Sludge: 24.8% alumina, $CaF_2$ 0%, CR ~ 2.3<br>- In cases with higher CR less amount of sludge or no sludge was noticed | [Allard et al., 2014a, 2014c] |
| Industrial bath, 5% $CaF_2$, 10% alumina, CR = 2.2 | Graphitized and graphitic cathodes, 955 °C, electrolysis at 0.9 A/cm$^2$ for 2-5 h; high/low heat transfer rate at walls of the cell; with two conditions of alumina underfeeding and overfeeding | - The blocks with higher thermal conductivity showed less sludge formation;<br>- Lower heat transfer at the walls leads to more bottom sludge formation;<br>- At similar conditions there is hardly any difference between the chemical composition of central deposits for two types of cathodes;<br>- At similar conditions, graphitized cathode had more central deposits | [Coulombe et al., 2016a] |
| 5% $CaF_2$, 5% alumina, CR = 1.5-4.0 | Inversed polarity electrolysis cell; Anthracitic and graphitic cathodes, 1000 °C, electrolysis at 0-0.7 A/cm$^2$ for 4 h | - Higher current density leads to thicker deposits (2-3 mm) at 0.15-0.20 A/cm$^2$<br>- At higher current densities, aluminum droplets act as wedges and partially remove the deposit<br>- For graphitic cathodes, the deposit contains more aluminum droplets<br>- Carbide formation is a function of current density and CR<br>- For a system with CR ~4.0 the deposit is a network of alumina particles trapping cryolite<br>- For a system with CR ~1.5 the deposit is larger and bulky; there is no network structure; the deposit contains carbon and silicon (5%) | [Herstad *et coll.*, 1983a, Herstad *et coll.*, 1983b] |

| Bath composition | Operational characteristics | Central deposit characteristics and remarks | Reference |
|---|---|---|---|
| Saturated alumina and cryolite, 10 % excess $AlF_3$, 2-4% LiF | Inversed polarity electrolysis cell; alumina particles size 40-150 μm; 1020 °C with cold finger at 975-997 °C | - When heated above the liquidus temperature the sludge kept its dimension and just lost some of the bath<br>- Alumina content was 65-85% and large crystallized α-alumina particles ( up to 5 mm) were visible<br>- Presence of aluminum metal decreased the size of the crystals up to 75%; changed the colorless crystals to yellowish/brownish; changed the random orientation of crystals into thin right angled growth<br>- Crystals are connected by recrystallization of interstitial dissolved alumina<br>- In case of more acidic baths, the deposit adherence to the cathode is stronger and the alumina plates are thinner<br>- Presence of LiF decreases the cathodic deposit coverage<br>- Sludge dissolves 2.5 times faster than bottom crust<br>- Dissolution rate of bottom crust is quite close to the dissolution rate of pure alumina. | [Thonstad et al., 1982] |
| 5% excess $AlF_3$, 2% alumina, 5% $CaF_2$ | 960 ºC | - Sludge with alumina content >10% acts like a fluid and wets the cathode; On slightest cooling alumina crystallizes<br>- Sludge with alumina content <10% forms bottom crusts that preserve their structure after heat losses | [Gerlach et Winkhaus, 1985] |

| Bath composition | Operational characteristics | Central deposit characteristics and remarks | Reference |
|---|---|---|---|
| Pure cryolite | 1020 ºC<br>Sludge samples with 25-50% alumina under 4 cm of molten aluminum covered by pure cryolite<br>Stirring rate of cryolite: 20-80 rpm | - Dissolution of sludge is hindered by the thickness of the metal pad<br>- In direct contact of sludge and cryolite, the dissolution rate is of first order in unsaturated bath<br>- Presence of metal pad creates an almost zero order dissolution rate (i.e. mass transfer is controlled through a bath film between the metal and the walls) | [Thonstad et al., 1980, 2013] |
| 40% alumina<br>60% cryolite | Stable top crusts (35-55% α-alumina) formed at 985 °C were kept for 48 h in sludge phase at 1000 °C and they were removed | - If stable top crust (35-55% α-alumina) forms sludge, such sludge will take much more time to dissolve in comparison to crusts formed by floury alumina (unstable crust).<br>- The transformation of γ-alumina to α-alumina is rapid and is catalyzed by cryolitic vapors/liquids; the order of catalytic effect is as follows: $AlF_3 > Na_3AlF_6 > NaF > CaF_2$ | [Ødegård *et coll.*, 1985, Ødegård *et coll.*, 2013a] |
| No bath. | Cubes of the top crust (1 g) were placed under the molten aluminum at 980 °C | - At 980 °C for 1 hour: sludge with lower α-alumina content (< 25 %) remains stable; sludge with intermediate α-alumina content (25-45 %) deforms and sludge with very high α-alumina content (97 %) disintegrates forming a film under the metal pad.<br>- At longer times ( 96 h) the sludge with intermediate α-alumina content also disintegrates but sludge with lower α-alumina content still remains stable. | [Kheiri *et coll.*, 1987] |

### 2.3.5 Influence of carbon cathode materials

The cathode is related to the sludge formation tendency through its thermo-electrical, geometrical and physicochemical characteristics. The most important characteristics of the cathode that may play a major role in the formation/dissolution of the sludge are the thermal conductivity, electrical resistance, porosity and design.

The propensity of a cell to form sludge is strongly related to the quality of alumina dissolution and the heat loss at the bottom of carbon cathode block. Approximately 50 % of the total heat loss occurs through the cell sidewall and bottom, therefore the thermal properties of the carbon cathode lining become a significant parameter [Solheim, 2018]. Consequently, as long as the sludge does not freeze due to the excessive heat loss at the bottom of the cell, it can be back-fed through several phenomena including interfacial and hydrodynamics movements. As a result, it is not wrong to say that the primary purpose of the cell heat balance is to avoid the formation and freezing of the sludge [Grjotheim et Kvande, 1993b].

Heat transfer across the cathode construction materials is proportional to the thermal resistance of each layer of material. The thermal conductivity of the carbon materials increases with the level of graphitization and it is a function of the age of the cell and temperature. The thermal conductivity of anthracite increases with temperature but graphitized materials' thermal conductivity decreases with temperature. However, graphitic materials show contradictory behaviors (i.e. decrease or increase). The intriguing point here is that the behavior of cathode blocks does not always follow a definite increase or decrease pattern. Such different behavior can be attributed to the complex phenomena that each cathode block undergoes during the operation life such as carbide/deposit formation, sodium/thermal expansion, sodium/bath penetration and surface corrosion of cathode block. [Sørlie et Øye, 2010]

The thermal conductivity of the side walls also affects the dynamics of the cell through its interaction with the buffer layer of frozen cryolite (i.e. side ledge). The thickness of the side ledge is influenced by the heat transfer rate. Side walls with lower thermal conductivities transfer the heat from the side ledge at a slower rate, hence cells using such materials may be more prone to have higher superheat levels and sludge dissolution ability. Nevertheless, the more conductive side wall materials may also be prone to dissolve the sludge but with another mechanism [Coulombe et al., 2016a]. Such mechanism involves the extensive formation of the

ledge toe (i.e. bottom freeze) and its contact with the sludge. The interaction of such cryolite rich phases and the sludge produces liquid deposits less dense than the aluminum metal, helping the back-feeding of sludge into the main bath [Solheim, 2002].

In addition to thermal conductivity, the electrical resistance of the cathode block also plays a major role in the complex dynamics of the cells. Song *et coll.* (2016) have shown, by using a modeling approach, that a cathode material with higher electrical resistivity may cause a higher cathode voltage drop; however, such high resistivity, forces the current paths to follow the most energy efficient path, which is a straight line towards the cathodic bar (i.e. less horizontal current). According to this criterion, the magnitude of horizontal currents versus the cathode type in decreasing order is: graphitized, semi-graphitized, full graphitic, 50/50 anthracite/artificial graphite, 70/30 anthracite/artificial graphite and full anthracite. Moreover, horizontal currents can be decreased by up to 20 % with a cathode bottom inclination of 2°. Likewise, other types of modifications such as addition of cylindrical or trapezoidal protrusions on the bottom surface of the conventional cathodes may help to achieve lower and more uniform metal velocity [Wang *et coll.*, 2014, Song *et coll.*, 2017a, Song *et coll.*, 2017c]. Better metal stability can also be achieved by the use of copper inserts which not only reduce the CVD but also can halve the amount of horizontal current density; however, application of such copper inserts may also lead to an extended ledge elongation on the cathode surface because of the high thermal conductivity of copper [Singh *et coll.*, 2017b, Von Kaenel *et coll.*, 2017]. Consequently, the use of copper inserts in modern cells has created a renewed interest for cathodes with lower thermal conductivity (e.g. graphitic grades) letting a better control over the thermal balance of the cell (i.e. limiting sludge formation and freezing) [Rivoaland, 2016a].

In addition to thermal, electrical and geometrical characteristics of the cell, the physicochemical characteristics of the cell linings such as porosity, tortuosity and air permeability may play a major role in the dynamics of the cell [Wang *et coll.*, 2009a]. The later properties define the effective diffusivity of gaseous sodium through the linings and carbon materials (i.e. changing the chemistry of the thin bath that separates the ledge from the metal). The changed chemistry within the aforementioned thin film affects the corresponding interfacial phenomena, which play a major role in the dissolution/formation of sludge and are extensively explained in another section of this article. Furthermore, there is a direct relationship between the carbide formation,

porosity of the cathode block and the sludge formation [Landry *et coll.*, 2018a, James *et coll.*, 1995b]. Such relationship could be easily explained by the fact that as sludge is formed, it acts as a medium for the dissolution of the carbide. Later, when the sludge is gradually back-fed, the carbide finds its way into the cell and changes the batch chemistry [Fallah Fini et al., 2017a, James et al., 1995b]. In addition, innovative cathode design such as drained cathodes may also eliminate the problem of sludge formation. Drained cathodes only require a film of molten aluminum on the surface of the cathode and consequently the sludge dissolution happens with more ease. Pawlek (2010b) has reviewed some of the proposed innovative cell designs and patents of drained cells.

### 2.3.6 Fluid dynamics

It is quite well established that without proper agitation around the fed alumina particles, alumina feed cannot dissolve and distribute evenly in the bath. Irrespective to the interfacial movements which are explained separately in this article, the most effective dynamic forces in an aluminum electrolysis cell are anodic bubble movements and magnetic agitations. Bubble induced agitation is the most effective phenomenon to dissolve the alumina particles since detrimental hydro-magnetic waves at the bath-metal interface leads to excessive dissolution of metallic species in the bath and alter the anode cathode distance (i.e. more back reaction and loss of current efficiency) [Thonstad et al., 2001a]. In order to minimize the detrimental effect of magnetohydrodynamics (MHD) forces, a typical layer of 25 cm of molten aluminum is maintained during the operation [Tabereaux et Peterson, 2014].

Modern cell technologies all use magnetic compensation systems to reduce the bath-metal agitation and to keep the anode cathode distance as even and low as possible. On the other hand, the application of other technologies such as the insertion of copper rods in the cathode bars has dramatically reduced the metal pad movements [Von Kaenel et al., 2017]. In such situation, alumina dissolution and distribution in the cell is mostly dependent on the bubble movements. In order to exploit the turbulence of bubble movements, application of slotted anodes has been practiced [Moxnes *et coll.*, 1998]. The slots in the anodes guide the bubbles towards the central channel before leaving the cell in order to exploit the bubble turbulence most efficiently.

Although the hydrodynamics of the cell affects the alumina dissolution and distribution, the formation of sludge also tempers with the hydrodynamics of the cell. As the sludge is formed,

it acts as an electrical insulation on the cathode block and this creates local horizontal current distribution. Such horizontal current lines create local vortexes that disturb the total hydrodynamics of the cell [Tarapore, 2013].

While talking about the hydrodynamics of the electrolysis cells, it is important to mention that one of the oldest questions in the aluminum industry has always been how the sludge is back-fed to the mother bath. In order to answer this question, there have been three theories, namely interfacial phenomena (i.e. a thin bath film between the ledge and metal pad [Thonstad et al., 1980], direct contact of the bath and sludge [Welch, 1995] and finally the metal pad movements [Kalgraf et Torklep, 1998a, Torklep *et coll.*, 1997]. Irrespective to the interfacial theory, which is explained extensively in its proper section, the other two theories are directly related to the hydrodynamics of the cell.

The direct contact of sludge and the bath was mostly practical in old feeding systems, such as side work and center break ones in which the cells were mostly run by sludge dissolution and on average just 25% of the fed alumina was dissolved shortly after introduction into the cell [Welch, 1995, Thonstad, 1977]. Nevertheless, in cases that a significant amount of sludge is formed, metal tapping (i.e. lower level of metal) can expose the sludge directly to the bath and expedite the sludge dissolution. Sludge dissolution is a long and time-consuming process since the sludge is not in direct contact with the bulk bath, so consequently, lowering the liquid metal height not only creates a direct contact between the sludge and the bath but also increases the metal pad hydromagnetic movements [Sele, 1977]. Such temporary elevated hydromagnetic movement, while the bath and sludge are in direct contact, is an excellent approach to deal with the extensive amount of sludge. Moreover, according to sediment transport theory [Torklep et al., 1997, Kalgraf et Torklep, 1998a], the increased horizontal movement of metal pad on the fresh sludge, by creating a considerable drag force, may be able to lift up the sludge particles, as big as 1 mm, and move them through the metal pad into the bath.

In severe situations, in order to dissolve the sludge as soon as possible, the synergistic effect of hydrodynamics, superheat and bath chemistry is implemented. In such cases, it is common to practice lower metal depth, less acidity (i.e. reduction of $AlF_3$ addition) and higher temperature (i.e. superheat level) [Hove et Kvande, 1982, Stam *et coll.*, 2008]. Increasing the metal tapping not only increases the hydromagnetic movements but also, by increasing the anode cathode

distance, increases the superheat level. On the other hand, the decreased amount of $AlF_3$ addition increases both the alumina solubility and the rate of alumina dissolution [Grjotheim et Kvande, 1993b].

### 2.3.7 Interfacial phenomena

Interfacial phenomena are quite significant in the Hall-Héroult process, since the main cathodic reaction occurs at an interface. Interfacial phenomena may affect the dynamics of the cell through numerous ways. Interfacial tension (IFT) gradient, induced by change in local temperature or bath chemistry, can play a major role in creating certain circulation within the metal-melt interface. Interfacial forces may resist the formation and movement of the gas bubbles or dampen the oscillation at the bath-metal interface; however, surface active species may speed up the renewal of the interface and enhance the mass transfer [Utigard *et coll.*, 1989]. Besides, the interfacial tension between the bath and metal is a barrier against the undissolved alumina agglomerates and other precipitated cryolitic species.

It is well established that as surface-active sodium ions travel towards the metal/bath interface, such concentration polarization lowers the IFT of metal/bath [Utigard et al., 1989]. On the other hand, since there is a difference between the current density exactly under the anode, and the areas at its vicinity, such IFT gradient causes an outward movement from under the anode (Figure 2.4). Moreover, since usually the deposited sludge has a lower $AlF_3$ content than the bulk of the melt, and the fact that higher excess $AlF_3$ increases the interfacial tension, another IFT gradient exists between the metal/bath and metal/sludge. This latter IFT gradient induces a film movement from the sludge towards the bulk melt. Besides, since sodium is continuously lost to the cathode lining, the thin layer of melt in contact with the cathode linings must have a higher $AlF_3$ (i.e. higher interfacial tension) compared to metal/bath interface. Such higher IFT induces a film of the bath to move downwards from the metal/bath interface (lower interfacial tension) towards the metal/sludge interface (higher interfacial tension). [Utigard et Toguri, 1991b, Utigard et al., 1989].

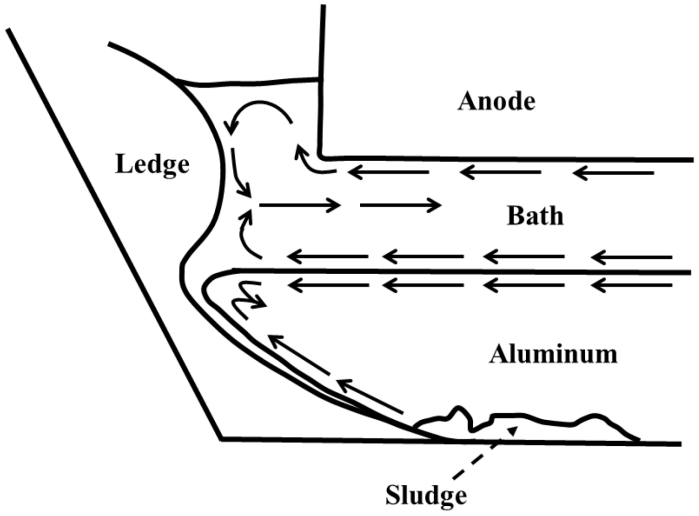


**Figure 2.4 Interfacial movements within the aluminum electrolysis cells [Utigard et Toguri, 1991b] "Copyright 1991 by The Minerals, Metals & Materials Society. Used with permission."**

Based on such interfacial movement patterns, a slow back-feeding of the sludge through a thin film of the bath between the ledge and the metal pad has been proposed by Thonstad et al. (1980). Such speculation is based on the two following observations: first, in a laboratory experiment, it was found out that dissolution rate of sludge was approximately independent of bath agitation rate and diffusion controlled. Secondly, after cooling down the experimental setup, a thin bath film was always surrounding the metal pad. Later on , Thonstad et al. (1980) also noticed a fairly rapid transfer rate of sludge in industrial cases. Based on such industrial observations, and assuming an interfacial layer of 0.25-1.0 mm thick, Utigard (1987) has calculated a net back-feeding of 5.5-88 liters of sludge per hour through the thin bath film, which corresponds well with the high exchange rate observed in previous commercial cases [Thonstad et al., 1980].

On the other hand, as it was mentioned before, $AlF_3$ feeding may also cause sludge formation and such sludge interacts very differently with the bath. For instance, its dissolution time is much longer than the sludge formed by alumina agglomerates. The elongated dissolution time is explained by the interfacial movement from the low IFT at bath towards the high IFT (due to excessively high amount of $AlF_3$) at the sludge, exactly opposite of the flow pattern speculated for alumina formed sludge. As $AlF_3$ gradually dissolves in the film layer, a mixture of solid $AlF_3$ and $AlF_3$-rich bath is formed. At a certain point, the density of this solid-liquid mixture becomes less than the aluminum pad and a sudden batch of $AlF_3$ is introduced into the bath. Furthermore,

it is shown that the IFT plummets in the range between pure cryolite and 13% of excess $AlF_3$; beyond such amount of excess $AlF_3$, no further significant change is noticed in IFT values [Utigard et Toguri, 1985]. Accordingly, it has been speculated that it is better to operate the electrolysis cells at an excess $AlF_3$ value of 10-13 % in order to keep a tangible driving force to enhance the movement of bath film and back-feeding of sludge [Utigard, 1987].

Moreover, Utigard (1993) has argued that when the low density liquid fraction of the sludge is back-fed, either through the metal pad or through a thin film between the ledge and metal pad, the remaining solid bottom crust is also capable of being removed. He speculates that the dissolution of such bottom crust is dependent on two phenomena that are, first, the downward movement of the bath through the thin bath film that separates the ledge from the metal. Such downward movement is due to the low sodium and $AlF_3$ activities of alumina-rich cryolite in contact with the bottom crust. Secondly, such low activities, enhance the mass transfer of sodium from sodium-rich cathode block towards the sludge. These two phenomena gradually provide enough bath to gradually dissolve the bottom crust.

Furthermore, in cases when the heat loss at the bottom of the cell is enough to crystallize cryolite, such solidification increases the local $AlF_3$ concentration, leading to enhanced movement of the bath within the thin film from the bulk to the bottom of the cell. Consequently, a thin layer of solid cryolite may form and extend astonishingly fast (up to 10 cm/day) on the surface of the carbon cathode [Utigard, 1987]. At high bath acidity, irrespective of the problem of increased bath resistivity, increased anodic/cathodic overvoltage, less alumina solubility and lower rate of alumina dissolution, it is also possible that a solid layer of cryolite precipitates on the bath-metal interface [Utigard, 1987]. Such phenomenon has been noticed in cases with very high amount of excess $AlF_3$ and low superheat levels due to the sodium overvoltage at the bath metal interface and increased interfacial liquidus temperature [Sleppy et Cochran, 2013]. The precipitation of cryolite at the metal-bath interface may be enhanced in systems that possess high amount of excess $AlF_3$, stable bath-metal interface (i.e. magnetically compensated) and no lithium [Haupin, 1997].

Additionally, Solheim (2002) has calculated the amount of cryolite and alumina that may crystallize at the bath-metal interface in case of sodium concentration polarization, considering the fact that lower superheat level as well as higher excess $AlF_3$, favor the crystallization.

According to Haupin (1997), the increased electrical resistance due to the precipitated cryolitic species at the bath-metal interface, ultimately dissolves such layer (by creating local heat) creating a cycle of precipitation and dissolution in a repetitive manner. In addition, if such cryolitic crystals form sludge, those may act as a solvent for alumina particles. The dissolution of alumina particles in the precipitated cryolite crystals not only decreases the acidity of the sludge, but also lowers the liquidus temperature and density of the liquid fraction of the sludge [Solheim, 2002]. The consequence of such phenomena for the molten mixture of cryolite and alumina is either rising through the metal pad in small batches or dissolution in the thin film that exists between the ledge and metal pad.

### 2.3.8 Temperature

Probably the most effective parameter in the formation/dissolution of sludge is the operational temperature. The operational temperature of the cell is directly related to the heat balance of the cell and the primary purpose of checking the heat balance of the cell is to avoid the formation and freezing of the sludge [Grjotheim et Kvande, 1993b]. Based on the phase behavior of the bath (i.e. bath chemistry), operational temperature is also related to the superheat level of the bath according to Figure 2.5. For more detailed information for the influence of temperature on the formation and dynamics of different deposits within the electrolysis cells refer to Fallah Fini et al. (2017a).

Moreover, it deserves to be mentioned that the summation of the dissolution energy and sensible heat is enough to decrease the temperature of the melt by 15˚C if 1 wt% of alumina (with respect to total mass of the bath) at room temperature is introduced into the cell [Welch et Kuschel, 2007]. Such calculations show that heat transfer within the cell is crucial for proper dissolution of the alumina and further prevention of sludge formation [Hove et Kvande, 1982]. On the other hand, as it was mentioned before, the dissolution/disintegration of the frozen bath layer around the agglomerated alumina particles is heat transfer controlled. On top of that, in order to reduce the required sensible heat for the dissolution of alumina particles, preheating of the alumina particles has been proposed which is further explained in the section concerning the physicochemical characteristics of alumina [Kobbeltvedt, 1997].

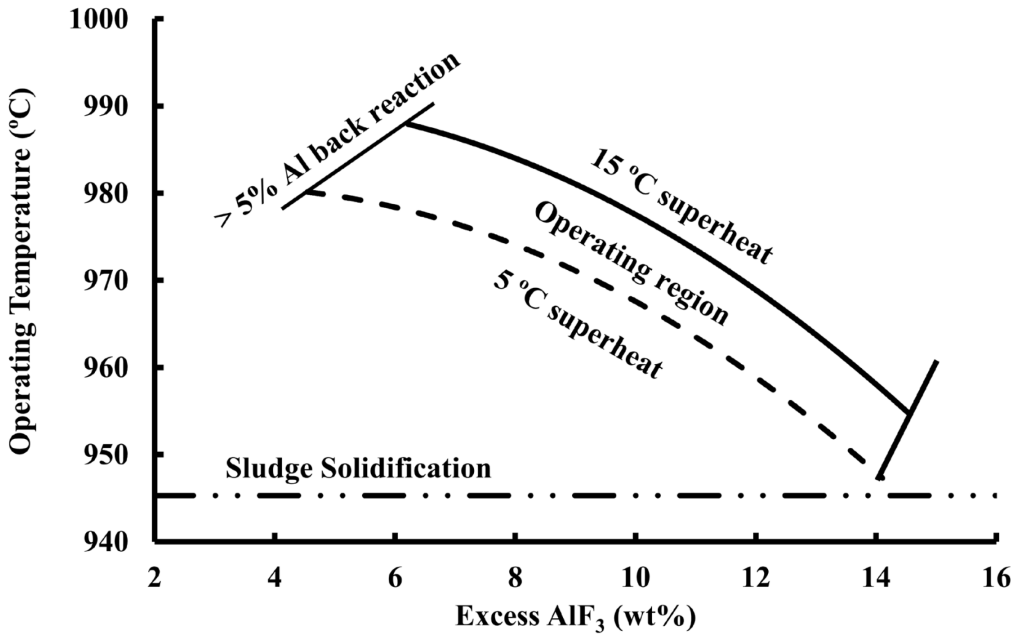


**Figure 2.5 The schematic influence of temperature and bath acidity on the operation of the cells; the bath includes 0.5 wt% $MgF_2$, 3 wt% alumina and 5 wt% $CaF_2$. [Taylor, 1997]**

Also, in order to enhance the chance of back-feeding of the sludge, it is always necessary to keep the temperature of the bottom of the cells at least at the eutectic temperature of the operating bath [Utigard, 1999b]. The latter consideration is due to the fact that the liquid bath in contact with sludge is saturated in alumina and the lowest temperature that allows the dissolution of sludge in the bath is the eutectic temperature. However, the liquid fraction of the sludge is rich in sodium which increases the threshold saturation temperature (i.e. eutectic temperature).

Another important parameter regarding the operational temperature of the cell is related to the rate of heat transfer through the cell walls affecting the growth or melting of the side ledge. Coulombe et al. (2016a), by using a bench scale setup, have demonstrated the influence of the heat transfer rate at the sidewalls of the cell on the sludge formation/dissolution tendency. It has been shown that more sludge is formed at low heat transfer rate from the cooled wall of an experimental cell, in comparison to tests with higher heat transfer rate. They justify such contradictory results by claiming that for tests with higher heat transfer rate, the side ledge extends on the bottom surface of the cathode forming an elongated ledge toe. Such ledge toe creeps towards the sludge and upon linking to the sludge, creates a less dense liquid, which is gradually back-fed into the bath either through interfacial phenomena or through the aluminum

metal. Such conclusion is quite comprehensible since the ledge is mostly consisting of cryolite and its contact with alumina particles can dissolve them and create a low-density alumina-saturated bath with lower liquidus temperature [Solheim, 2002].

### 2.3.9 Bath chemistry

A typical electrolysis cell uses 9-11% $AlF_3$, 4-6% $CaF_2$, 1.5-4% $Al_2O_3$ and in some cases 2-4% $MgF_2$/LiF [Tabereaux et Peterson, 2014]. Table 2.4 shows the influence of various additives on the physicochemical properties of a typical bath. There is no doubt that the presence of each chemical in the bath affects the phase equilibria. However, the study of the phase equilibria in each system is out of the scope of this research and avid readers are referred to extensive references [Thonstad et al., 2001a, Grjotheim *et coll.*, 1982].

Table 2.4 : Influence of additives on physicochemical properties of the bath; ↑ increase, ↓ decrease [Habashi, 2003, Grjotheim et Kvande, 1993b]

| Property | LiF | NaF | $CaF_2$ | $MgF_2$ | $AlF_3$ |
|---|---|---|---|---|---|
| Liquidus temperature | ↓ | ↓ | ↓ | ↓ | ↓ |
| Alumina solubility | ↓ | ↓ | ↓ | ↓ | ↓ |
| Rate of alumina dissolution | ↓ | ↓ | ↓ | ↓ | ↓ |
| Vapor pressure | ↓ | ↓ | ↓ | ↓ | ↑ |
| Density | ↓ | ↓ | ↑ | ↑ | ↓ |
| Viscosity | ↓ | ↓ | ↑ | ↑ | ↓ |
| Interfacial tension (bath-metal) | ↑ | ↓ | ↑ | ↑ | ↑ |
| Electrical conductivity | ↑ | ↑ | ↓ | ↓ | ↓ |

The reduction of liquidus temperature is a beneficial phenomenon since it reduces the operating temperature (i.e. less energy consumption) and enhances the current efficiency. This is also beneficial since at constant operating temperature, lower liquidus temperature reduces the chance of sludge solidification. Nevertheless, the combination of lower superheat levels and higher acidity not only reduces the alumina solubility and its dissolution rate but also increases the difference between the melting point of the side ledge and the bath [Utigard, 1993]. Besides, in the systems using LiF as additive, the liquidus and hence the eutectic temperature of the system is lower, allowing for a possible lower bottom temperature in the cell [Utigard, 1999b]. Nevertheless, Thonstad et al. (1982) indicate that the application of LiF in acidic baths exacerbates the bottom crust formation [Thonstad et al., 1982]. Such problem may be related

to the fact that the application of LiF not only reduces the liquidus/eutectic temperature but also reduces the eutectic alumina concentration and dissolution rate of alumina.

All the additives affect the density of the bath. Lower bath density may decrease the terminal velocity of the alumina particles. Keller (1984) mentions that lower density of the bath consequently reduces the density of the alumina agglomerates and hence it can hinder the sludge formation. On the other hand, since the density of aluminum pad (~2300 kg/m$^3$) does not change significantly with temperature within the range of 940-970 ˚C [Leitner *et coll.*, 2017], most of the density difference between the bath and metal is accounted for by the cryolitic melt. Dissolution of alumina in the bath reduces the density of the bath up to the eutectic point [Thonstad et al., 2001a] and hence any contact between the sludge and a cryolite rich phase could enhance the back-feeding of sludge. Such cryolite rich phases could be provided by the molten side ledge (i.e. high superheats) or precipitation of cryolite due to sodium concentration polarization at bath-metal interface [Solheim, 2002].

After alumina particles agglomerate and sink through the bath, there is yet another barrier (i.e. interface of metal-melt) for them to reach to surface of the cathode block. According to Table 2.4, all additives increase the metal-melt interfacial tension (IFT). Lower CR and higher alumina content also increase the interfacial tension [Utigard, 1999b]. In addition to IFT, the viscosity of the electrolyte also affects the hydrodynamics of fluids through interaction with gas bubble detachment and terminal velocity of undissolved alumina particles. A high viscosity can reduce the metal dissolution within the bath and enhance the alumina dissolution rate by reducing the back reaction rate. In addition to the above-mentioned factors, evaporation of volatile species also affects the chemistry of the bath. The most volatile species are the sodium and aluminum fluoride or the combination of these species as $NaAlF_4$ [Grjotheim et Kvande, 1993b]. Evaporation of such chemicals increases the CR and it is required to control the CR by introduction of fresh materials. Higher CR increases the liquidus temperature and consequently the sludge finds more opportunities to transform into a solid deposit [Allard et al., 2014a].

### 2.3.10Physicochemical characteristics of alumina

One of the other significant factors in normal operation of the electrolysis cells is the physicochemical traits of the alumina feed, since it directly influences the solubility rate of the alumina and the chemistry of the bath. Such characteristics include different phases of alumina,

BET (Brunauer-Emmett-Teller) surface area, density, loss on ignition (LOI), particle size distribution and flow funnel time. There are already extensive literature reviews about the influence of alumina traits on its dissolution behavior [Grjotheim et al., 1982, Grjotheim et Kvande, 1993b, Thonstad et al., 2001a, Wang, 2009, Welch et Kuschel, 2007], consequently, only some important points will be addressed here. Furthermore, typical characteristics of the smelter grade alumina feed has been summarized by Tabereaux et Peterson (2014).

Alumina is present in the cryolitic bath samples as dissolved alumina or several crystalline structures (i.e. β, γ, θ, δ, α). The two most common alumina phases are the α-alumina (high temperature calcined) and γ-alumina (low temperature calcined). γ-alumina (also known as sandy alumina) has a lower flow funnel time, higher surface area and higher dissolution rate which makes it more ideal for aluminum electrolysis cells; however, pure γ-alumina creates very hard top crusts (i.e. excessive crust feeding). Hence typical α-alumina (also known as floury alumina) content of smelter grade alumina (SGA) is 2-15% [Tabereaux et Peterson, 2014]. Moreover, the rate of dissolution for different alumina phases is as follows: $\beta > \gamma > \theta > \delta > \alpha$ [Gerlach *et coll.*, 1975]. Upon addition to the melt, γ-alumina exothermally transforms into α-alumina, which is less soluble, and later, endothermally dissolves within the bath [Gerlach et Winkhaus, 1985]. γ-alumina transformation into α-alumina creates thin plates (*ca.* 0.5 μm) while thicker alumina plates (*ca.* 1.5 μm) are the initial feed α-alumina content that has precipitated without dissolution and act as building blocks of the agglomerates [Thonstad et al., 2001a].

What's more, alumina particles which easily flow (i.e. less flow funnel time) tend to disperse over the bath rather than forming clumps, therefore a faster dissolution rate is observed. Flow funnel time is inversely proportional to the percentage of fine alumina particles. High number of fine particles may lead to the creation of densely packed alumina aggregates (i.e. higher density) that in return increase the possibility of sludge formation. Of course, fine particles dissolve individually faster than coarse particles but their higher flow funnel time and poor wetting properties lead to a slower dissolution rate. Because of such poor wetting properties, electrolyte cannot penetrate within the intergranular voids of the alumina particles and instead, finer particles fill the voids between the coarse particles creating an elongate floating period for the formed rafts. Besides, the volatile content of the alumina (i.e. LOI) in contact with the hot

bath not only creates agglomerates that are more porous (i.e. lower density) but also provides a local turbulence that helps to enhance the dissolution rate of alumina. Upon addition of the alumina into the cell, the volatile content of the alumina is released in two steps, 1) a short rapid release of vapor from $Al(OH)_3$ and 2) a more extended vapor release during α-phase transition catalyzed by $NaAlF_4$. [Rye *et coll.*, 1990, Isaeva *et coll.*, 2009, Dando *et coll.*, 2010, Keller, 1984]

Moreover, preheating the alumina (≥ 600 °C) is an effective method to make sure that most of the alumina is dissolved at rates close to single particle dissolution rate; nevertheless, the agglomerates formed at such condition, are much denser and hard to dissolve [Kobbeltvedt, 1997]. According to Rye et al. (1990), the reason for increased rate of dissolution in case of preheated alumina is due to the formation of a thinner bath layer around the agglomerates which in return disintegrates faster. The short life span of such alumina agglomerates inhibits extensive sintering, so less dense α-alumina aggregates are formed. It has to be emphasized that the most effective method to enhance the dissolution rate of the single alumina particles as well as the alumina agglomerates is to have enough superheat [Kobbeltvedt, 1997]. In recent years, there have been some attempts to construct preheating equipment (e.g. countercurrent heat exchanger) that can use the top crust heat loss of the smelters to preheat the alumina particles [Schubert Severo et Gusberti, 2017].

Yang *et coll.* (2015) have investigated the difference between two grades of alumina namely primary and secondary alumina. Based on observations made with transparent quartz cells, it has been shown that secondary alumina dissolves 50% faster than primary alumina. In order to explain the higher dissolution rate of the secondary alumina, parameters such as higher values of loss on ignition (25-300˚C), fluoride content and burning of adsorbed carbon dust have been proposed. It has been claimed that the burning of adsorbed carbon dust after introduction of the feed can decrease the temperature drop up to 0.5% as compared to primary alumina.

Furthermore, according to Wang (2009), there are contradictory research results pertaining to the effect of BET surface area on alumina particles' dissolution rate. Some results indicate that higher surface area enhances the dissolution rate [Bagshaw et Welch, 2013], whereas some others mention that surface area has a negligible effect on the dissolution rate [Jain *et coll.*, 1983a, Jain *et coll.*, 1983b]. In addition, it has to be emphasized that most of the alumina

characteristics such as BET, α-alumina content, LOI and flowability are interlinked which makes the study of individual parameters very hard [Wang, 2009]. On the other hand, it is well established that the dissolution of alumina in the bath is mostly governed by superheat level, bubble agitation and feeding strategy rather than the characteristics of feed stock [Kobbeltvedt, 1997, Kuschel et Welch, 2013, Lavoie *et coll.*, 2016, Welch et Kuschel, 2007].

Archer (1983), Archer (2013) has presented a qualitative model to predict the sludge formation tendency of the alumina feedstock with respect to alumina characteristics that are governed by Bayer process. Accordingly, two parameters were reported to have medium levels of confidence in the prediction of sludge formation tendency, namely big alumina particles (>149 μm) and Gibbsite content, while the other two parameters (i.e. specific surface area and particle size distribution) showed low levels of confidence. At the end, no data has been reported on the relationship between the fine particles (<45 μm) and the tendency towards sludge formation.

At the end, it has to be emphasized that in some cases the situation is much more complex and a more in-depth analysis is required to investigate the influence of alumina characteristics on the dynamics of the cell. Consequently, some dramatic and unpredictable changes may occur by changing the alumina feed from one batch to another batch. In one case, for example, a change to an alumina feed containing higher gibbsite and moisture content has shown two different behaviors either leading to lower bath acidity (i.e. from 10.6% to 8.8%) or no change in bath acidity [Meyer *et coll.*, 2012]. On top of that, investigation of some parameters such as pore size distribution or particle size distribution has failed to account for the unpredictable response of the smelter. Such contradictory behavior requires further studies to a) compare the difference between the effect of moisture content of various alumina phases; and b) investigate the different behavior of moisture content depending on particles' pore size distribution.

### 2.3.11Alumina feeding strategy

Upon the introduction of alumina into the aluminum smelting cells, alumina particles (depending on their physicochemical characteristics and feeding strategy) either undergo a rapid path of dissolution, with no problem of sludge formation, or agglomerate and follow a slower regime of dissolution [Solheim, 2014]. As Table 2.5 indicates, there are three main feeding strategies, namely center worked (CW), side worked (SW) and point feeding (PF).

Table 2.5 : Comparison between different feeding systems [Grjotheim *et coll.*, 1989].


| Property | | Feeding system | | |
|---|---|---|---|---|
| | | PF* | CW** | SW*** |
| Break and feed | Frequency (1/hr) | 10-30 | 0.3-0.5 | 0.2-0.3 |
| | Immersion time (s) | 0.7-2 | 2-4 | 2.5-4 |
| | Discharge mass (kg) | 0.5-3 | 60-100 | 100-160 |
| | Crust feeding (kg) | 0.2 | 30-50 | 60-100 |
| | Bath quantity (kg) | 30-50 | 350-450 | 500-700 |
| Heat demand | (kJ/kg bath) | 50 | 700 | 800 |
| Sludge tendency | | Low | High | Very high |

*Point feeding, **Center working, ***Side working

The CW and SW technologies are the oldest feeding technologies which had several drawbacks such as higher anode effect frequency and extensive sludge formation. The benefits of the center worked (CW) cells versus the side worked (SW) cells is a greater volume of bath close to feeding zone and faster recovery from thermal effects. However, the location of sludge in SW cells is better than CW cells since during the heating period, the partially molten side ledge is closer to the sludge formed in the SW cells. On the other hand, the magnetically driven motion of the metal pad tends to force the sludge towards the side ledge hence enhancing the back-feeding [Welch et Grjotheim, 1988]. The main problem of CW cells is the excessive sludge formation that stems from two operational facts namely, big mass of alumina dumps and big amount of top crust feeding [Welch et Grjotheim, 1988]. Considering that the thickness of the crust is typically 100 mm in the CW and SW cells, sometimes several beam actions are required to break the crust properly. Consequently, in addition to the excessive crust feeding, volume of the bath is also reduced because a lot of bath freezes over the beams. Based on these facts, most of the sludge formation problems in the CW and SW cells arise from the considerable amount of crust that is suddenly dumped into the cell [Grjotheim et al., 1989, Welch, 1990, Welch et Grjotheim, 1988].

In order to alleviate the muck formation problem, various attempts were made to better adjust the following parameters: bath acidity, alumina quality, temperature (i.e. superheat), dump size, crust-breaking technology, feeding position, bath volume, alumina discharge technology and agitation level of the bath [Welch, 1990]. So far, the most influential technique which not only minimizes the muck (sludge) formation but also addresses several other control issues such as short-term variation in temperature, anode effect frequency and enhancement of current efficiency, has been the implementation of point-feeding systems [Tarcy et al., 2011, Welch et Grjotheim, 1988, Welch, 2007]. The main concept behind the point feeding systems is to reduce the amount of alumina dumps but increase the frequency of alumina addition. Such approach not only helps to avoid excessive sludge formation but also decreases the frequency of anode effect.

The batch size and frequency of alumina addition mainly depends on the corresponding temperature drop and the heat balance of the cell. According to Hove et Kvande (1982), the state of sludge formation is related to the volume of the fed alumina batch, rate of the feeding and duration of feeding time. Walker *et coll.* (1995) have compared the temperature drop of two industrial cells with two different feeding strategy (i.e. PF versus CW). As it is shown in Figure 2.6, the larger quantity and the more sudden addition of alumina lead to excessive and a much wider temperature drop and hence more possibility for sludge formation. According to Welch (1990), every cell has its own dump-size to break-frequency ratio which has to be recognized through experience and modeling strategies.

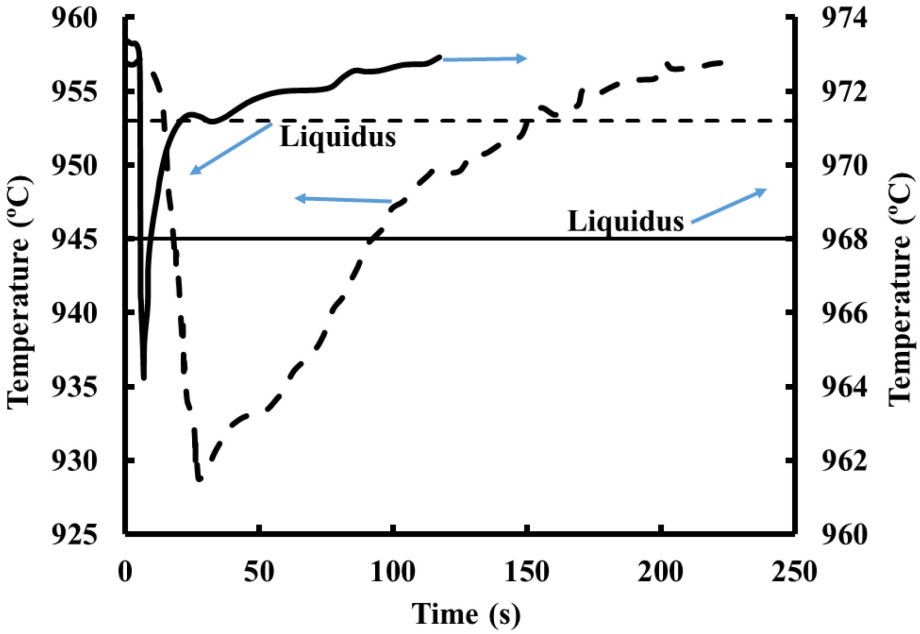


**Figure 2.6 Comparison of bath temperature change versus time for two feeding strategies; The solid lines and dashed lines correspond to point feeding and center working respectively [Walker et al., 1995]. "Copyright 1995 by The Minerals, Metals & Materials Society. Used with permission."**

Jain et al. (1983b) have monitored two distinct behaviors during two feeding regimes. The first regime shown in Figure 2.7 happens when alumina is added in a manner that every alumina particle is well dispersed (i.e. slow feeding rate and small dumps) and a rapid dissolution regime is followed. The second behavior is according to the slow dissolution path, usually happening when alumina is not well dispersed and agglomerates are formed. If the heat transfer is not enough, the dissolution of agglomerates will be hindered and as Walker et al. (1995) have shown, agglomerates' density may surpass the density of the molten aluminum.

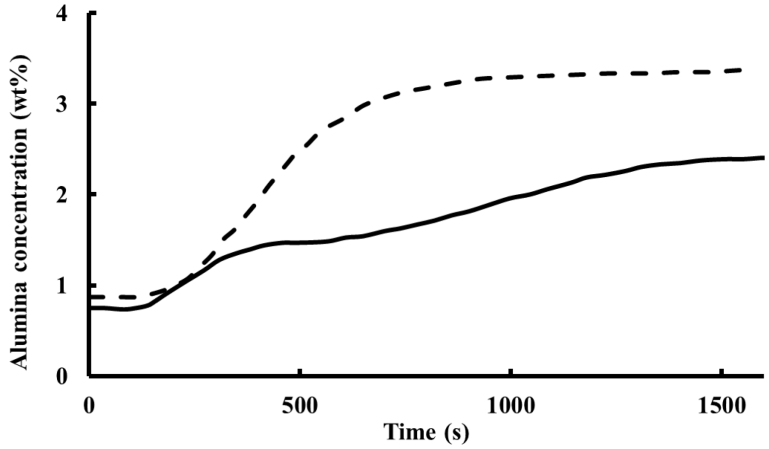


**Figure 2.7 Dissolution behavior of one-stage well dispersed (dashed line) and two-stage agglomerated alumina particles (solid line) [Jain et al., 1983b]. "Copyright 1983 by The Minerals, Metals & Materials Society. Used with permission."**

The agglomeration or fast dissolution of alumina particles are also influenced by the feeding height and area [Bagshaw *et coll.*, 1985]. Of course, the addition of alumina in a widely dispersed manner creates occasional rafts; nevertheless, alumina feeding to a confined area enhances the possibility of alumina particles' agglomeration. Moreover, as Figure 2.8 shows, the dissolution rate of alumina particles is quite dependent on impact-induced turbulence and increased penetration velocity of the particles into the bath [Bagshaw et al., 1985].

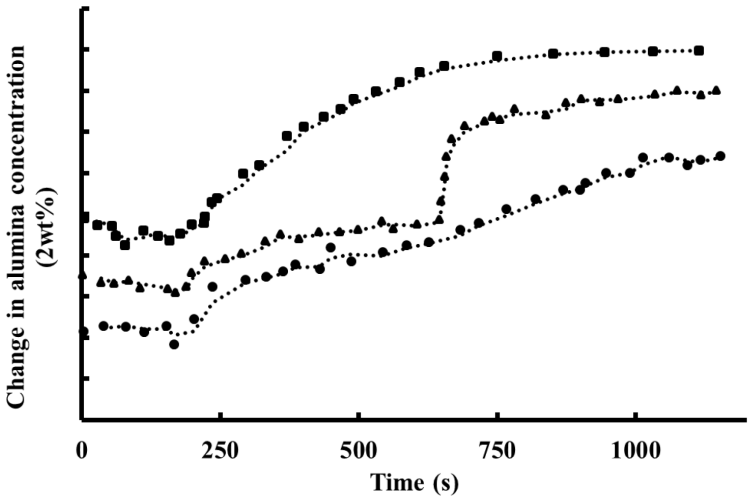


**Figure 2.8 Effect of dumping height (h) on the dissolution behavior of alumina; ● (h=2 cm), ■ (h=10 cm), ▲ (h=60 cm) [Bagshaw et al., 1985]. "Copyright 1985 by The Minerals, Metals & Materials Society. Used with permission."**

Recently Solheim (2014) has argued about the ideal case of feeding strategy which is continuous feeding (i.e. very high frequency + very low quantity). In an ideal continuous feeding, the

alumina concentration is constantly kept at low values avoiding any anode effect or sludge formation. Nevertheless, point feeders that are used nowadays are far away from completely dispersed feeding systems. Solheim (2014) has also reviewed several patents and articles concerning the continuous feeding of alumina as well as the problems that may arise by their implementation.

Considering the fact that nowadays most of the smelters in the world use point-feeding systems [Tabereaux, 2000], the frequency and batch size of the alumina is quite dependent on the number of feeders and their location [Walker *et coll.*, 2013]. On the other hand, the number of feeders and their location are determined based on proper dissolution and distribution of alumina, which means that the hydrodynamics of the bath is a crucial parameter [Kobbeltvedt et Moxnes, 2013]. It is well established that in order to enhance the alumina distribution in the bath, the best location for feeders is in the center channel near to the corner of anodes along the anodes' width and close to the inter-anode slots [Welch, 1990, Zhan *et coll.*, 2014]. Such feeding location, not only widens the effective mixing of the bath by bubble movements, but also approximately halves the number of required point feeders [Zhan et al., 2014].

The other parameter that may determine the batch size and frequency of alumina addition is based on demand-feed technology. This concept is based on the variation of bath resistivity between two extremes of underfeeding (i.e. anode effect) and overfeeding (i.e. sludge formation) [Robilliard et Rolofs, 2013, Welch, 2007, Kvande *et coll.*, 1994, Moxnes *et coll.*, 2009]. Consequently, one common approach is to add the alumina based on the bath resistance, keeping the alumina concentration around a mean value by having underfeeding and overfeeding periods. Flow adapted alumina feeding is yet another recently developed strategy and it tries to optimize the cell operation through keeping a uniform alumina content. In this method, the uniformity of alumina concentration in the cell is adjusted by controlling the local feeding rate of each feeder as a function of anodic current density. Such an approach leads to higher current efficiency, lower anode effect frequency and less sludge formation [Moxnes et al., 2009].

Another important factor for having a sludge free operation is related to the condition of feeding holes. Kobbeltvedt *et coll.* (1996) have argued about the plugging effect of feeding holes that leads to the excessive formation of agglomerates/sludge. It is mentioned that alumina may plug

feeding holes due to design features or bath splashing. Consequently, the next crust breaking action will push into the bath an amount of alumina higher than expected. As it can be seen in Figure 2.9, there is a vivid variation of temperature in case of plugged feeding holes compared to the almost equal temperature drop of the open feeding holes (i.e. easy to control). Besides, in case of plugged feeding holes, the alumina dissolution behavior shows a two-stage pattern in accord with extensive agglomeration of alumina particles. [Kobbeltvedt et al., 1996, Lavoie et al., 2016]

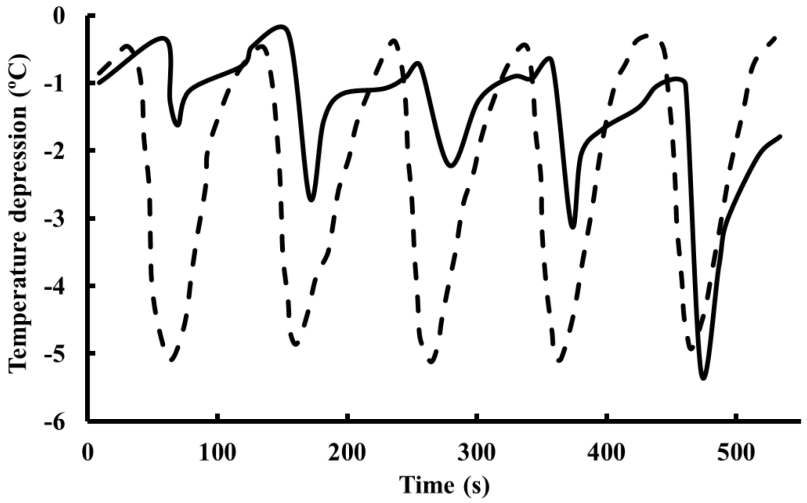


**Figure 2.9 Temperature drop when bath was fed with plugged holes (solid line) and open holes (dashed line) [Kobbeltvedt et al., 1996]. "Copyright 1996 by The Minerals, Metals & Materials Society. Used with permission."**

Considering the above-mentioned factors related to alumina feeding, it has to be emphasized that anode change can also introduce a considerable amount of top crust and anode cover materials (150-250 kg per anode) into the cell [Taylor et Welch, 2004]. Such crust feeding may create a domino of undesirable events such as reducing bath volume, dropping superheat, changing bath chemistry, altering cell's resistivity, and agitating magnetic forces [Grjotheim et al., 1989]. Besides, anode change may also contribute to the formation of cryolite-rich sludge if lumps of anode freeze (containing less $AlF_3$ and alumina compared to the main bath) fall on the bottom of the cell [Utigard, 1999b].

## 2.3.12Conclusion

Sludge formation in Hall-Héroult cells causes numerous operational problems leading to higher energy demand and lower current efficiency. As it is reviewed in this article, sludge formation

is quite a complex phenomenon, interlinked with several operational and fundamental parameters. Such parameters include the heat balance, feeding strategy, characteristics of alumina, type and geometry of the cathode, hydrodynamics, interfacial tension and bath chemistry. It is evident that with a proper superheat throughout the cell, not only the fed alumina is dissolved but also in case of sludge formation, the sludge may not find enough time to form resistive hard-to-dissolve bottom crust. However, proper dissolution and distribution of alumina in the cell is also quite dependent on the bath chemistry, hydrodynamics, feeding strategy and the characteristics of the fed alumina. It has been well established that the introduction of small batches of alumina in short intervals not only keeps the cell's heat balance in check but also provides more opportunities for fine tuning the bath chemistry and hydrodynamics. Anode gas release, magnetic movements and geometry of the cell are the key factors in hydrodynamics of the cell. In modern cells that are typically magnetically compensated, anode gas release has become the main source of agitation in the bath. Withal, recent developments in application of certain protrusions at the bottom of the cell or tilting the bottom of the cell have shown even more potential to reduce the metal pad movements. Nevertheless, the local turbulence of the bath, upon introduction of fresh alumina into the cell is another crucial factor in efficient dissolution and distribution of alumina throughout the anode cathode distance. Of course, it has to be emphasized that such local agitation induced by the alumina introduction into the cell is mainly governed by the physicochemical characteristics of the alumina. Moreover, the undeniable effect of interfacial phenomena in the Hall-Héroult process must not be forgotten since the main cathodic reaction leading to aluminum production occurs at an interface. Considering all the above-mentioned factors, sludge formation is quite common, whether it is related to alumina feeding, anode change, collapse of the top crust or change of bath chemistry. The important questions at the end of this review would be first to understand how all these factors interact with each other and enhance or alleviate the problem of sludge formation. The first question has been dealt with in different sections of this article but the second question is how to avoid sludge formation and enhance the operation of the cells in order to reduce the energy consumption and increase the current efficiency. The answer to this question is simply to keep all the parameters in check (i.e. keeping enough superheat, controlling the feeding, etc.). Such task has been following a one-hundred-year old path of improvement and fine-tuning because of interlinked nature of all the operational parameters. The most recent improvements

include the continuous monitoring of anodic current density, preheating the alumina and implementing the concept of continuous alumina feeding. These innovations seem to be able to eliminate or drastically reduce the sludge formation in the near future.

## 2.3.13 References


Abd El All, S., Gerlach, J. & Hennig, U. 1980. "Interactions between powdered alumina and fluoride melts with regard to the properties of the reaction products." Erzmetall, 33(10), pp. 504-509.

Allard, F., Coulombe, M.-A., Soucy, G. & Rivoaland, L. 2014a. "Cartography and chemical composition of the different deposits in the hall-heroult process." Light Metals, pp. 1233-1238.

Allard, F., Soucy, G. & Rivoaland, L. 2014b. "Formation of deposits on the cathode surface of aluminum electrolysis cells." Metallurgical and Materials Transactions B, 45(6), pp. 2475-2485.

Allard, F., Soucy, G., Rivoaland, L. & Désilets, M. 2015. "Thermodynamic and thermochemical investigation of the deposits formed on the cathode surface of aluminum electrolysis cells." Journal of Thermal Analysis and Calorimetry, 119(2), pp. 1303-1314.

Archer, A. M. 1983. "Considerations in the selection of alumina for smelter operation." Journal of Metals, 35(9), pp. 43-46.

Archer, A. M. 2013. Considerations in the selection of alumina for smelter operation. In: Bearne, G., Dupuis, M. & Tarcy, G. (eds.) Essential Readings in Light Metals. Hoboken, NJ, USA: John Wiley & Sons, Inc., pp. 569-573.

Bagshaw, A. N., Kuschel, G., Taylor, M. P., Tricklebank, S. B. & Welch, B. J. 1985. "Effect of operating conditions in the dissolution of primary and secondary (reacted) alumina powders in electrolytes." Light Metals, pp. 649-659.

Bagshaw, A. N. & Welch, B. J. 2013. The Influence of alumina properties on Its dissolution in smelting electrolyte. In: Donaldson, D. & Raahauge, B. E. (eds.) Essential Readings in Light Metals. Hoboken, NJ, USA: John Wiley & Sons, Inc., pp. 783-787.

Bray, E. L. 2018. Aluminum Statistics and Information [Online]. U.S. Geological Survey. Available: https://minerals.usgs.gov/minerals/pubs/commodity/aluminum/index.html#myb [Accessed 13-05-2018].

Bugnion, L. & Fischer, J. C. 2016. "Effect of carbon dust on the electrical resistivity of cryolite bath." Light Metals, pp. 587-591.

Coulombe, M.-A., Soucy, G., Rivoaland, L. & Davies, L. 2016. "Factors leading to the formation of a resistive thin film at the bottom of aluminum electrolysis cells." Metallurgical and Materials Transactions B., 47(2), pp. 1280-1295.

Dando, N., Wang, X., Sorensen, J. & Xu, W. 2010. "Impact of thermal pretreatment on alumina dissolution rate and HF evolution." Light Metals, pp. 541-546.

Davidson, P. A. & Lindsay, R. I. 1998. "Stability of interfacial waves in aluminium reduction cells." Journal of Fluid Mechanics, 362, pp. 273-295.

Fallah Fini, M., Soucy, G., Désilets, Martin, Pelletier, P., Lombard, D. & Rivoaland, L. 2017. Sludge formation in Hall-Héroult Process: an existing problem. Proceedings of ICSOBA Conference. Hamburg, Germany: ICSOBA, pp. 987-996.

Gasik, M. M. & Gasik, M. I. 2003. Smelting of aluminum. In: Totten, G. E. & MacKenzie, D. S. (eds.) Handbook of Aluminum. NY, USA: Marcel Dekker, pp. 47-79.

Geay, P.-Y., Welch, B. J. & Homsi, P. 2013. Sludge in operating aluminum smelting cells. In: Bearne, G., Dupuis, M. & Tarcy, G. (eds.) Essential Readings in Light Metals. Hoboken, NJ, USA: John Wiley & Sons, Inc., pp. 222-228.

Gerlach, J., Hennig, U. & Kern, K. 1975. "The dissolution of aluminum oxide in cryolite melts." Metallurgical and Materials Transactions B, 6(1), pp. 83-86.

Gerlach, J. & Winkhaus, G. 1985. "Interactions of alumina with cryolite-based melts." Light Metals, pp. 301-313.

Grjotheim, K., Krohn, C., Malinovský, K., Matiašovský, J. & Thonstad, J. 1982. Aluminium Electrolysis: Fundamentals of the Hall-Héroult Process, Düsseldorf, Germany: Aluminium-Verlag.

Grjotheim, K. & Kvande, H. (eds.) 1993. Introduction to Aluminium Electrolysis: Understanding the Hall-Héroult Process, Düsseldorf, Germany: Aluminium-Verlag GmbH.

Grjotheim, K. & Welch, B. J. 1989. "Technological developments for aluminum smeltinq as the industry enters the 21st century." JOM, 41(11), pp. 12-16.

Grjotheim, K., Welch, B. J. & Taylor, M. P. 1989. "Relating operating strategy and performance in aluminium smelting cells - an overview." Light Metals, pp. 255-260.

Habashi, F. 2003. Extractive metallurgy of aluminum. In: Totten, G. E. & MacKenzie, D. S. (eds.) Handbook of Aluminum. NY, USA: Marcel Dekker, pp. 1-45.

Haupin, W. 1997. "Understanding boundary layers." Light Metals, pp. 319-323.

Herstad, O., Krohn, C. H., Soerlie, M. & Øye, H. A. 1983a. "Precipitation of alumina and aluminum carbide during electrolysis of cryolite-alumina melts." Light Metals, pp. 347-356.

Herstad, O., Krohn, C. H., Soerlie, M. & Øye, H. A. 1983b. "Precipitation of solid components during electrolysis of cryolite-alumina melts." Aluminium, 59(3), pp. 200-206.

Hove, S. J. & Kvande, H. 1982. "Center-break alumina feeding and sludge control of prebaked cells." Light Metals, pp. 513-529.

Isaeva, L. A., Braslavskii, A. B. & Polyakov, P. V. 2009. "Effect of the content of the α-phase and granulometric composition on the dissolution rate of alumina in cryolite-alumina melts." Izvestiya VUZ. Tsvetnaya Metallurgiya, (6), pp. 35-40.

Jain, R. K., Taylor, M. P., Tricklebank, S. B. & Welch, B. J. 1983a. A study of the relationship between the properties of alumina. Its interaction with aluminium smelting electrolytes. Proceedings of the 1st International Symposium on Molten Salt Chemistry and Technology. Kyoto, Japan: Electrochemical Society of Japan, pp. 59-64.

Jain, R. K., Tricklebank, S. B., Welch, B. J. & Williams, D. J. 1983b. "Interaction of aluminas with aluminium smelting electrolytes." Light Metals, pp. 609-622.

James, B. J., Welch, B. J., Hyland, M. M., Metson, J. B. & Morrison, C. D. 1995. "Interfacial processes and the performance of cathode linings in aluminum smelters." JOM, 47(2), pp. 22-25.

Kachanovskaya, I. S. & Arakelyan, O. I. 1976. "Behavior of alumina in the deposits and crust of an aluminum electrolytic cell." Tsvetnye Metally, (4), pp. 37-40.

Kalgraf, K. & Torklep, K. 1998. "Sediment transport and dissolution in Hall-Heroult Cells." Light Metals, pp. 455-464.

Keller, R. 1984. "Alumina dissolution and sludge formation." Light Metals, pp. 513-518.

Keller, R. 2005. "Alumina dissolution and sludge formation revisited." Light Metals, pp. 147-150.

Keller, R., Burgman, J. W. & Sides, P. J. 1988. "Electrochemical reactions in the Hall-Heroult cathode." Light Metals, pp. 629-631.

Kheiri, M., Gerlach, J., Hennig, U. & Kammel, R. 1987. "Formation and behavior of crusts and bottom sludge in alumina reduction electrolysis." Erzmetall, 40(3), pp. 127-131.

Kobbeltvedt, O. 1997. Dissolution Kinetics for Alumina in Cryolite Melts. Distribution of Alumina in the Electrolyte of Industrial Aluminium Cells. PhD Thesis, Norwegian University of Science and Technology. Trondheim, Norway.

Kobbeltvedt, O. & Moxnes, B. P. 2013. On the bath flow, alumina distribution and anode gas release in aluminium cells. In: Bearne, G., Dupuis, M. & Tarcy, G. (eds.) Essential Readings in Light Metals. Hoboken, NJ, USA: John Wiley & Sons, Inc., pp. 257-264.

Kobbeltvedt, O., Rolseth, S. & Thonstad, J. 1996. "On the mechanisms of alumina dissolution with relevance to point feeding aluminium cells." Light Metals, pp. 421-427.

Kuschel, G. I. & Welch, B. J. 2013. Further studies of alumina dissolution under conditions similar to cell operation. In: Bearne, G., Dupuis, M. & Tarcy, G. (eds.) Essential Readings in Light Metals. Hoboken, NJ, USA: John Wiley & Sons, Inc., pp. 112-118.

Kvande, H., Chen, J. & Haupin, W. E. 1994. "Minimizing energy consumption through optimizing alumina concentration in the bath of Hall-Heroult Cells." Light Metals, pp. 429-440.

Landi, M. F., Bacchiega, R. & Battaglia, A. 1968. "Oriented recrystallization of alumina from cryolite baths for the production of aluminum by electrolysis of the separated ore." La Metallurgia Italiana, 60(11), pp. 939-44.

Landry, J.-R., Fallah Fini, M., Soucy, G., Désilets, M., Pelletier, P., Rivoaland, L. & Lombard, D. 2018. "Laboratory study of the impact of the cathode grade on the formation of deposits on the cathode surface in Hall-Héroult Cells." Light Metals, pp. 1229-1233.

Lavoie, P., Taylor, M. P. & Metson, J. B. 2016. "A review of alumina feeding and dissolution factors in aluminum reduction cells." Metallurgical and Materials Transactions B, 47(4), pp. 2690-2696.

Leitner, M., Leitner, T., Schmon, A., Aziz, K. & Pottlacher, G. 2017. "Thermophysical properties of liquid aluminum." Metallurgical and Materials Transactions A, 48(6), pp. 3036-3045.

Liao, X. & Øye, H. A. 2013. Carbon cathode corrosion by aluminium carbide formation in cryolitic melts. In: Tomsett, A. & Johnson, J. (eds.) Essential Readings in Light Metals. Hoboken, NJ, USA: John Wiley & Sons, Inc., pp. 992-998.

Liu, X. 1995. Thermochemistry of electrolyte, sludge/ridge, ledge and cell cover. Proceedings of the 5th Australasian Aluminum Smelter Technology Workshop. Queenstown, New Zealand: Royal Australian Chemical Institute and University of South Wales, pp. 619-627.

Meyer, A., Børset, O., Sommerseth, C., Osen, K., Rosenkilde, C. & Kristiansen, L. 2012. Examination of drop in bath acidity due to change-over of alumina qualities in the sunndal aluminium smelter, Norway. Proceedings of the 9th International Alumina Quality Workshop, Perth, Australia. Sidney, Australia: AQW Inc., pp. 316-321.

Moxnes, B., Solheim, A., Liane, M., Svinsås, E. & Halkjelsvik, A. 2009. "Improved cell operation by redistribution of the alumina feeding." Light Metals, pp. 461-466.

Moxnes, B. P., Aga, B. E. & Skaar, J. H. 1998. "How to obtain open feeder holes by installing anodes with tracks." Light Metals, pp. 247-255.

Ødegård, R., Roenning, S., Rolseth, S. & Thonstad, J. 1985. "Crust formation in aluminum cells." JOM, 37(11), pp. 25-28.

Ødegård, R., Roenning, S., Rolseth, S. & Thonstad, J. 2013a. On alumina phase transformation and crust formation in aluminum cells. In: Bearne, G., Dupuis, M. & Tarcy, G. (eds.) Essential Readings in Light Metals. Hoboken, NJ, USA: John Wiley & Sons, Inc., pp. 622-629.

Ødegård, R., Sterten, Å. & Thonstad, J. 2013b. On the solubility of aluminium carbide in cryolitic melts - influence on cell performance. In: Bearne, G., Dupuis, M. & Tarcy, G. (eds.) Essential Readings in Light Metals. Hoboken, NJ, USA: John Wiley and Sons Inc., pp. 25-32.

Pawlek, R. P. 2010. "Wettable cathodes: an update." Light Metals, pp. 377-382.

Rivoaland, L. 2016. Development of a new type of cathode for aluminium electrolysis. Proceedings of ICSOBA Conference. QC, Canada: ICSOBA-RioTinto-REGAL, pp. 9.

Robilliard, K. R. & Rolofs, B. 2013. A demand feed strategy for aluminium electrolysis cells. In: Bearne, G., Dupuis, M. & Tarcy, G. (eds.) Essential Readings in Light Metals. Hoboken, NJ, USA: John Wiley & Sons, Inc., pp. 747-751.

Rye, K. A., Rolseth, S., Thonstad, J. & Zhanling, K. 1990. Behaviour of alumina on addition to cryolitic baths. Proceedings of the 2nd International Alumina Quality Workshop. Perth, Australia: AQW Inc., pp. 24-37.

Schubert Severo, D. & Gusberti, V. 2017. Heat exchanger for alumina preheating in aluminium reduction cells. Proceedings of ICSOBA Conference. Hamburg, Germany: ICSOBA, pp. 1059-1069.

Sele, T. 1977. "Instabilities of the metal surface in electrolytic alumina reduction cells." Metallurgical Transactions B, 8(4), pp. 613-618.

Singh, R., Das, K., Mishra, A. K. & Kalo, N. 2017. "An approach for estimation of cathode voltage drop in an aluminum reduction cell with an inclined carbon block and a copper Insert." Transactions of the Indian Institute of Metals, 70(7), pp. 1795-1804.

Sleppy, W. C. & Cochran, C. N. 2013. Bench scale electrolysis of alumina in sodium fluoride–aluminum fluoride melts below 900°C. In: Bearne, G., Dupuis, M. & Tarcy, G. (eds.) Essential Readings in Light Metals. Hoboken, NJ, USA: John Wiley & Sons, Inc., pp. 1089-1094.

Solheim, A. 2002. "Crystallization of cryolite and alumina at the metal-bath interface in aluminium reduction cells." Light Metals, pp. 225-230.

Solheim, A. 2014. "A novel design criterion for alumina feeders in aluminium electrolysis cells." Light Metals, pp. 709-716.

Solheim, A. 2018. "Inert anodes—the blind alley to environmental friendliness?" Light Metals, pp. 1253-1260.

Song, Y., Peng, J., Di, Y., Wang, Y. & Feng, N. 2017a. "Metal flow performance in aluminium electrolytic cells with different side-wall types." Canadian Metallurgical Quarterly, pp. 1-9.

Song, Y., Peng, J., Di, Y., Wang, Y. & Feng, N. 2017b. "Performance of the cathodes with trapezoidal protrusions in aluminum electrolysis cells." JOM, 69(12), pp. 2844-2850.

Song, Y., Peng, J., Di, Y., Wang, Y., Li, B. & Feng, N. 2016. "The impact of cathode material and shape on current density in an aluminum electrolysis cell." JOM, 68(2), pp. 593-599.

Sørlie, M. & Øye, H. A. 2010. Cathodes in Aluminium Electrolysis, Düsseldorf, Germany: Aluminium Verlag GmbH.

Stam, M. A., Taylor, M. P., Chen, J. J. J., Mulder, A. & Rodrigo, R. 2008. "Common behaviour and abnormalities in aluminium reduction cells." Light metals, pp. 309-314.

Tabereaux, A. 2000. "Prebake cell technology: a global review." JOM, 52(2), pp. 23-29.

Tabereaux, A. T. & Peterson, R. D. 2014. Aluminum production. In: Seetharaman, S. (ed.) Treatise on Process Metallurgy. Boston, MA, USA: Elsevier, pp. 839-917.

Tarapore, E. D. 2013. The effect of some operating variables on flow in aluminum reduction cells. In: Bearne, G., Dupuis, M. & Tarcy, G. (eds.) Essential Readings in Light Metals. Hoboken, NJ, USA: John Wiley & Sons, Inc., pp. 322-329.

Tarcy, G. P., Kvande, H. & Tabereaux, A. 2011. "Advancing the industrial aluminum process: 20th century breakthrough inventions and developments." JOM, 63(8), pp. 101-108.

Taylor, M. P. 1997. Challenges in optimizing and controlling the electrolyte in aluminum smelters. Proceedings of the International Conference on Molten Slags, Fluxes and Salts. Warrendale, PA, USA: Iron and Steel Society of AIME, pp. 659-674.

Taylor, M. P., Liu, X., Fraser, K. & Welch, B. J. 1990. "Dynamics and performance of reduction cell electrolytes." Light Metals, pp. 259-266.

Taylor, M. P. & Welch, B. J. 2004. "The future outlook and challenges for smelting aluminium." Aluminium International Today, 16(2), pp. 20-24.

Thonstad, J. 1977. "Semicontinuous determination of the concentration of alumina in the electrolyte of aluminum cells." Metallurgical Transactions B, 8(1), pp. 125-130.

Thonstad, J., Fellner, P., Haarberg, G. M., Híveš, J., Kvande, H. & Sterten, Å. 2001. Aluminium Electrolysis: Fundamentals of the Hall-Héroult Process, Düsseldorf, Germany: Aluminium-Verlag.

Thonstad, J., Johansen, P. & Kristensen, E. W. 1980. "Some properties of alumina sludge." Light Metals, pp. 227-239.

Thonstad, J., Nordmo, F. & Paulsen, J. B. 1972. "Dissolution of alumina in molten cryolite." Metallurgical Transactions, 3(2), pp. 407-412.

Thonstad, J., Roenning, S. & Entner, P. 1982. "Formation of bottom crusts in aluminum pots. a laboratory study." Light Metals, pp. 485-497.

Thonstad, J., Solheim, A., Rolseth, S. & Skar, O. 2013. The dissolution of alumina in cryolite melts. In: Bearne, G., Dupuis, M. & Tarcy, G. (eds.) Essential Readings in Light Metals. Hoboken, NJ, USA: John Wiley & Sons, Inc., pp. 105-111.

Torklep, K., Kalgraf, K. & Nordbo, T. 1997. "Alumina distribution in point-fed Hall-Heroult Cells." Light Metals, pp. 377-386.

Utigard, T. 1987. "Mass transfer in Hall-Heroult Electrolysis induced by interfacial tension gradients." Aluminium, 63(6), pp. 608-613.

Utigard, T., Rolsetht, S., Thonstad, J. & Toguri, J. M. 1989. Interfacial phenomena in aluminum electrolysis. In: Closset, B. (ed.) Production and Electrolysis of Light Metals. Oxford, UK: Pergamon, pp. 189-199.

Utigard, T. & Toguri, J. M. 1985. "Interfacial tension of aluminum in cryolite melts." Metallurgical Transactions B, 16(2), pp. 333-338.

Utigard, T. & Toguri, J. M. 1991. "Marangoni flow in the Hall-Heroult Cell." Light Metals, pp. 273-281.

Utigard, T. A. 1993. "An analysis of the effect of bath density variations on the behaviour of Hall-Heroult Cells." Canadian Metallurgical Quarterly, 32(4), pp. 327-333.

Utigard, T. A. 1999. "Why best pots operate between 955 and 970 °C." Light Metals, pp. 319-326.

Veneraki, I. E., Romanko, K. S., Urda, N. N. & Semenov, V. S. 1973. "Thermal conductivity of materials of aluminum electrolytic cells." Energetika i Elektrifikatsiya, (2), pp. 52-54.

Von Kaenel, R., Bugnion, L., Von Kaenel, L., Spinetti, G. & Pfeffer, M. 2017. The use of copper in cathodes of aluminium reduction cells. Proceedings of ICSOBA Conference. Hamburg, Germany: ICSOBA, pp. 879-889.

Walker, D. I., Utigard, T. A. & Taylor, M. P. 1995. "Alumina agglomerates in aluminum smelters." Light Metals, pp. 425-434.

Walker, M. L., Purdie, J. M., Wai-Poi, N. S., Welch, B. J. & Chen, J. J. J. 2013. Design considerations for selecting the number of point feeders in modern reduction cells. In: Bearne, G., Dupuis, M. & Tarcy, G. (eds.) Essential Readings in Light Metals. Hoboken, NJ, USA: John Wiley & Sons, Inc., pp. 752-759.

Wang, L., Tabereaux, A. T. & Richards, N. E. 1994. "Electrical conductivity of cryolitic melts containing aluminum carbide." Light metals, pp. 177-185.

Wang, Q., Li, B., He, Z. & Feng, N. 2014. "Simulation of magnetohydrodynamic multiphase flow phenomena and interface fluctuation in aluminum electrolytic cell with innovative cathode." Metallurgical and Materials Transactions B, 45(1), pp. 272-294.

Wang, X. 2009. "Alumina dissolution in aluminum smelting electrolyte." Light Metals, pp. 383-388.

Wang, Z., Skybakmoen, E. & Grande, T. 2009. "Spent Si3N4 bonded SiC sidelining materials in aluminium electrolysis cells." Light Metals, pp. 353-358.

Welch, B. J. 1990. The role cell design and cell operating conditions can play in reducing problems from alumina. Proceedings of the 2nd International Alumina Quality Workshop. Perth, Australia: AQW Inc., pp. 15-22.

Welch, B. J. 1995. Sludge/muck in smelting cells. Proceedings of the 5th Australasian Aluminum Smelter Technology Workshop. Sidney, Australia: Royal Australian Chemical Institute and University of South Wales, pp. 651–659.

Welch, B. J. 2007. Gaining that extra 2 percent current efficiency. In: Peterson, W. S. & Miller, R. E. (eds.) Hall-Héroult Centennial. Hoboken, NJ, USA: John Wiley & Sons, Inc., pp. 120-129.

Welch, B. J. & Grjotheim, K. 1988. Alumina's and cell feeding technologies. Proceedings of the 1st International Alumina Quality Workshop. Gladstone, Australia: AQW Inc., pp. 75-86.

Welch, B. J. & Kinery, J. T. 2000. "Advancing the hall heroult electrolytic process." Light Metals, pp. 17-25.

Welch, B. J. & Kuschel, G. I. 2007. "Crust and alumina powder dissolution in aluminum smelting electrolytes." JOM, 59(5), pp. 50-54.

World-Aluminium. 2017. Primary aluminium smelting energy intensity [Online]. The International Aluminium Institute. Available: http://www.world-aluminium.org/statistics/primary-aluminium-smelting-energy-intensity/#data [Accessed 18.04.2017].

Yang, Y., Gao, B., Wang, Z., Shi, Z. & Hu, X. 2015. "Study on the dissolution of alumina in cryolite electrolyte using the see-through cell." Light Metals, pp. 583-588.

Zhan, S., Li, M., Zhou, J., Yang, J. & Zhou, Y. 2014. "CFD simulation of dissolution process of alumina in an aluminum reduction cell with two-particle phase population balance model." Applied Thermal Engineering, 73(1), pp. 805-818.

# CHAPITRE 3 MÉTHODOLOGIE

## 3.1 Montage expérimental

Ce projet de recherche est de nature expérimentale. L'étude de la formation des dépôts au fond des cellules d'électrolyse d'aluminium est faite sur des cellules faites de matériaux cathodiques de taille expérimentale provenant de l'industrie. Les expériences sont effectuées à l'Université de Sherbrooke dans le laboratoire d'électrolyse de l'aluminium contenant des fours à haute température conçus pour de telles expériences. Le four utilisé dans le cadre de cette étude fut utilisé par les étudiants précédents et permet de reproduire certaines conditions industrielles en laboratoire. Le banc d'essai utilisé est illustré dans la Figure 3.1.


**Figure 3.1 Banc d'essai pour expériences d'électrolyse à haute température**

Le montage est relié à un ordinateur avec interface LabVIEW© pour le contrôle du système et l'acquisition des données. La cellule expérimentale est déposée sur une plaque de carbure de silicium au fond d'un porte-creuset en Inconel© scellé durant l'expérience. Le fond du porte-creuset est couvert d'alumine calcinée qui servirait à absorber toute fuite de bain au besoin. Le couvercle du porte-creuset contient des cheminées permettant l'alignement et le branchement des tiges de contact électrique et l'insertion des thermocouples tout en restant étanche. Les cellules sont assemblées au préalable et placées au centre du porte-creuset, tel que schématisé à la Figure 3.2.

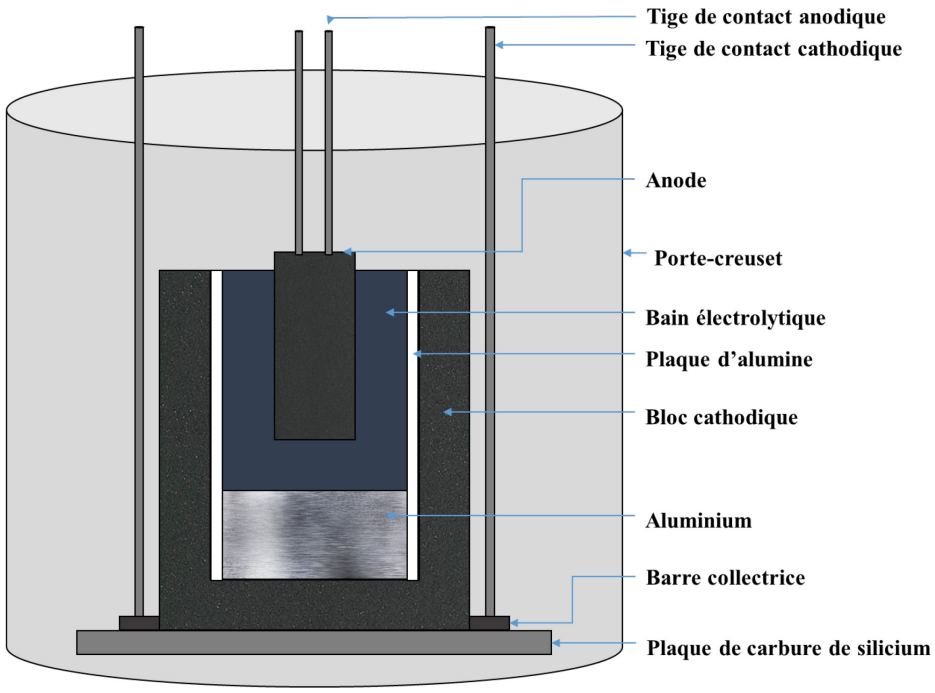


**Figure 3.2 Schéma du montage expérimental (vue de côté)**

Un tube d'alimentation continue en azote est aussi connecté à une cheminée afin d'assurer une atmosphère inerte durant les expériences. La température est mesurée dans le bain, dans la paroi du bloc cathodique et dans le porte-creuset, tel qu'illustré sur la Figure 3.3.

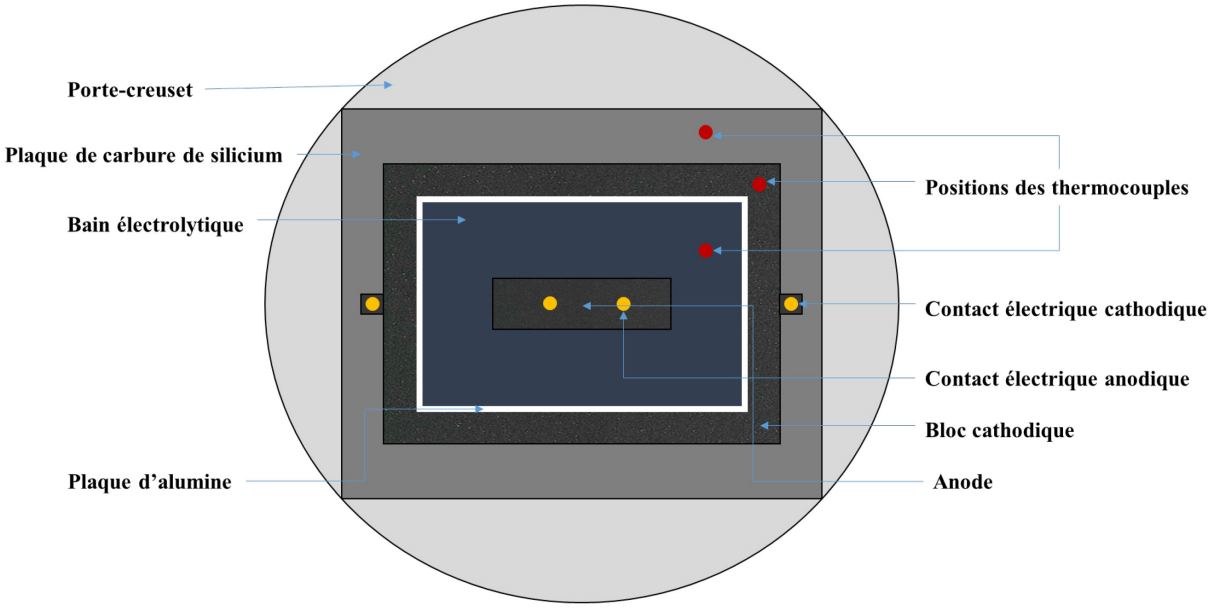


**Figure 3.3 Schéma du montage expérimental (vue de haut)**

Les quatre parois verticales de l'intérieur du bloc cathodique sont recouvertes de plaques d'alumine afin d'isoler électriquement les murs. Lors de l'assemblage de la cellule, un bloc

d'approximativement 500 g d'aluminium est déposé au fond de la cellule. D'après les expériences passées sur ce banc d'essai, l'introduction d'une nappe d'aluminium avant l'électrolyse empêche le bloc cathodique de fendre durant l'expérience. Le bain électrolytique, fourni par Rio Tinto, est ensuite entassé par-dessus la nappe d'aluminium en même temps que l'anode est centrée dans la cellule. Les dimensions des toutes les composantes du système sont illustrées dans la Figure 3.4.

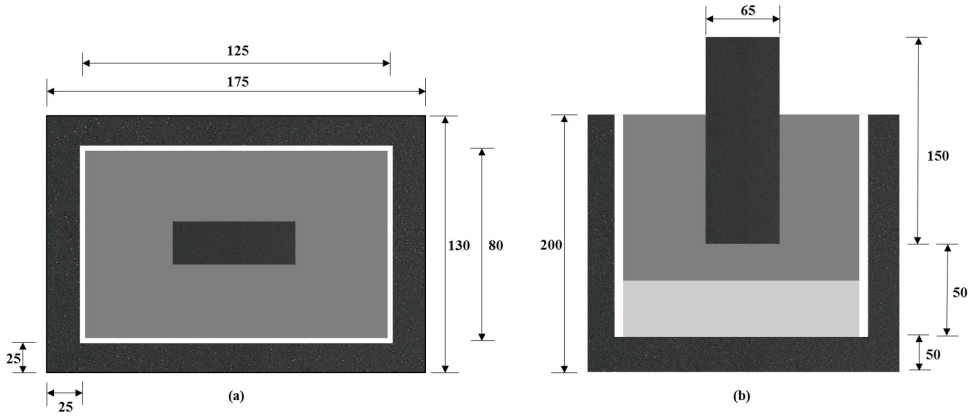


**Figure 3.4 Dimensions des composantes des cellules expérimentales (mesures en millimètres)**

Avant l'expérience, le couvercle du porte-creuset est recouvert de laine d'alumine afin de minimiser les pertes de chaleur. Lors des expériences, les thermocouples sont recouverts d'une gaine en alumine afin d'éviter qu'ils n'entrent en contact avec le bain corrosif. Cependant, il a été observé que la gaine de thermocouple se faisait dissoudre dans le bain au fil du temps. Pour cette raison la gaine d'alumine du thermocouple du bain fut changée à une gaine de carbure de silicium. De plus, il fut observé que les plaques d'alumine étaient aussi partiellement dissoutes lors de l'électrolyse. Ce phénomène est discuté dans le chapitre 5.

## 3.2 Conditions expérimentales

L'objectif principal de cette étude est de déterminer l'impact de la nuance de bloc cathodique sur la formation de dépôts à l'interface bloc cathodique-aluminium. Il est donc important d'assurer que toute autre condition expérimentale ne soit pas variée afin de bien faire refléter l'influence des différentes propriétés physico-chimiques des nuances de bloc à l'étude. Ainsi, le seul paramètre varié dans cette étude est la nuance de bloc cathodique. Les conditions expérimentales utilisées pour cette étude sont présentées dans le Tableau 3.1.

Tableau 3.1 : Conditions expérimentales

| | |
|---|---|
| Température d'électrolyse (°C) | 960 |
| Intensité (A) | 73 |
| Densité de courant cathodique ($A/cm^2$) | 0.9 |
| Ratio de cryolite initial du bain (CR) | 2.2 |
| Teneur initiale en alumine du bain (wt. %) | 10 |
| Teneur initiale en $CaF_2$ du bain (wt. %) | 5 |
| Durée d'électrolyse (h) | 8 |
| Atmosphère dans le porte-creuset | $N_2$ |

Cinq différentes nuances industrielles de blocs cathodiques sont étudiées dans ce projet. L'intérêt de ces nuances provient de leurs comportements divergents en termes d'embourbement, observé en industrie. Les propriétés physico-chimiques de ces nuances sont présentées dans la section traitant de la méthodologie dans les articles des chapitres 4 et 5. Toutes les cellules des cinq nuances étudiées ont les mêmes dimensions afin d'assurer la représentativité des résultats.

Les expériences d'électrolyse sont généralement faites sur trois jours. La première journée sert à la préparation du système. La cellule est d'abord assemblée : insertion des quatre plaques en alumine sur les murs et de la nappe de métal au fond du bloc cathodique en carbone, remplissage de la cellule avec le bain, positionnement de l'anode dans le centre et compactage du bain. La cellule est ensuite placée dans le four et le reste du montage est préparé. Le reste de la préparation du montage consiste en l'alignement de l'anode, la connexion des tiges de contact cathodiques et anodiques, l'emballage du système avec quatre couches de réfractaires en alumine et la connexion des prises pour l'azote. L'électrolyse est faite durant la deuxième journée. Cette journée inclut le temps de chauffage du four et l'électrolyse. Pour chaque expérience, le système met de 4 à 5 heures pour atteindre et se stabiliser à la température

d'opération (960 °C), il est donc judicieux de commencer le chauffage tôt en matinée. Tel qu'indiqué dans le Tableau 3.1, l'électrolyse est maintenue durant 8 heures. Lorsque le temps d'électrolyse est terminé, la consigne de la fournaise est ajustée à la température de la pièce et le système est refroidi. La durée du refroidissement est d'environ 30 heures, durant la nuit suivant l'électrolyse et la troisième journée. Lorsque la cellule a atteint la température de la pièce, elle est placée dans une chambre sous atmosphère d'argon. L'analyse post-mortem de la cellule est faite promptement dans les jours suivant l'expérience afin d'éviter la dégradation de la cellule avec le temps.

## 3.3 Autopsies et caractérisation

### 3.3.1 Autopsies

Les coupes des cellules sont effectuées avec des scies de calibre industriel au laboratoire de machinage à l'Université de Sherbrooke sous la supervision de Mr André Bilodeau et Serge Gagnon. Les cellules sont coupées directement avec une lame en diamant. Les positions des coupes sont indiquées à la Figure 3.5.

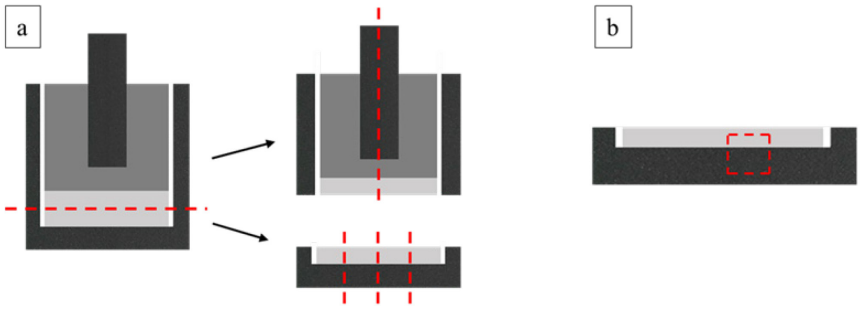


**Figure 3.5 Positions des coupes (pointillés rouges) au début des autopsies**

La cellule est d'abord coupée dans le milieu de la bille d'aluminium, tel qu'indiqué. La partie du bas de la cellule, contenant l'interface carbone-aluminium, est ensuite sectionnée en quatre tranches. La partie du haut de la cellule est séparée en deux. Les sections du bas contenant l'interface carbone-aluminium sont premièrement observées avec le microscope optique. Bien que la bille de métal se détache souvent de la cellule lors du sectionnement de la section du bas, il est préférable de tenter de minimiser le déplacement de l'aluminium afin de ne pas endommager les dépôts présents et de ne pas compromettre la qualité des photos de l'interface carbone-aluminium. Cependant, le détachement de la bille de métal est presque inévitable durant les coupes. Lorsque les observations au microscope sont faites, des échantillons de la surface du

bloc sont coupés pour les observations au microscope électronique, tel qu'illustré à la Figure 3.5b.

### 3.3.2 Microscopie optique

Le stéréomicroscope Leica© MZ FLIII fut utilisé pour faire les premières observations de l'interface carbone-aluminium et des photos avec la caméra numérique Leica© DC300. Le microscope permet un grossissement allant de 8x à 100x avec une résolution maximale de 3,15 mégapixels. Les photos numériques prises avec cet appareil sont mises en panorama afin d'obtenir une vue complète de l'interface carbone-aluminium. Il est ainsi possible de mesurer les dépôts de pied de talus, de boues et aussi vérifier pour des marques d'érosion à la surface du bloc.

### 3.3.3 Diffraction des rayons X

Des échantillons de bain sont prélevés à différentes positions et à différentes hauteurs dans la cellule afin d'analyser leur composition par diffraction des rayons X (DRX). La DRX est une technique non destructive servant à analyser la structure cristalline d'un matériau. Un faisceau de rayons X est envoyé sur l'échantillon à des angles spécifiques. Il en résulte un diffractogramme dont les pics sont la signature de la distribution des espèces à l'intérieur du réseau.

La prise d'échantillons pour DRX est faite avec un marteau et pic sous forte ventilation. Des échantillons sont prélevés ainsi dans le lit du bain (*bulk*) tout comme dans la partie du bas (boues, pieds de talus) et ensuite concassés dans un broyeur. Les échantillons sont compactés et placés dans un porte-échantillons rotatif à 1 $s^{-1}$. L'analyse DRX est effectuée avec un diffractomètre X'Pert PRO MPD et la mesure totale du calcium est effectuée avec un détecteur XRF POTFLUX CHANNEL. Un détecteur PIXcel$^{1D}$ muni d'un filtre de nickel est utilisé pour collecter les données de diffraction. Pour diriger le faisceau vers l'échantillon et ensuite vers le détecteur, les éléments suivants ont été placés : une fente divergente de 1/4°, une fente convergente de 1/2°, un masque de 20 mm et une fente d'antidispersion de 7,5 mm. Le voltage et l'intensité du générateur sont respectivement 40 kV et 40 mA.

La quantification Rietveld a été utilisée afin de quantifier les phases cristallines présentes dans les échantillons analysés par DRX. Cette méthode similaire à celle de Feret (2008) permet

l'identification des phases : $Na_3AlF_6$, $Na_5Al_3F_{14}$, $NaAlF_4$, $Na_2Ca_3Al_2F_{14}$, $NaCaAlF_6$, $Na_4Ca_4Al_7F_{33}$, $CaF_2$, NaF, $AlF_3$, α-$Al_2O_3$, γ-$Al_2O_3$, δ-$Al_2O_3$, θ-$Al_2O_3$, $NaAl_{11}O_{17}$ (β-$Al_2O_3$), $Al_4C_3$, Al et C. L'identification de ces phases sert principalement à déterminer l'acidité du mélange cryolitique des échantillons, dont l'indicateur est le ratio de cryolite (CR), calculé selon l'équation 3.1.

$$\frac{(0.60w_{Na_3AlF_6}) + (0.33w_{NaAlF_4}) + (0.45w_{Na_5Al_3F_{14}}) + (0.20w_{NaCaAlF_{6-a}}) + (0.20w_{NaCaAlF_{6-b}}) + (0.17w_{NaCa_{1.5}AlF_7}) + (0.15w_{Na_4Ca_4Al_7F_{33}}) + (w_{NaF})}{(0.40w_{Na_3AlF_6}) + (0.66w_{NaAlF_4}) + (0.54w_{Na_5Al_3F_{14}}) + (0.41w_{NaCaAlF_{6-a}}) + (0.41w_{NaCaAlF_{6-b}}) + (0.34w_{NaCa_{1.5}AlF_7}) + (0.55w_{Na_4Ca_4Al_7F_{33}}) + (w_{AlF_3})} \quad (3.1)$$

### 3.3.4 Microscopie électronique à balayage et spectroscopie par dispersion d'énergie

La cartographie élémentaire est faite à des sites d'intérêt de l'interface carbone-aluminium par microscopie électronique à balayage (MEB). La MEB (*Scanning Electron Microscopy*) est une technique de caractérisation donnant des images à haute résolution à la surface des échantillons. Avec un détecteur auxiliaire EDS (*Energy Dispersive X-ray Spectroscopy*), cette technique permet l'obtention d'une identification élémentaire, résultant en une cartographie élémentaire de l'image obtenue. Le microscope Hitachi© modèle S-4700 et le module EDS Oxford Instruments modèle X-Max 50 $mm^2$ ont été utilisés dans ce projet. L'échantillon est mis sous vide puis la tension d'accélération et l'intensité du rayon sont respectivement 20 kV et 10 µA. Les éléments cartographiés sont principalement C, Al, Na, F, O et Ca. Certains types de dépôts, tels que les carbures d'aluminium, peuvent être oxydés par l'air ambiant au fil du temps, il est donc nécessaire de préserver les échantillons fraichement coupés sous atmosphère inerte et d'en faire l'analyse au MEB-EDS promptement après électrolyse. Ceux-ci sont entreposés dans une boîte à gants sous atmosphère d'argon. Lors des observations MEB, le long de l'interface carbone-aluminium de chaque échantillon est scruté et des photos sont prises dans des régions semblant présenter un certain intérêt (couche de bain, érosion, etc.). Les images prises sont ensuite traitées avec le logiciel INCA afin de différencier les diverses phases présentes à l'aide d'un code de couleur. De cette manière, il est possible de rendre visibles des dépôts de bain ou de carbures d'aluminium.

## 3.4 Conclusion de la méthodologie

La génération de dépôts de boues est effectuée avec un montage expérimental d'électrolyse d'aluminium utilisant des nuances de blocs cathodiques provenant de l'industrie. Après l'électrolyse, les cellules expérimentales sont découpées et plusieurs méthodes d'analyse sont utilisées pour retirer l'information nécessaire à l'interprétation des mécanismes de formation des boues. Les techniques de caractérisation utilisées permettent des observations détaillées de chaque section des blocs cathodiques et aussi la détermination de la composition cristalline des échantillons d'intérêt. Ces techniques permettent ainsi de récupérer une multitude d'indices aidant l'interprétation des mécanismes de formation des boues et de déterminer en quoi les nuances de cathode interviennent lors de ces phénomènes.

# CHAPITRE 4 ÉTUDE EN LABORATOIRE DE L'IMPACT DE LA NUANCE DE CATHODE SUR LA FORMATION DE DÉPÔTS À LA SURFACE DE LA CATHODE DES CELLULES HALL-HÉROULT

## 4.1 Avant-propos

**Auteurs et affiliations:**

**Jean-René Landry** : Département de génie chimique et biotechnologique, Université de Sherbrooke, Québec, Canada.

**Mojtaba Fallah Fini** : Département de génie chimique et biotechnologique, Université de Sherbrooke, Québec, Canada.

**Gervais Soucy** : Département de génie chimique et biotechnologique, Université de Sherbrooke, Québec, Canada.

**Martin Désilets** : Département de génie chimique et biotechnologique, Université de Sherbrooke, Québec, Canada.

**Patrick Pelletier** : Rio Tinto, Centre de Recherche et Développement Arvida, Saguenay, Québec, Canada.

**Loig Rivoaland** : Carbone Savoie, Vénissieux, France.

**Didier Lombard** : Rio Tinto, St-Jean-de-Maurienne, France.

**Date de l'acceptation :** 2 février 2018.

**Journal :** The Minerals, Metals and Material Society, Light Metals division.

**Référence de l'article :**

Landry, J.-R., Fallah Fini, M., Soucy, G., Désilets, M., Pelletier, P., Rivoaland, L., Lombard, D. (2018). Laboratory study of the impact of the cathode grade on the formation of deposits on the cathode surface in Hall-Héroult cells. *Light Metals*, p. 1229-1233.

**Contribution du document au mémoire :**

Ce document présente les résultats des premiers tests de ce projet de recherche dans le cadre de conférence annuelle TMS (2018). Les dépôts de boues, de talus, de pieds de talus et de bain sont analysés en plus de la couche de carbures d'aluminium typiquement présente à la surface du bloc cathodique. L'accent est mis sur les mesures effectuées au microscopes optique et électronique des dépôts de boues et de carbures d'aluminium. Ma contribution est d'avoir effectué les expériences d'électrolyse en laboratoire, leur caractérisation, l'interprétation des données et la rédaction de l'article.

## 4.2 Titre et résumé français

**Titre :**

Étude en laboratoire de l'impact de la nuance de cathode sur la formation de dépôts à la surface de la cathode des cellules Hall-Héroult

**Résumé :**

Cette étude expérimentale investigue l'effet de la nuance de bloc cathodique sur la formation de dépôts à l'interface carbone-aluminium des cellules Hall-Héroult. Cinq différentes nuances de cathodes industrielles sont testées sur un banc d'essai d'électrolyse d'aluminium avec les conditions d'opération suivantes : densité de courant de 0.9 A/cm$^2$, sous atmosphère d'azote à 960 °C durant 8 heures, teneur initiale en alumine du bain de 10 % (massique), ratio de cryolite initial du bain de 2,2, Teneur initiale en $CaF_2$ du bain de 5 % (massique). L'analyse post-mortem inclut la diffraction des rayons X sur les échantillons de pied de talus, de talus, de boue et de bain en plus de la microscopie électronique à balayage avec analyse dispersive en énergie et la microscopie optique de l'interface carbone-aluminium. Les premiers résultats suggèrent que l'épaisseur de la couche de carbures d'aluminium augmente avec la porosité du matériau

cathodique. Deuxièmement, la quantité de boue semble plus reliée à la nuance de cathode qu'à d'autres paramètres opératoires comme la température.

## 4.3 Étude en laboratoire de l'impact de la nuance de cathode sur la formation de dépôts à la surface de la cathode des cellules Hall-Héroult

### 4.3.1 Title

Laboratory study of the impact of the cathode grade on the formation of deposits on the cathode surface in Hall-Héroult cells

**Keywords :** cathode grade; carbon-aluminium interface; aluminium carbide; sludge; graphitized; impregnated graphite.

### 4.3.2 Abstract

This experimental study investigates the effect of the cathode grade on the formation of deposits at the carbon aluminium interface in Hall-Héroult electrolysis cells. Five different industrial cathode grades are tested in a bench scale aluminum electrolysis setup with the following operational parameters: cathodic current density of 0.9 A/cm$^2$, under a nitrogen atmosphere at 960 °C for 8 hours with initial bath composition of 9 % alumina, cryolite ratio of 2.18 and 5 % $CaF_2$. Post mortem analyses include X-Ray diffraction on the ledge toe, ledge, sludge and bath samples as well as scanning electron microscopy- energy dispersive spectroscopy and optical microscopy of the carbon aluminum interface. Early results suggest that the thickness of the aluminium carbide layer increases with the porosity of the carbon material. Secondly, the amount of sludge seems to be more related to the cathode grade than to the other operational parameters such as the temperature.

### 4.3.3 Introduction

The formation of deposits on the surface of the cathode in Hall-Héroult cells is a phenomenon that disturbs the electrical current paths and accelerates the cathode wear [Geay *et coll.*, 2001, Keller, 2005a]. Nowadays, for high amperage cells, industrials are leaning towards graphitized types of cathode blocks because of their higher thermal conductivity and low electrical

resistivity compared to semi-graphitic or graphitic types of cathode [Wang *et coll.*, 2016]. Although the physical properties have improved, the formation of deposits on the cathode surface is still an ongoing problem at the industrial level. Investigations on this problem often focus on the operating conditions of the cell and little on the equipment type such as cathode grade. Industrials have reported different behaviours among graphitized cathode types regarding deposit formation. This may be attributed to the differences in properties such as porosity, permeability or density. These differences may induce various behaviours in the electrolyte, thus potentially affecting the formation of deposits [Novak *et coll.*, 2012].

Distinct types of deposits at the carbon-aluminium interface have been identified:

The formation of a layer of aluminium carbide ($Al_4C_3$) infiltrated in the carbon block has been established [Coulombe *et coll.*, 2016b]. Moreover, it is stipulated that the combined formation and dissolution of this layer wears off the carbon surface of the block and that the use of graphitized blocks result in a higher wear of the cathodic carbon block [Tschöpe *et coll.*, 2013b]. Aluminum carbides are formed by the contact of the metal with the carbon interface (equation 4.1) or by the interaction of carbon with the intercalated bath components according to equations 4.2 and 4.3 [Zoukel *et coll.*, 2009].

$$Al_{(l)} + C_{(s)} \rightarrow Al_4C_{3\,(s,diss)} \tag{4.1}$$

$$8Al_2O_{3\,(s)} + 12Na_{(in\,C)} + 3C_{(s)} \rightarrow Al_4C_{3\,(s)} + 12NaAlO_{2\,(s)} \tag{4.2}$$

$$3C + 4AlF_{3\,(diss)} + 12e^- \rightarrow Al_4C_{3\,(s,diss)} + 12F^-_{(diss)} \tag{4.3}$$

$$Al_4C_{3\,(s)} + 5AlF_{3\,(diss)} + 9NaF_{(l)} \rightarrow 3Na_3Al_3CF_{8\,(diss)} \tag{4.4}$$

The subsequent dissolution of aluminium carbides is described by equation 4.4.

In addition, the presence of sludge in the center of aluminium reduction cells is often found under alumina point feeders. It is often said to be caused by the cover material falling during anode changes. It is also thought to be attributed to incomplete dissolution of alumina, leading to agglomerates, which may carry bath components through the metal pad down to the carbon interface [Keller, 2005a, Dassylva-Raymond *et coll.*, 2014]. Aluminum carbides may dissolve in the sludge found under the aluminium [James *et coll.*, 1995a].

Furthermore, the heat losses through sidewalls and bottom of cell may cause the side ledge to grow at the carbon-aluminium interface [Allard *et coll.*, 2014b]. The impact of all these phenomena is the enhanced erosion of the block at the tip of the frozen ledge and disturbed current paths with an increase in cathode voltage drop [Siew *et coll.*, 2005, Einarsrud *et coll.*, 2014].

The formation of these deposits are certainly affected by the cathode block properties. This experimental study will investigate the role of the cathode grade by making further links between specific properties of the block and the formation of deposits.

### 4.3.4 Methodology

Experimental setup

Aluminum electrolysis tests are done using five industrial cathode grades (A, B, C, D and E) provided by a specialized Hall-Héroult cathode producer. Grades A to D are graphitized block grades and E is impregnated graphite (block graphitized then impregnated with pitch and rebaked). The properties of these grades were given by the supplier and are listed in Table 4.1.

Table 4.1 : Cathode block properties at room temperature (*: horizontal; **: vertical)

| Properties | A | B | C | D | E |
|---|---|---|---|---|---|
| Thermal conductivity (W/m.K) | 125*<br>112** | 130*<br>115** | 145*<br>135** | 130*<br>105** | 130*<br>105** |
| Open porosity (%) | 18 | 14 | 15 | 20 | 14 |
| Air permeability (nPerm) | 8 | 7 | 3 | 6 | 5 |

The propensity to form sludge by grade generally seen in industry is D = E > A > B > C, D and E being the grades that equally form the most sludge. This study aims to evaluate the behavior of the experimental cells for comparison with the real life behavior reported.

Rectangular experimental blocks of the five grades have been machined for laboratory electrolysis tests. All dimensions of the cell components are shown in Figure 4.1.

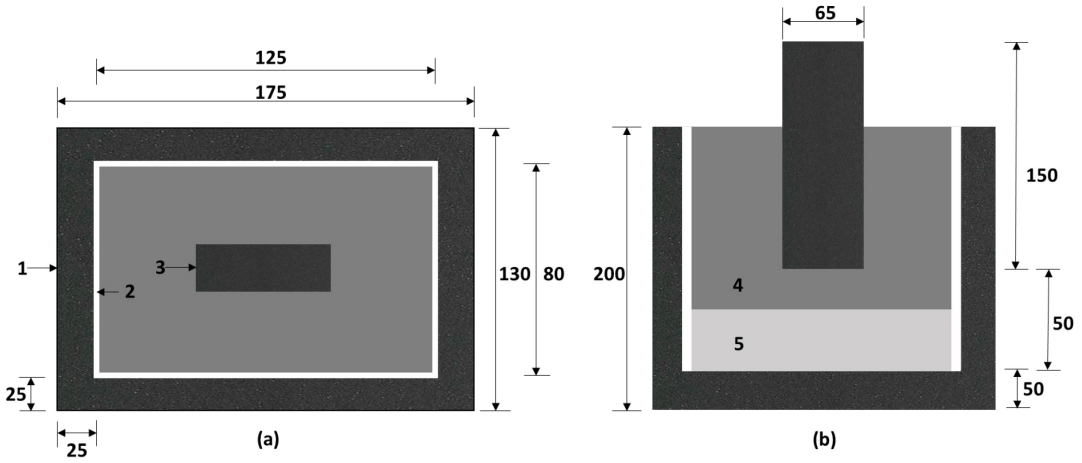


**Figure 4.1 Sizing of experimental Hall-Héroult cell for this study, top view (a) and side view (b). All dimensions are in millimeters (mm). 1: carbon crucible, 2: alumina plates, 3: anode, 4: bath, 5: aluminium**

The cell is filled with 1700 g of industrial bath initially containing 9 % (w/w) alumina with a cryolite ratio (CR) of 2.18. A block of approximately 500 g of aluminium is placed at the bottom of the cell prior to the electrolysis and 5 mm thick alumina plates cover all vertical walls of the carbon block to limit bath infiltrations. The cell is positioned inside a crucible made of Inconel placed inside an oven. The temperature is measured in three locations: inside the bath, in the carbon sidewall and outside the cell.

The electrolysis tests are done at a bath temperature of 960 °C, a current density of 0.9 A/cm$^2$ for 8 h under a $N_2$ atmosphere. The current is set to 73 A and is kept constant. The temperature and voltage are measured continuously during electrolysis. In all cases, a sudden increase in temperature up to 970 °C is observed at the beginning of electrolysis, which may be attributed to Joule effect. The temperature reaches then 960 °C and is kept stable during electrolysis. The anode to cathode distance is set to 2 cm. In order to highlight the impact of the cathode grade, no feeding is used and all parameters are kept constant during the cell operation for all cathode grades.

Autopsies and characterization

At the end of the electrolysis time, the electricity is cut off and the furnace is set to room temperature for cooling. In order to observe the deposits at the carbon-aluminium interface, the cooled cell is cut using a diamond blade saw. Cuts are made in the center of the cell and in periphery. Each section of the carbon-aluminium interface is observed with a stereomicroscope.

Pictures are taken to recreate panoramic views of the interface. For composition, harvested samples are powdered using a ball mill then put in the rotating sample holder of the X-Ray diffraction (XRD). The chemical composition is provided by the Rietveld analysis of the sample. Scanning electron microscopy-energy dispersive spectroscopy (SEM-EDS) was used for surface analysis and elemental cartography. This method of analysis allows observation and easy measurements of the aluminium carbide layer in the carbon block.

### 4.3.5 Results

Aluminium carbide observation

Scanning electron microscopy was used to observe the carbon-aluminium interface. For each site of interest, the elemental cartography included mapping of carbon, aluminium, oxygen, fluoride, calcium and sodium. Figure 4.2 shows the observable carbide layer.

A noticeable distinct red layer containing atoms of aluminium was visible at the interface for every sample taken. The values of the measured thickness of the carbide layer for each cathode grade are summarized in

Table 4.2. The following data were obtained by averaging all direct measurements of the layer. The samples were taken under the sludge, under the ledge toe and in the “cleaner” areas in between (direct contact of aluminium and carbon).

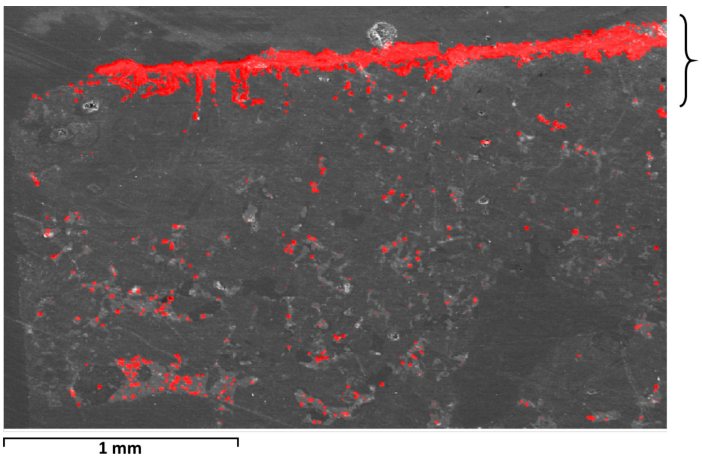


**Figure 4.2 Scanning electron microscopy of the carbon-aluminium interface of experimental cell E (impregnated graphite). The position of the aluminium carbide layer is shown by the bracket symbol**

Table 4.2 : Average aluminium carbide layer thickness (± 4 μm).
The average data for two tests of each grade is displayed

| Cathode type | Graphitized | | | | Impregnated graphite |
|---|---|---|---|---|---|
| Cathode grade | A | B | C | D | E |
| Carbide layer thickness (μm) | 54 \| 55 | 65 \| 66 | 41 \| 48 | 89 \| 96 | 65 \| 72 |

The impregnated graphite grade had the sharpest and most distinct layer of aluminium carbide. Other graphitized grades had a dispersed carbide layer.

Ledge and sludge observations

Microscopic observations revealed the presence of sludge accumulated near the center of the carbon-aluminium interface under the anode tip. Typical profiles of sludge are exhibited in Figure 4.3.

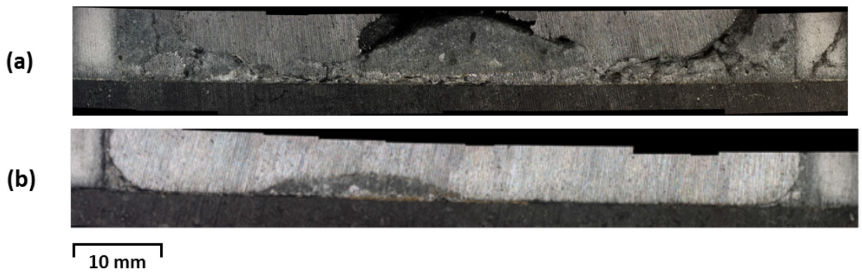


**Figure 4.3 Typical sludge profiles for graphitized grade A (a), impregnated graphite grade E (b)**

All grades displayed a central deposit of sludge. As indicated in Table 4.3, graphitized grade A had the thickest central sludge with a thick bath film covering the carbon-aluminium interface and thicker ledge. The experimental cell of grade A had the highest sludge propensity and the four other grades showed thinner layer than grade A. At this stage, it is difficult to conclude a sludge propensity trend between the other grades.

For each experiment, the central deposit was harvested along with a ledge toe sample from the same cell. The CR and alumina content of these samples are also summarized in Table 4.3.

Table 4.3 : CR, total alumina content and height of ledge toe and central sludge deposits from XRD analysis

| | Ledge toe | | Central sludge | | |
|---|---|---|---|---|---|
| Cathode grade | CR | Total $Al_2O_3$ (%) | CR | Total $Al_2O_3$ (%) | Height (± 0.5 mm) |
| A (graphitized) | 2.34 | 22.3 | 2.44 | 14.6 | 8.1 |
| B (graphitized) | 2.66 | 19.9 | 2.91 | 11.8 | 3.4 |
| C (graphitized) | 2.68 | 22.9 | 2.85 | 21.0 | 4.7 |
| D (graphitized) | 2.75 | 21.1 | 2.64 | 16.8 | 3.2 |
| E (imp. graphite) | 2.04 | 22.4 | 2.46 | 19.0 | 5.1 |

## 4.3.6 Discussion

Aluminum carbide layer – effect of porosity

The data for the thickness of the aluminium carbide layer has been plotted in Figure 4.4.

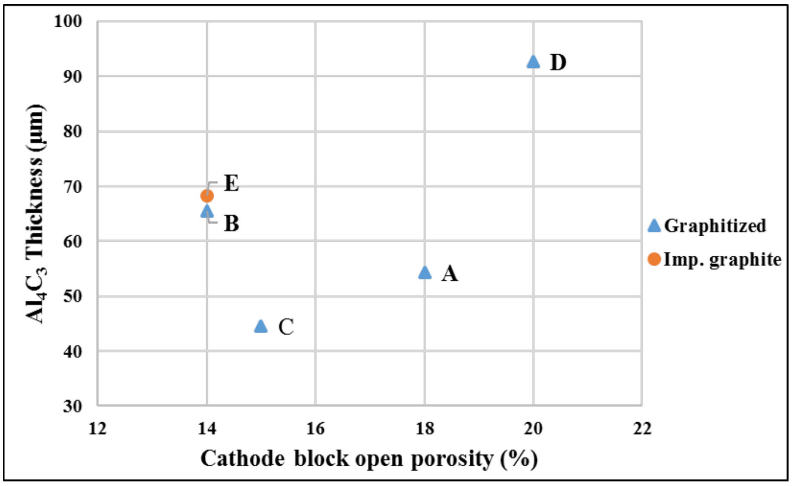


**Figure 4.4 Thickness of the aluminium carbide layer at the carbon-aluminium interface of the five experimental cells (triangles: graphitized blocks; circles: impregnated graphite)**

Measurements for graphitized cathode blocks A, C and D show a trend between the block's open porosity and the thickness of the aluminium carbide layer at the carbon-metal interface. The thicker layer of B may be explained by its permeability that is roughly 60 % higher than the one of grade C, thus allowing more bath species to infiltrate and further react according to equation 4.2. In this way, the thickness of the aluminum carbide layer may be affected by the combination of both open porosity and air permeability of the cathode block. This is shown with the case of grades B and E that have similar porosity, permeability and carbide thickness. The high amount of sludge in grade A may explain the thinner than expected carbide layer. This could be attributed to a combination of two phenomena. The high presence of sludge reduces carbides formed by equation 4.1. Moreover, sludge areas corresponding to lower current density lessens sodium intercalation and carbides formed by equation 4.2. The second phenomenon being aluminum carbide dissolution in sludge.

Central sludge

The presence of a central sludge deposit at the carbon-aluminium interface was not foreseeable since there was no direct feeding of alumina during all experiments. The absence of point feeding or anode change in this study insinuates that sludge may come from other phenomena.

Considering that the cell dimensions are too short for considerable MHD forces, only the generated gas at the anode tip will agitate the layer of bath and the metal pad. The detachment of metal from the main pad may lead to the access of some bath to the carbon-aluminium interface. A proof of this agitation was obtained by running a test during which the electrolysis was maintained during cooling until the entire system was solid. The agitated metal may also cause the tip of the ledge toe to be dragged towards the center of the carbon-aluminium interface (under the anode), contributing to the accumulation of sludge. In this experimental study, the sludge may well come from ledge by agitation since Table 4.3 shows that the composition of the sludge and ledge are close. Furthermore, for a grade with thick ledge such as A, there is a film of bath connecting the central sludge to the ledge toe visible on Figure 4.3a. The lower alumina content and CR of the central sludge in cell A may be explained by back feeding of alumina into the film and acidification through sodium loses [Whitfield *et coll.*, 2004].

Knowing that the side ledge and ledge toe are formed when their temperatures reaches a value below the liquidus of the bath, in that regard the thermal conductivity of the block may affect the extent of ledge toe elongation, thus the amount of sludge.

### 4.3.7 Conclusions

Aluminum carbide behavior

The higher porosity of graphite deepens the reacting zone of infiltrated bath components, thus enlarging the apparent thickness of the carbide layer. Furthermore, the permeability of the carbon block may enhance the effect of porosity. On the contrary, the presence of sludge at the carbon-aluminium interface reduces the thickness of the aluminium carbide layer by diminution of current density and dissolution of the carbides in the sludge. For graphitized grades, a thinner carbide layer can be obtained with blocks that have a low porosity, a low permeability and a high tendency to form sludge.

Sludge formation

This study has shown that sludge may form even without alumina point feeding or any manipulation with the anode.

The behavior of the five grades was not the same in experimental tests than in industrial cells regarding sludge propensity. The comparison between the laboratory tests with the industrial cell behavior of these grades regarding sludge formation is still under investigation. It may be achieved by further investigating the impact of other operating conditions such as feeding strategy or electrolysis time.

Analyses of sludge deposits suggest that the thermal conductivity of the carbon block may influence the amount of ledge, which can be transported along the carbon-aluminium interface by metal agitation.

### 4.3.8 References

Geay, P.-Y., B.J. Welch, and P. Homsi: Sludge in operating aluminum smelting cells, Light Metals 2001, 541-548.

Keller R.: Alumina dissolution and sludge formation revisited, Light Metals 2005, 147-150.

Wang, Z., et al. Cathode Wear in Electrowinning of Aluminum Investigated by a Laboratory Test Cell, Light Metals 2016, 897-902.

Novak, B., et al.: Fundamentals of aluminium carbide formation, Light Metals 2012, 1343-1348.

Coulombe, M.-A., et al. (2016), Factors Leading to the Formation of a Resistive Thin Film at the Bottom of Aluminum Electrolysis Cells, Metall. Mater. Trans. B, 1280-1295, doi: 10.1007/s11663-015-0567-8.

Tschöpe, K., et al.: Critical reflections on laboratory wear tests for ranking commercial cathode materials in aluminium cells, Light Metals 2013, 1251-1256.

Zoukel, A., P. Chartrand, and G. Soucy: Study of Aluminum Carbide Formation in Hall-Heroult Electrolytic Cells, Light Metals 2009, 1123-1128.

Dassylva-Raymond, V., et al.: Modeling the Behavior of Alumina Agglomerate in the Hall-Heroult Process, Light Metals 2014, 603-608.

James, B.J., et al. (1995): Interfacial Processes and the Performance of Cathode Linings in Aluminum Smelters, JOM, 22-25, doi: 10.1007/BF03221401.

Allard, F., G. Soucy, and L. Rivoaland (2014): Formation of Deposits on the Cathode Surface of Aluminium Electrolysis Cells, Metall. Mater. Trans. B, 2475-2485, doi: 10.1007/s11663-014-0118-8.

Siew, E.F., et al.: A study of the fundamentals of pothole formation, Light Metals 2005, 763-769.

Einarsrud, K.E., E. Skybakmoen, and A. Solheim: On the influence of MHD driven convection on cathode wear, Light Metals 2014, 485-490.

Whitfield, D., et al.: Aspects of alumina control in aluminium reduction cells, Light Metals 2004, 249-255.

# CHAPITRE 5 ÉTUDE EXPÉRIMENTALE DE LA NUANCE DE CATHODE SUR LA FORMATION DE BOUES DANS LES CELLULES HALL-HÉROULT

## 5.1 Avant-propos

**Auteurs et affiliations :**

**Jean-René Landry** : Département de génie chimique et biotechnologique, Université de Sherbrooke, Québec, Canada.

**Mojtaba Fallah Fini** : Département de génie chimique et biotechnologique, Université de Sherbrooke, Québec, Canada.

**Gervais Soucy** : Département de génie chimique et biotechnologique, Université de Sherbrooke, Québec, Canada.

**Martin Désilets** : Département de génie chimique et biotechnologique, Université de Sherbrooke, Québec, Canada.

**Patrick Pelletier** : Rio Tinto, Centre de Recherche et Développement Arvida, Saguenay, Québec, Canada.

**Loig Rivoaland** : Carbone Savoie, Vénissieux, France.

**Didier Lombard** : Rio Tinto, St-Jean-de-Maurienne, France.

**Date de soumission :** 18 juillet 2018

**État et date de l'acceptation :** accepté le 5 octobre 2018

**Journal :** Metallurgical and Materials Transactions B.

**Référence de l'article :** https://doi.org/10.1007/s11663-018-1435-0

**Contribution du document au mémoire :**

Ce document rassemble et traite principalement les dépôts de boue (*sludge*) et de pieds de talus observées durant la totalité des expériences de ce projet de recherche. L'accent est mis sur le rôle des propriétés de la nuance de cathode dans les mécanismes de formation de boue. Les principaux facteurs gouvernant la formation de boue, énoncés dans la revue de littérature, sont discutés et mis en relief avec les observations faites sur les cellules expérimentales. Une brève section est dédiée à l'érosion des blocs et fait un lien avec les mesures de carbures d'aluminium présentées dans l'article du chapitre précédant. Ma contribution est d'avoir effectué toutes les expériences en laboratoire, leur caractérisation, interprétation ainsi que la rédaction de l'article. Ce chapitre constitue le cœur de ce projet de recherche et de ma contribution originale à la recherche.

## 5.2 Titre et résumé français

**Titre :**

Étude expérimentale de l'impact de la nuance de cathode sur la formation de boues à l'interface carbone-aluminium des cellules Hall-Héroult

**Résumé :**

La présence de boue (sludge) électriquement résistives à la surface de la cathode dans les cellules Hall-Héroult augmente les coûts de production d'aluminium et réduit la durée de vie des cellules. Les cathodes de nuances graphitisées utilisées dans les cellules modernes ont un taux de détérioration plus élevé en vertu de la présence excessive de dépôts formés et des forts courants électriques utilisés. Cependant, les nuances de types graphitisées n'ont pas toutes la même tendance observable à former des boues et peu d'attention est typiquement portée sur l'impact de la nuance et des propriétés de cathode sur la formation des boues. Dans cette étude, cinq nuances de cathodes industrielles avec des propriétés variées sont testées sur un banc d'essai d'électrolyse d'aluminium avec les conditions suivantes : densité de courant de 0.9 A/cm$^2$, sous atmosphère d'azote à 960 °C durant 8 heures, teneur initiale en alumine du bain de 10 % (massique), ratio de cryolite initial du bain de 2,2, teneur initiale en $CaF_2$ du bain de 5 % (massique) et sans point d'alimentation d'alumine. La caractérisation post-mortem inclut l'analyse Rietveld des dépôts, les observations de l'interface carbone-aluminium aux

microscopes optique et électronique avec analyse dispersive en énergie. Un dépôt de boue distinct situé au centre des cellules a été généré malgré l'absence de point d'alimentation d'alumine. Le profil des boues était variable et semble être lié aux conductivités thermiques horizontale et verticale des blocs cathodiques. Cette étude a aidé à pousser plus loin la compréhension des mécanismes de formation des boues ainsi que le rôle de la nuance de cathode sur ces mécanismes.

## 5.3 Étude expérimentale de l'impact de la nuance de cathode sur la formation de boues dans les cellules Hall-Héroult

### 5.3.1 Title

Experimental investigation of the impact of cathode grade on sludge formation at the cathode block-aluminum interface of Hall-Héroult cells

**Keywords :** Cathode grade; sludge; carbon-aluminum interface.

### 5.3.2 Abstract

The presence of resistive sludge on the cathode surface in Hall-Héroult cells can increase the aluminum production costs and reduces cell lifetime. Modern cells with graphitized cathode blocks generally operate satisfactorily but some are exhibiting excessive deposit formation, thus lower performances. Little attention has ever been given to the role of the cathode grade and its properties on sludge formation. In this investigation, five graphitized industrial cathode grades with varying properties are tested on a bench scale aluminum electrolysis setup with cathodic current density of 0.9 A/cm$^2$, under a nitrogen atmosphere at 1233 K (960 °C) for 8 hours with initial bath composition of 10 % alumina, cryolite ratio of 2.2, 5 % $CaF_2$ and no point feeding. Postmortem characterization includes Rietveld refinement of deposits, optical microscopy and SEM-EDS observations of the carbon-aluminum interface. Sludge located near the center of the cathode surface was generated during the experiments despite the absence of point feeding. The sludge profile was variable among grades and could be related to the horizontal and vertical thermal conductivities of the blocks. This study has pushed further the understanding of the mechanisms of sludge formation and dissolution concerning the cathode grade properties.

### 5.3.3 Introduction

The problem concerning sludge

The main drawback of the Hall-Héroult process is its high electrical energy consumption. The formation and accumulation of electrically resistive sludge (aka *muck*) at the cathode block surface increase the electrical resistance of the cell, which boosts cathode voltage drop (CVD). The net effect is the higher energy requirement and thereby, higher aluminum production costs. Due to high electrical resistance of the sludge compared to the metal, the presence of sludge at the carbon-aluminum interface redirects the electrical current and creates high current density spots, prompting cathode block electrochemical wear [Liao et Oye, 1999]. Another consequence of the presence of sludge on the cathode surface is the generation of horizontal currents, which increase metal pad movement [Allard et al., 2014b]. The increased metal flow and resulting oscillation of the bath-metal interface greatly contribute to difficulty in reducing the ACD and increases aluminum solubility, prompting current efficiency losses [Grjotheim et Kvande, 1993a, Song *et coll.*, 2017b]. The control over the formation of sludge in Hall-Héroult cells is a key factor in avoiding high CVD, current efficiency losses and excessive cathode wear.

Description of deposits

During the regular operation of a typical alumina reduction cell, there is a variety of inevitable deposits that form within the process through time. Figure 5.1 displays the deposits that occur in modern point feeding cells.

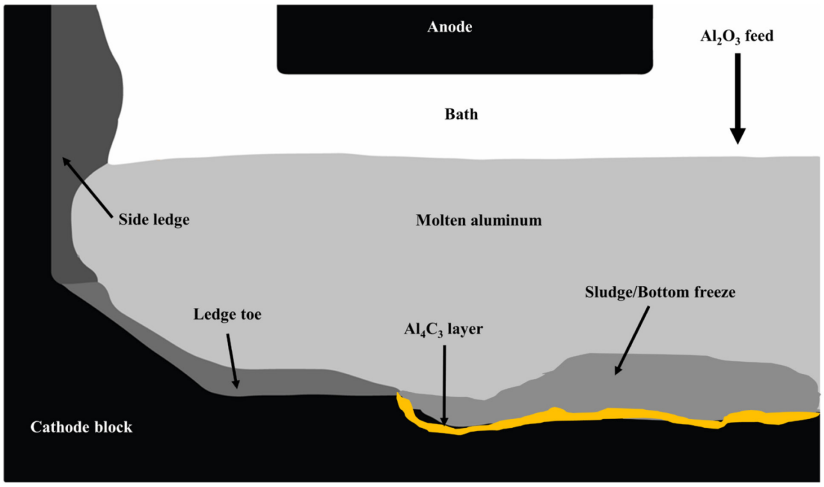


**Figure 5.1 Deposits at the carbon-metal interface of Hall-Héroult cells**

The protective side ledge is necessary in order to avoid molten metal and electrolyte attacks and infiltrations in the sidewall that cause premature cell failures [Sorlie et Oye, 2010]. Ideally, this frozen layer of bath should cover the entire surface of the side lining. The ledge toe is a horizontal elongation of the side ledge formed on the cathode surface. In alumina point feeding cells, sludge mainly originates from alumina incomplete dissolution, collapse of top crust, anode change or failure in the heat balance of the cell [Utigard et Toguri, 1991a]. A typical sludge is a mixture of undissolved solid alumina particles and saturated bath with density around 2400 kg/m$^3$, 20 - 50 % alumina, 2 – 10 % $AlF_3$ and 2 – 5 % $CaF_2$ [Grjotheim et Kvande, 1993a, Allard *et coll.*, 2014b]. Bottom crust is caused by the complete solidification of sludge when its temperature reaches below the eutectic point of the sludge [Geay et al., 2001]. According to Fallah Fini *et coll.* (2017b) the most important factors that influence the sludge formation or dissolution are cell's hydrodynamics, operational temperature, electrolyte chemistry, physicochemical properties of alumina and alumina feeding techniques. It has to be underlined that sludge formation and solidification can be effectively reduced by keeping an appropriate superheat in the bath with respect to the acidity and alumina concentration in the cell.

Sludge back feeding mechanisms

Once sludge is formed at the cathode surface, several mechanisms are stipulated to contribute to its back feeding into the bulk. The presence of a bath film between the carbon block and the metal was said to be related to sludge formation and dissolution [Li *et coll.*, 2015]. It was argued that sludge may be back fed through such a film wherein fluid flow is induced by interfacial tensions (IFT) differences [Utigard et Toguri, 1991a, Utigard, 1999a]. The bath film may also dissolve aluminum carbides formed at the carbon-aluminum interface, leading to net carbon losses of the block and cathode bottom wear [Liao et Oye, 1998, Novak et al., 2012, Zoukel et al., 2009]. A layer containing such aluminum carbides at the cathode block-aluminum interface was observed in both industrial and laboratory cells [Novak *et coll.*, 2018, Coulombe et al., 2016b]. However, hardly any laboratory study has explicitly shown signs of erosion visibly related to aluminum carbide formation and dissolution. Sludge may also be back fed into the bulk by the means of hydrodynamics. Accordingly, sludge could be dragged along the cathode surface by saltation caused by the moving metal and eventually be transported through the metal and dissolve in the bulk. [Kalgraf et Torklep, 1998b].

Cathode grades in modern Hall-Héroult cells

The cathode material is of great importance, as it has to endure several electrical, thermal and chemical phenomena during the lifetime of the cell. The optimal criteria for cathode lining material are as follows: chemical inertness, low permeability towards the environment, sufficient thermal and mechanical strength, ability to distribute current evenly, allow low CVD, controlled heat losses and lowest possible cost [Grjotheim et Kvande, 1993a]. Carbon in the allotropic form of graphite is the material that fulfills the most of the latter requirements. With desired increased productivity, graphitized types of cathode blocks are attractive because of their higher thermal conductivity and lower electrical resistivity [Wang et al., 2016] [Tschöpe *et coll.*, 2012]. However, graphitized cathode blocks in modern cells show higher wear rates because of increased amperage which has recently been correlated with high local current density and wear areas [Tschöpe *et coll.*, 2013a, Skvbakmoen *et coll.*, 2011, Dreyfus et Joncourt, 1999]. Cells with graphitized cathode blocks of high thermal conductivity are more prone to bottom freeze, which increases the CVD [Rivoaland, 2016b]. The thermal conductivity of the cathode block is also of major importance regarding the heat balance and the control of the thickness of the ledge and sludge formation. Controlled heat losses may also help to keep appropriate superheat, which disfavors sludge formation.

The impact of the cathode grade on sludge formation has not explicitly been investigated in literature. In fact, the industry has reported that distinctive cathode grades have shown variable propensities to form sludge. This experimental study will help to better understand the sludge formation phenomenon and to make further links between the graphitized cathode grade and the formation of deposits at the carbon-aluminum interface.

### 5.3.4 Methodology

Experimental setup

Laboratory aluminum electrolysis tests were conducted using five industrial cathode grades (A, B, C, D and E) provided by a Hall-Héroult cathode producer. The grades A to D are graphitized and the grade E is impregnated graphite (i.e. graphitized then impregnated with pitch and rebaked). The properties of these grades were provided by the supplier and are listed in Table 5.1.

Table 5.1 : Cathode block properties at room temperature (*: horizontal; **: vertical)

| Properties | A | B | C | D | E |
|---|---|---|---|---|---|
| Thermal conductivity (W/m.K) | 125*<br>112** | 130*<br>115** | 145*<br>135** | 130*<br>105** | 130*<br>105** |
| Electrical resistivity (μΩ.m) | 12.0 | 10.5*<br>11.5** | 8.0*<br>9.0** | 10.5*<br>13.0** | 10.5*<br>13.0** |
| Open porosity (%) | 18 | 14 | 15 | 20 | 14 |
| Air permeability (nPerm) | 8 | 7 | 3 | 6 | 5 |

From experience with these types of blocks, the industry has noticed that the sludge formation tendency differed typically from one grade to another. The sludge formation tendency of cathode grades, that was observed and reported by the industry, is D = E > A > B > C; D and E being the grades that forms the most sludge. This study aims to evaluate the behavior of the different grades of block in the experimental cells for comparison with the real-life behavior reported.

Rectangular experimental blocks of the five grades have been machined for laboratory electrolysis tests. All dimensions of the cell components are shown in Figure 5.2.

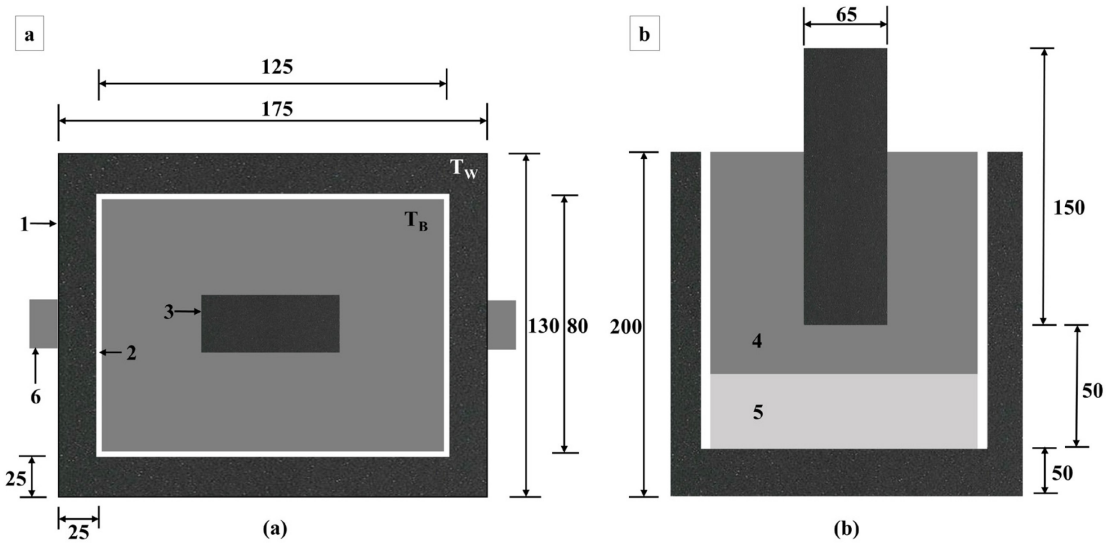


**Figure 5.2 Sizing of experimental Hall-Héroult cells for this study, top view (a) and side view (b). All dimensions are in millimeters (mm). 1: carbon crucible, 2: alumina plates, 3: anode, 4: bath, 5: aluminum, 6: bus bar. $T_W$ and $T_B$ refer respectively to the positions of the thermocouples in the sidewall and in the bath**

Alumina plates of 5 mm thickness are positioned on each cathode sidewall so that the current passes through the bottom. A plate of approximately 500 g of aluminum is placed at the bottom of the cell. The cell is then filled with 1700 g of industrial bath initially containing 10 % (w/w) alumina with a cryolite ratio (CR) of 2.2. The anode is centered as the cryolite is being compacted in the cell. The cell is positioned inside a crucible made of Inconel placed inside a furnace. The temperature is measured in three locations: inside the bath, in the carbon sidewall and inside the crucible. The type K thermocouples are placed inside alumina sleeves in order to protect them from bath corrosion and to prevent short-circuiting the system. The bath thermocouple is left inside the bath until the electrolysis is stopped.

The electrolysis tests are done at a 0.9 A/cm$^2$ current density for 8 h under a $N_2$ atmosphere with a 2-cm ACD. The current is set to 73 A and is kept constant. The temperature and voltage are measured continuously during electrolysis. The bath is preheated between 1233 K and 1273 K (960 °C and 1000 °C) then the temperature is stabilized at 1233 K (960 °C) before the start of electrolysis. In order to highlight the impact of the cathode grade, no point feeding is used and all parameters are kept constant during the cell operation for all cathode grades. At the end of the electrolysis time, the electricity is cut off and the furnace is set to room temperature for

cooling under nitrogen atmosphere. The time for the cell to reach room temperature is close to 30 hours in every case.

Autopsies

During its characterization, the cell is stored under argon atmosphere to avoid any oxidation reaction. In order to observe the deposits at the carbon-aluminum interface, the cell is cut using a diamond blade saw, as illustrated in Figure 5.3.

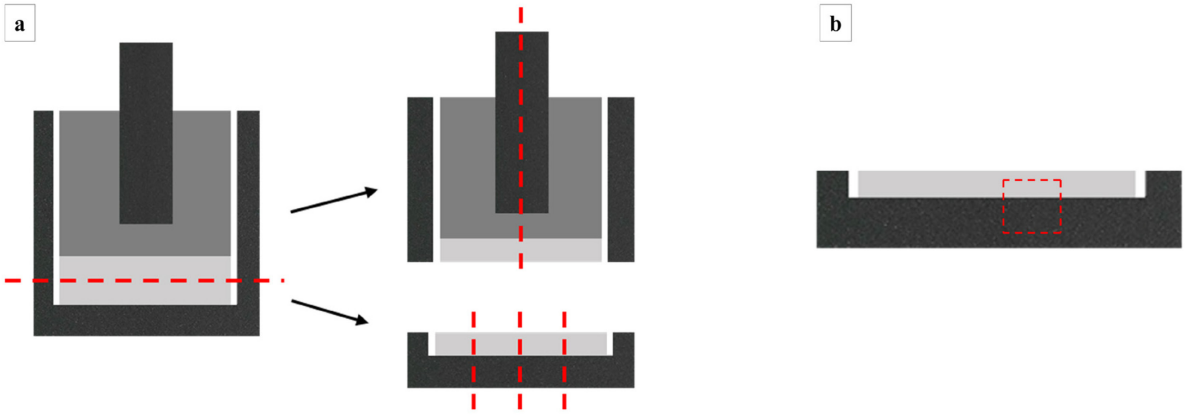


**Figure 5.3 Positions of cuts for deposit observation (red dashed lines); a) cuts of the cell and cathode surface for microscopic sludge observations; b) cutting for SEM observations of the carbon-aluminum interface**

The cathode surface is separated by first cutting through the metal pad. The top of the cell is cut in two in the middle of the anode and the cell bottom part is cut in three positions as shown in Figure 5.3 (section a). After microscopic observations of the obtained slices of the cathode floor, cubes of the carbon-aluminum interface are carved with a diamond blade as shown in Figure 5.3 (section b).

Optical microscopy

Microscopic observations of the carbon-aluminum interface are done with a stereomicroscope Leica MZ FLIII. Panoramic views of the interface are made in order to obtain size and position of deposits. The microscopic observation of the carbon-aluminum interface allows to measure the size of sludge, the extent of the ledge toe and the existence of erosion marks, if any.

X-Ray diffraction (XRD) and quantification of chemical composition

For the top part of the cathode block, samples are harvested from various regions of the bulk for chemical composition quantification. All deposits found at the bottom part of the block are harvested for quantification (sludge, ledge toe). The harvested samples are powdered using a ball mill, back loaded as pressed powder in a cavity and analyzed by XRD. The equipment used for XRD is a PANalytical X'Pert PRO MPD diffractometer and a PIXcel$^{1D}$ detector with a nickel filter. An XRF Potflux Channel was used to determine the total calcium content of samples. The quantitative analysis of each sample is obtained by the Rietveld refinement [Feret, 2008]. The CR based on stoichiometry (moles of NaF/moles of $AlF_3$) calculation is similar to the one used in previous studies on sludge formation as described by Allard et al. (2014b).

Scanning-electron microscopy (SEM)

The surface analysis for elemental cartography is done using the scanning electron microscope Hitachi S-4700 on samples of the carbon floor. The acceleration voltage is set to 20 kV. The intensity of the beam is 10 μA and the working distance 12 mm. The elemental analysis is done with an Oxford X-Mas 50 mm$^2$ energy-dispersive X-ray spectroscopy module (EDS). Electronic microscopy of the carbon-aluminum interface allows evaluating the topography of the interface and measuring the aluminum carbide layer typically formed under the metal.

### 5.3.5 Results

For each experiment, the temperature was recorded with thermocouples in the bath, in the carbon sidewall and inside the Inconel crucible. Figure 5.4 depicts the temperature profile in the bath for the first five runs done for each cathode grade. The temperature of the bath is raised between 1233 K and 1273 K (960 °C and 1000 °C) before the start of electrolysis in order to assure that the bath is completely molten. Afterwards, the temperature of the bath is brought down to 1233 K (960 °C) before electrolysis is initiated. Immediately after the start of the electrolysis, there is a sudden increase in bath temperature due to the Joule effect. After about a thirty-minute period, the bath temperature suddenly drops by approximately 6 to 8 degrees in a one-minute timeframe, as it is observed in Figure 5.4. Subsequently, the bath temperature stabilizes back to 1233 K (960 °C) before it steadily decreases afterwards.

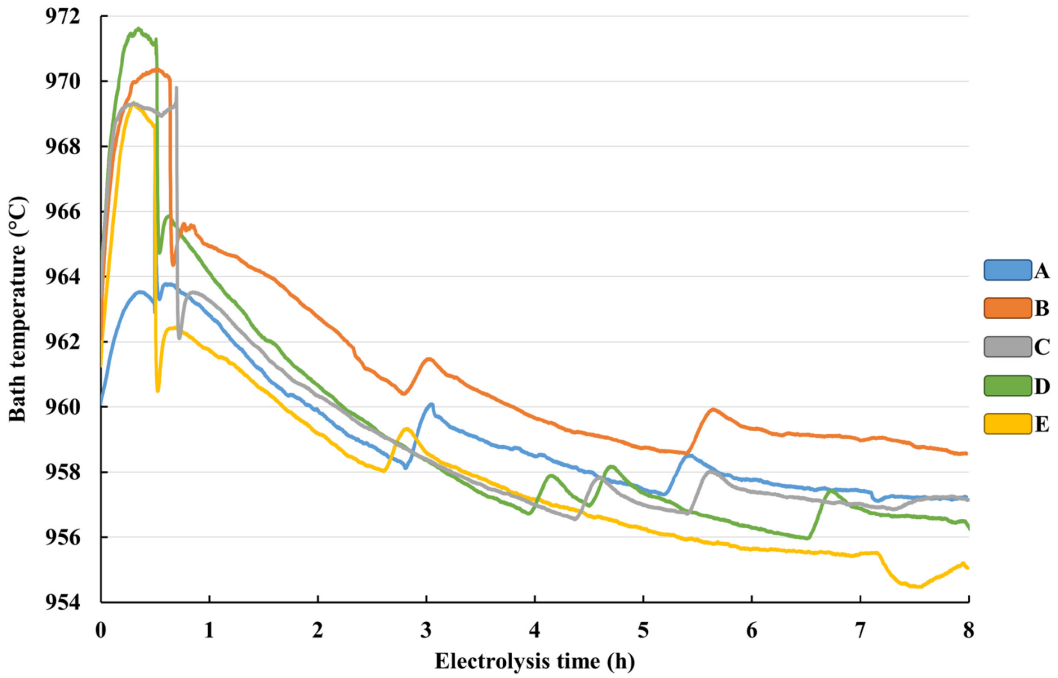


**Figure 5.4 Temperature profile of the bath for the five experimental grades during electrolysis**

The heat generated by the Joule effect in the cell is transferred to the carbon walls of the experimental cell. Due to the constant nitrogen flow inside the crucible, the heat generated in the cell is lost to the surroundings by different heat transfer mechanisms, including conduction through the walls, convection at the surface of the bath and evaporation of the bath. On the other hand, there is considerable amount of radiative heat transfer between different elements, like the Inconel wall and the exterior of the cell. Consequently, the temperature of the bath is affected by a combination of the aforementioned heat transfer mechanisms. Nevertheless, the temperature recorded in the sidewall and in the crucible remained close to 1233 K (960 °C). Because of heat losses to the surrounding of the cathode block, the bath temperature has a tendency to decrease during operation. In order to keep the bath temperature as close as possible to 1233 K (960 °C), the temperature of the furnace is adjusted accordingly (in the range between 1223 K and 1228 K), causing the small bumps on the bath temperature profiles in Figure 5.4. As it can be seen, all five grades have a similar bath temperature profile during electrolysis with a roughly 5 degree margin. At the end of the 8-hour electrolysis period, the furnace is turned off and the cell is let to cool down under nitrogen atmosphere.

After electrolysis, the bottom part of the block is cut in four sections as described in Figure 5.3. Each cut may or may not show a vivid sludge formation at the carbon-aluminum interface. Accordingly, the states of the carbon-aluminum interface associated with the temperature profiles of Figure 5.4 are presented in Figure 5.5.

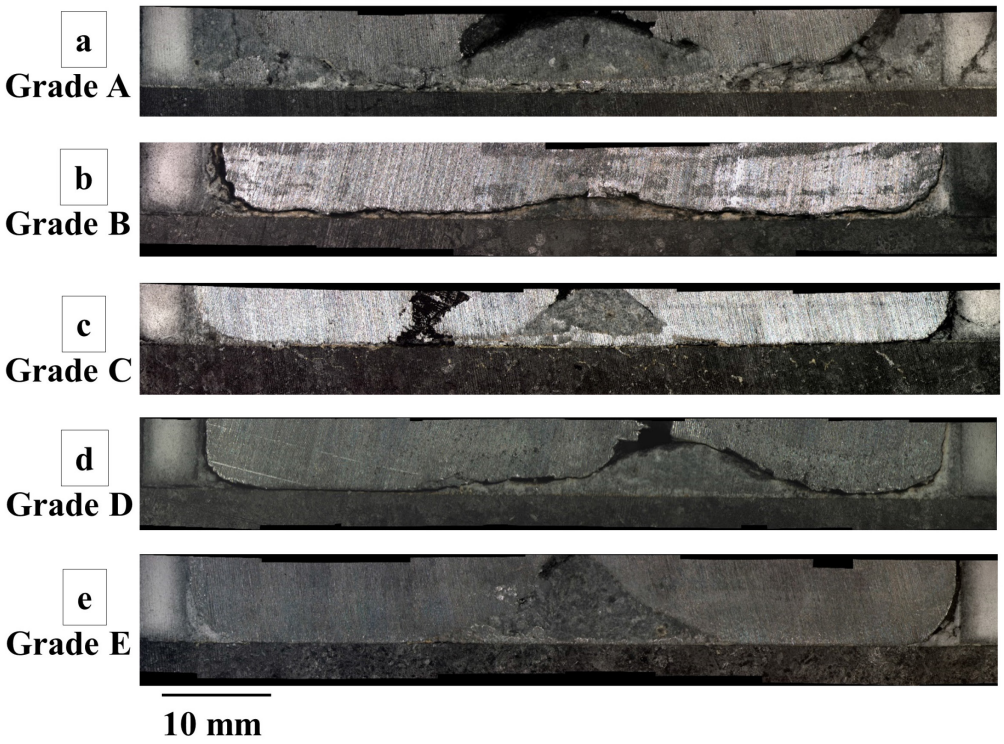


**Figure 5.5 Microscopic observations of the carbon-aluminum interface profile in the center of the cell for the five cathode grades; grade A (a), grade B (b), grade C (c), grade D (d) and grade E (e)**

As it is shown in Figure 5.5, the sludge profile is variable among the grades. An interesting cone shaped sludge deposit was found near the center of the cell. Moreover, a variable amount of bath fills the peripheral corners of the cell bottom, which represents the ledge toe in this experimental study. The ledge toe becomes more and more thin as it elongates towards the center of the cathode floor, leaving a bath layer between the carbon and the metal. However, during autopsies, it could be seen that this layer is not always covering the total surface of the cathode. The thin bath layer observable at the carbon-aluminum interface of grades B and C has a yellowish color and bright yellow marks appear clearly in the carbon of grade C. The thickness of the ledge toe is often variable within a single cell, making the carbon-metal interface profile asymmetrical. In Figure 5.5 (section c), there is an apparent empty space in the metal which can be explained by the contraction of the metal during cooling. For each run illustrated in

Figure 5.5, the characterization of the visible central sludge deposit and the ledge toe is summarized in Table 5.2.

Table 5.2 : Total alumina content (from Rietveld refinement) and cryolite ratio of central and ledge toe sampled in cells from Figure 5.5

| Cathode grade | Central sludge | | Ledge toe | |
|---|---|---|---|---|
| | CR | $Al_2O_3$ (wt %) | CR | $Al_2O_3$ (wt %) |
| A (graphitized) | 2.8 | 22 | 2.2 | 23 |
| B (graphitized) | N/A | N/A | 2.6 | 18 |
| C (graphitized) | 2.9 | 28 | 2.6 | 24 |
| D (graphitized) | 2.6 | 20 | 2.8 | 20 |
| E (graphitized) | 2.9 | 19 | 2.1 | 19 |

For the five runs shown in Figure 5.5/Table 5.2, the bulk of the electrolyte has an alumina content between 4 and 11 with a CR lower than 2 at the end of the electrolysis. The composition of the ledge toe has a higher alumina mass percentage and CR than the initial bath. Accordingly, it is a mixture of undissolved alumina and saturated bath. The central sludge deposits are also alumina-saturated bath and undissolved alumina with a CR less acidic than the initial composition of the bath (CR of 2.2 and 10 % alumina), which is also saturated bath. Besides, the sludge composition shown in Table 5.2 show little variability; nevertheless, the sludge profiles from Figure 5.5 differ significantly. However, when comparing each run with close conditions, it is evident that the size, shape, location and composition of the sludge vary considerably from one run to the other (Figure 5.6).

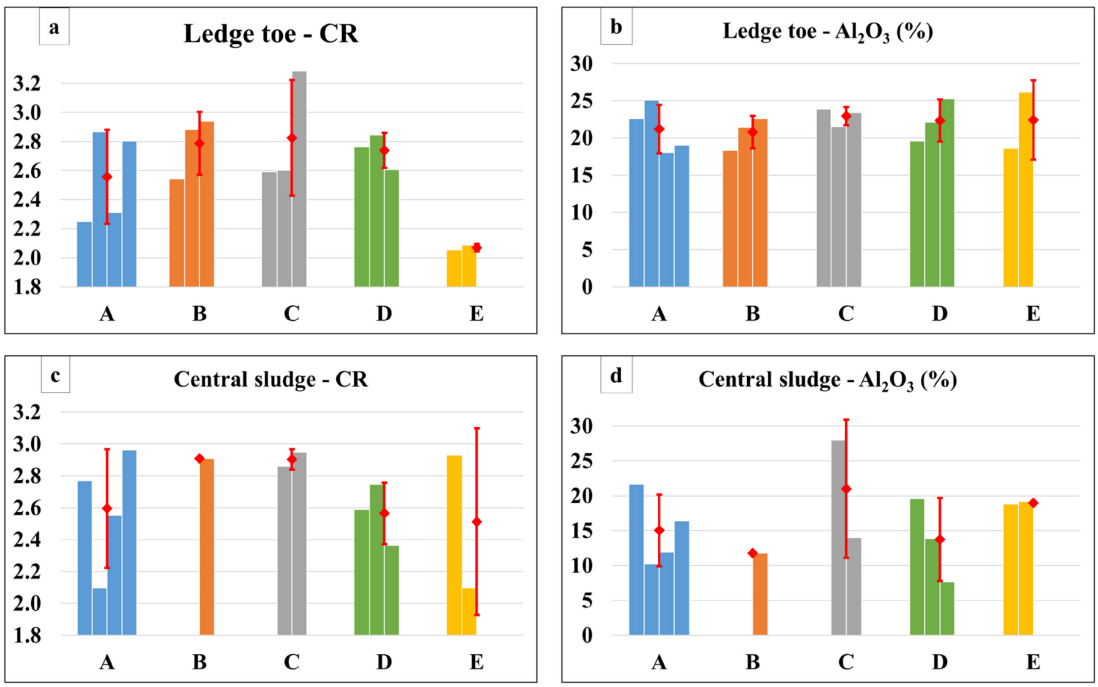


**Figure 5.6 Characterization summary of all experiments; the red markers are the average values by grade with the standard deviation; CR of ledge toe (a), total alumina mass percentage of ledge toe (b), CR of central sludge (c) and total alumina mass percentage of central sludge (d)**

Nonetheless, in every case, the average CR of the ledge toe in impregnated graphite (grade E) is the lowest among all the grades. Moreover, grades B and C, which have high thermal/electrical conductivities, have the highest average CR while grade E has the lowest value. As sections c and d in Figure 5.6 reveal, the number of times that samples of central sludge were analyzed reflects the actual number of times that central sludge had formed. Evidently, grade A is the grade that contained the most sludge in this study although it was listed as the grade with second highest sludge propensity by the industry. Moreover, a distinct central deposit was found only once for grade B.

Observations related to the post-mortem analysis of the bulk bath

The interior of the cell above the metal was also analyzed. It was found that the electrically insulating alumina plates were being dissolved during the experiments, implying an uncontrolled alumina feeding to the bath. The maximum point of erosion of the plates, shown on Figure 5.7, was at the bath-air interface, due to bubble-induced movement of the surface and the alumina dissolution in the low oxygen bath coming from the anode.

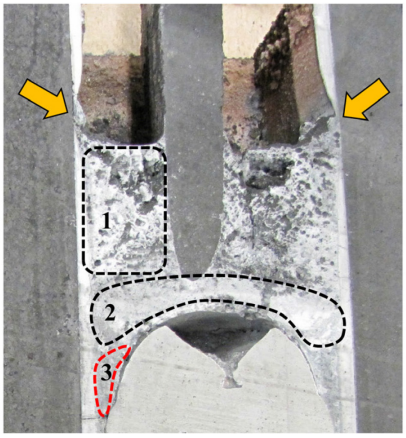


| Zone | $Al_2O_3$ (%) | St. dev. | CR | St. dev. | Density ($g/cm^3$) at 1233 K (960 °C) |
|---|---|---|---|---|---|
| 1 | 6 | 2 | 1.7 | 0.2 | 1.96 |
| 2 | 6 | 3 | 1.8 | 0.2 | 1.98 |
| 3 | 15 | 4 | 2.2 | 0.3 | Bath: 2.04 + solid $Al_2O_3$ |
| Central sludge | 16 | 6 | 2.7 | 0.3 | Bath: 2.09 + solid $Al_2O_3$ |
| Ledge toe | 21 | 4 | 2.6 | 0.3 | Bath: 2.09 + solid $Al_2O_3$ |

**Figure 5.7 Transversal cut of a typical experimental cell and the average alumina mass percentage and CR of the indicated zones; the yellow arrows indicate the typical region where the maximum erosion of alumina plates occurs. The region circled in red indicates that it is supersaturated in alumina**

As it is shown in Figure 5.7, the darker electrolyte above the tip of the anode (i.e. zone 1) is quite porous, caused by the bubbling at the anode. The electrolyte below the anode (i.e. zone 2), is much more packed. The characterization of samples taken in the indicated zones reveals a gradient of alumina concentration, CR and density from the point of erosion to the cathode bottom. Samples from zone 2 have an average alumina concentration and acidity similar to zone 1. However, samples collected in zone 3 (gray bath between the metal and the alumina plate) have a higher average alumina content and CR, which is similar to the bottom deposits. Zone 3 is the farthest region from the anode tip, which is a highly agitated area; therefore, it may be the ideal location of alumina accumulation when it precipitates. The alumina concentration exceeds saturation in zone 3, in the central sludge and in the ledge toe. Other laboratory scale electrolysis experiments have shown the presence of sludge containing 25 % alumina and a CR of 2.2 (i.e. acidic) [Allard *et coll.*, 2014a]. However, those experiments were done with alumina point feeding while the runs presented in this paper had no alumina point feeding. In this experimental study, the initial state of the electrolyte is a mixture of liquid bath and solid undissolved alumina. Considering the additional alumina is coming from the alumina plate erosion, it is not surprising to find considerable amounts of sludge at the bottom of each cell. This increasing of alumina concentration to the system originates from the corrosion of the alumina plates caused by the low oxygen content of the bath surrounding the anode region. The XRD analysis of the samples shown in Figure 5.7 reveals that the composition of the electrolyte at the end of the run, above the metal, has on average 6 % $Al_2O_3$ with an average CR of 1.8. According to the phase diagram

of the experimental system $Al_2O_3$-$AlF_3$-NaF-$CaF_2$, the onset of the experiment is within a two-phase region, requiring alumina precipitation enrichment of the bottom of the cell.

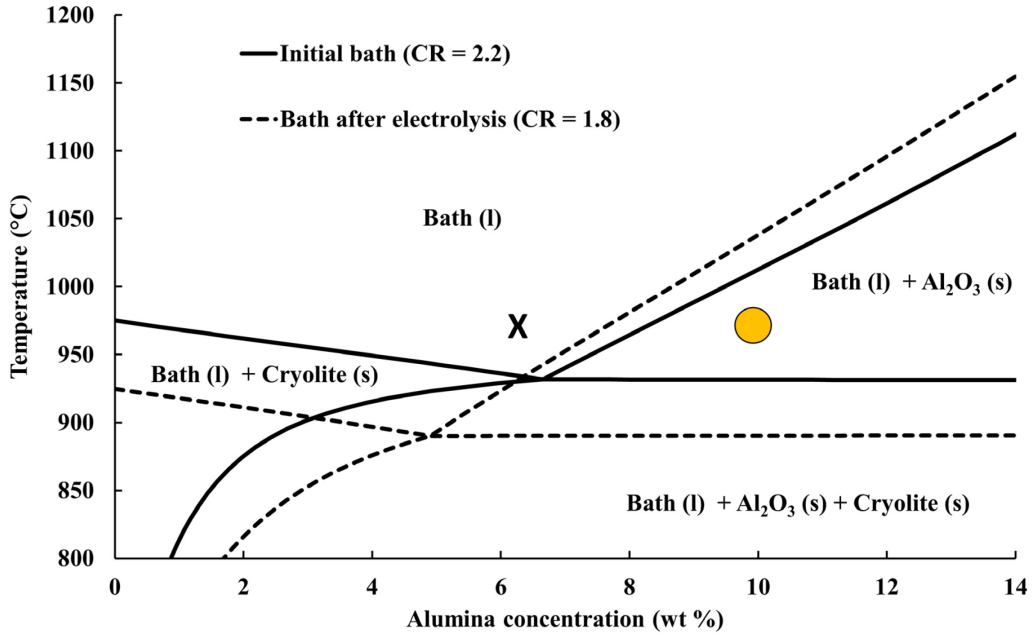


**Figure 5.8 Thermodynamic phase diagram from FactSage of the system $Al_2O_3$-$AlF_3$-NaF-$CaF_2$; the yellow circle (○) and X mark indicate respectively the initial condition of electrolysis and the composition of the bulk bath at the end of the run**

According to Figure 5.8, the acidification of the bulk has a stronger effect on the cryolite liquidus than on the alumina liquidus. Samples above the metal reached the liquid zone while deposits under the metal stayed in the alumina and bath mixture phase. The alumina concentration in the bulk at the end of the experiments suggests that the bath (initially supersaturated) reaches the saturation line during electrolysis. Upon alumina consumption from electrolysis, the alumina concentration in the bulk decreases. The bath depleted from alumina after electrolysis is circulated towards the top of the cell by the means of the bubble agitation, leading to more alumina from the plates getting dissolved, as observable in Figure 5.7. The undissolved alumina from the initial bath or the corrosion of the plates precipitates to the bottom.

Observations on the profile characteristics of the bottom deposits

Although sludge profiles vary from one experiment to the other, some distinctive characteristics of each cathode grade with regard to sludge and other bottom deposits have been noted and summarized in Table 5.3.

Table 5.3 : Qualitative observations of carbon-aluminum interface for each cathode grade

| Cathode grade | Observations |
|---|---|
| A (graphitized) | - High amount of ledge toe that stretches towards a continuous thick layer (> 1 mm).<br>- The thick layer always covers the entire area of the carbon-aluminum interface.<br>- The ledge toe is evenly distributed around the perimeter of the cell. |
| B (graphitized) | - The ledge toe is not evenly distributed, it tends to be thicker in some areas, leaving other regions free of deposits or covered with a thin layer (< 1 mm). |
| C (graphitized) | - Just like grade B, the ledge toe is not evenly distributed, but to a higher extent.<br>- The bath layer is thin (< 1 mm), non-continuous and with bright yellow marks.<br>- Erosion of the carbon surface is observed. |
| D (graphitized) | - High amount of ledge toe is observed, not evenly distributed along the perimeter.<br>- The thin layer (< 1 mm), does not cover the total area of the cathode surface.<br>- A small amount of central sludge is observed. |
| E (graphitized + impregnate.) | - An uneven ledge toe distribution is noticed.<br>- The thin layer (< 1 mm), does not cover the total area of the cathode surface.<br>- Variable amounts of central sludge are observed. |

Observations on the behavior of voltage during the electrolysis

The voltage for each run is measured continuously and the amperage is kept constant at 73 A. When current is launched, the voltage starts around 5.0 V, then decreases between 4.6 and 4.9 V before it generally starts to rise. The tendency for highly electrically conductive grade C and impregnated graphite grade E is to start rising after roughly 3 hours of electrolysis. For grade B,

the voltage typically starts to rise after 4 hours of electrolysis while graphitized grades A and D present steadier voltage behaviors under 5 V during the 8-hour operation period. The average voltage for each grade is presented in Figure 5.9.

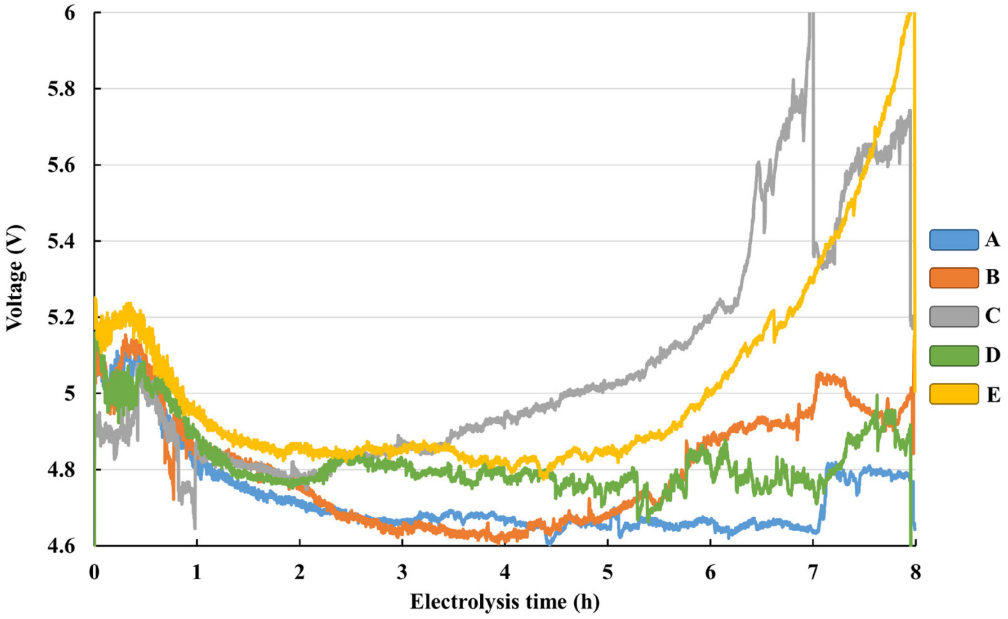


**Figure 5.9 Average voltage by cathode grade**

It does not seem likely that the voltage behavior in this study is directly correlated with the amount of sludge at the carbon-aluminum interface. On the other hand, as mentioned in Table 5.3, the cathode grade C also stood out for its visible erosion marks, which may explain the voltage rise. On the contrary, no visible signs of erosion were observed on impregnated graphite grade E.

SEM-EDS observations of the carbon-aluminum interface

The highest erosion is located where the tip of the elongated ledge toe or thin layer disappeared. Moreover, SEM-EDS observations of the carbon-aluminum interface revealed the presence of a layer containing aluminum covering the carbon surface and going inside the wear pits (Figure 5.10).

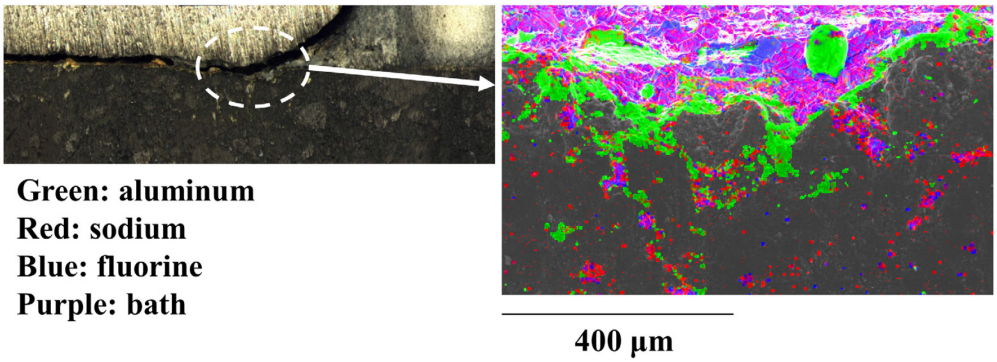


**Figure 5.10 SEM-EDS observation of the indicated zone of the carbon-aluminum interface for grade C**

The green layer containing aluminum in the SEM imaging appears to be aluminum carbide, which is nowadays thought to be highly responsible for cathode wear. This layer was observed with all five grades. The high wear, illustrated in Figure 5.10, suggests that the electrochemical formation of aluminum carbides and its subsequent dissolution in bath (from ledge toe or thin layer) is faster for cathode grades with a film that does not cover the entire cathode surface. Moreover, it may explain the voltage rise observable for grade C. The eroded parts of the carbon surface filled with bath may have prolonged the current paths around the pits, thus provoking voltage rise that is observed especially with grade C. The thickness of the aluminum carbide layer was measured for each block and an apparent correlation with the open porosity of the cathode grade has been previously established [Landry *et coll.*, 2018b]. In Figure 5.10, the aluminum carbide layer appears to be following the morphology of the carbon surface. Accordingly, erosion is taking place when aluminum carbides form around a small piece of carbon before dissolving inside the bath infiltrated in the pores. The detachment of the surrounded carbon piece accounts for the growing pit.

### 5.3.6 Discussion

Sludge formation is influenced by a myriad of phenomena that interact with each other during the regular operation of a cell. The major factors are temperature of the bath, interfacial phenomena, hydrodynamics, bath chemistry and alumina feeding strategy [Fallah Fini et al., 2017b]. Since no point feeding was used in this study, the impact of feeding strategy on sludge formation will not be discussed and reader is encouraged to refer to Fallah Fini et al. [Fallah Fini et al., 2017b]. Since the cathode block is an obligatory passage for heat, mass and

electricity, consequently the aforementioned factors (i.e. temperature of the bath, interfacial phenomena, hydrodynamics, bath chemistry and alumina feeding strategy) should also be influenced by the thermal, electrical and structural properties of the cathode block.

Effect of temperature

The proper dissolution of alumina and avoidance of sludge formation call for an appropriate superheat of the bath. Since close to half of the heat losses go through the carbon walls of the cathode [Grjotheim et Kvande, 1993a], the heat balance of the cell is partially controlled by the thermal conductivity of the cathode block. Expectantly, the cathode grade should have an impact on sludge formation through the cell heat balance. As it is seen in Table 5.1, the five cathode grades have different horizontal and vertical thermal conductivities, which suggests variable heat flows depending on the grade, thus variable sludge profiles. As mentioned earlier, the bath is heated by the Joule effect during electrolysis and cooled by several heat transfer modes. The heat generated inside the cell is transferred by conduction through the graphitized cathode block. The heat lost through the furnace walls and the nitrogen gas flow account for the convective cooling on the exterior of the cathode block. Moreover, the cell is subject to radiative heating coming from the furnace. Due to the complex combination of heat transfer modes affecting the bath temperature, it is not obvious to clearly discern the impact of the thermal conductivity of the cathode block on the heat transferred by conduction through the carbon phase. Nevertheless, during the more stable period of electrolysis (after the sudden temperature increase and decrease seen in Figure 5.4), the experimental cooling rate of the bath was calculated for each run and is plotted in Figure 5.11.

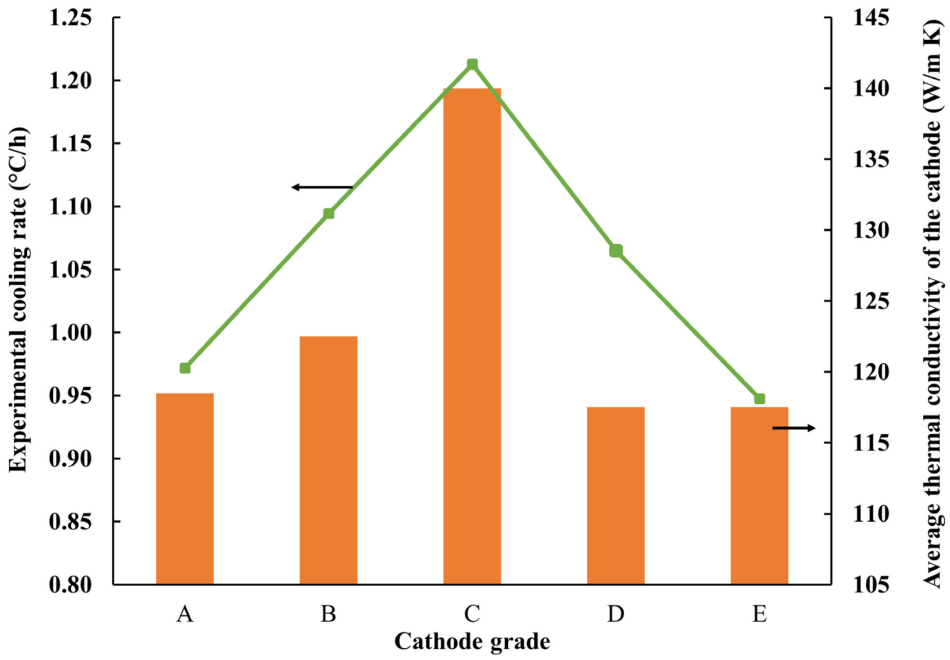


**Figure 5.11 Average cooling rate per cathode grade and average thermal conductivity of block: average conductivity was obtained by averaging the horizontal and vertical conductivities**

Consequently, it was found that the grade with a significantly higher average thermal conductivity (i.e. grade C) had the fastest cooling rate during the electrolysis. This foreseeable result highlights the sensitivity of cathode grades to heat losses even though those grades have close thermal conductivities. The different thermal behaviors seen with the experimental cells yet again emphasize the fact that the heat balance of the cell is greatly influenced by the cathodic carbon block. Knowing that heat losses must be well controlled in order to keep an appropriate superheat and limit sludge formation, the choice of cathode grade is important as it directly influences the rate and uniformity of heat losses. More uniform heat losses should help to control the position of the liquidus isotherm, thus keeping an appropriate uniform protective ledge. This may be easier to achieve by ensuring that the thermal conductivity of the carbon block is as uniform as possible in the whole block. However, it is known that the thermal conductivity of the cathode block changes during the life time of the cells and such changes are due to different phenomena that the cathode block endures [Yurkov, 2015]. Therefore, there must be a correlation between the cathode block raw microstructure (i.e. initial open porosity), infiltration depth of the bath and dynamic thermal conductivity during the operation. In fact, in a recent laboratory study, using similar cathode grades, the impregnated graphite with lower porosity had a lower bath penetration depth than non-impregnated graphite

[Brassard *et coll.*, 2016]. Consequently, in the current study, the impregnated grade E must have been filled with a smaller volume of bath. Despite its same raw thermal conductivity as grade E, grade D showed a significantly faster cooling rate than E during electrolysis. This could be due to a more intense change of thermal conductivity for grade D, resulting from a large bath infiltration enhanced by the higher open porosity of grade D. Although pitch impregnation of graphite blocks is typically used to decrease porosity and increase wear resistance, the pitch impregnation of grade E, while differentiating it from grade D, may have also helped to reduce the rate of heat losses.

Effect of interfacial tension (IFT)

At first, the formation of sludge was foreseeable because the initial bath composition was in the two-phase region (Figure 5.8). When central sludge was found, it was connected to the ledge toe by a bath layer more or less thin, as pictured in Figure 5.5. A similar bath layer was observed in previous experiments and was speculated to be resulting from the ledge toe/sludge displacement by MHD on the cathode block surface [Coulombe et al., 2016b]. Moreover, the existence of a bath film between the carbon and the aluminum was evoked and said to be related to the formation and dissolution of sludge [Li et al., 2015]. Studies on IFT between cryolitic melts and aluminum showed that the IFT between the cryolitic melt and the molten aluminum increases with increasing $AlF_3$ because of the higher activity of sodium [Utigard et Toguri, 1991a, Korenko, 2008, Dewing et Desclaux, 1977]. Accordingly, it was suggested that a movement in the liquid bath film can be induced if there is an IFT gradient between the bath at the aluminum-electrolyte interface and the film at the carbon-aluminum interface. Moreover, the direction of the movement of the film is from the region of lower IFT (i.e. low $AlF_3$) to the region of higher IFT (i.e. high $AlF_3$). The so-called Marangoni flow can back feed the sludge into the bulk if the direction is from the carbon-aluminum interface to the bulk. As it was mentioned previously, the thickness of the bath layer was variable among grades in this study. For grade A, the bath layer was thicker and clearly distinguishable. In order to further discuss the influence of IFT and cathode grade, a schematic diagram is proposed in Figure 5.12.

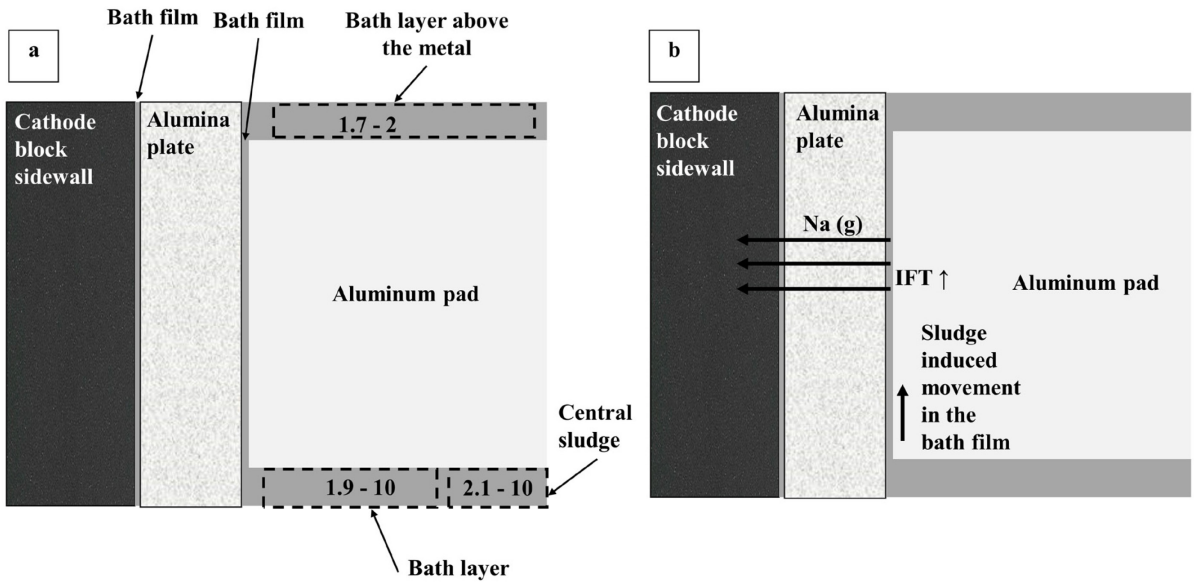


**Figure 5.12 a) Bath film connecting the bottom bath layer and the bulk (CR – alumina %) for one run with cathode grade A, b) film movement induced by sodium losses in cathode block**

The bath layer found below the aluminum seen in Figure 5.12 (section a) ) has a lower CR than the central sludge yet a similar alumina concentration. Also, a thin vertical bath film separating the aluminum pad and the alumina plate connects the bath layer and the bulk. Moreover, there is a gradient of CR from the bulk to the sludge, thus an IFT gradient. This suggests that central sludge may be back fed into the bulk through the bottom layer and the thin vertical film. As a result, alumina may back feed if fresh bath from the bulk can be circulated to the sludge through this film. Besides, the ability of the cathode block to pass sodium may tamper with the sodium depletion of the vertical bath film. As it is depicted in Figure 5.12 (section b), a high sodium diffusion through the cathode block and alumina plate may shift the CR of the bath film to more acidic, thus promoting sludge back feeding through this vertical film. The effective diffusion of sodium gas through the carbon may depend on its porosity, tortuosity and air permeability [Wang *et coll.*, 2009b]. Therefore, cathode grades with high sodium diffusivity may tend to have a lower CR in the bath between the sidewall and the metal, thus drawing mass transfer towards the bulk and promoting sludge back feeding. In this study, grade A was the grade with the highest air permeability, which may further explain the thicker bath layer observed. Other than the fact that grade A had a thick bath layer, no correlation was found between the cathode properties and the acidity of the bath in the bulk or in any other deposit. Nevertheless, if the cathode block has the potential to alter the acidity of the bath, it may well lead to IFT gradients

between the bottom deposits and the bulk, thus inducing Marangoni flows that affect sludge accumulation or back feeding. Furthermore, the Rietveld refinement of the bath samples at the aluminum-bath interface has shown too much variability to prove the presence of a consistent layer of bath rich in alumina that could sink through the metal pad. The agitation in the bath from the anode gas release, seen in Figure 5.7, may have caused such variability of concentration in the bath above the metal. With considerable agitation due to bubble movement and the small size of the cell, it is perceivable that hydrodynamics also play a major role in formation or dissolution of sludge.

Effect of hydrodynamics

Irrespective to IFT induced movement, bubble movement and magneto-hydrodynamics are the most effective forces in the cell. In industrial cells, proper bubble agitation contributes to dissolution of fed alumina particles while oscillation of the bath-metal interface leads to losses in current efficiency [Thonstad *et coll.*, 2001b]. Also, the large molten metal pad is constantly in movement due to MHD forces. In this study, it would take a considerable movement of the metal pad in order to lift the bottom sludge deposits right up into the bulk. With regard to this fact, Kalgraf et Torklep (1998b) have argued that the sludge back feeding process may be governed by the laws of sediment transport. Considering the fact that the sludge is a mixture of crystallized alumina particles and a saturated bath, sufficient turbulence of the metal pad movement could allow the sludge to be lifted (i.e. back-fed) into the bulk through the metal pad. In the present study, there is no obvious reason to believe that there was a sufficient metal pad movement from MHD near the cathode surface to transport sludge in such a manner. The agitation inside the cell is more likely to originate from bubble movement at the anode. Signs of agitation in the metal pad were only observed during the autopsy of a cell cooled during electrolysis. However, agitation signs were only observed in the ACD, which may be attributed to bubble induced movement or aluminum forming during cooling. Nevertheless, it is not clear at this point how the cathode grade can impact the sludge dissolution process through sediment transport-like movement.

### 5.3.7 Conclusions

Laboratory electrolysis tests with five different graphitized cathode grades were performed to study the formation of sludge at the cathode surface. This study has revealed the formation of a

distinct conical sludge deposit near the center of the carbon-aluminum interface for each grade, despite the absence of point feeding during electrolysis. The central sludge and ledge toe deposits had an alumina mass percentage ranging from 10 to 25 % and a CR from 2.4 to 2.9. No correlation was found between the composition of the bottom deposits and the cathode grade in this study.

The profile of sludge was variable among cathode grades, which further suggests that the cathode grade has an impact on sludge formation. However, no clear correlation between the thermal conductivity of the cathode block and the temperature profiles was found, due to the complex array of heat transfers involved during the experiments. The observable temperature profile variations testify of the sensibility of the experimental setup used in this study. Nevertheless, a certain amount of sludge was always found at the carbon-metal interface in each experiment. The phenomenon of sludge formation may be repeatable, granted that conditions inside the cells (especially temperature profiles) are replicated.

The higher CR of the central sludge vs the CR of the bulk suggested an induced movement in the vertical bath film, resulting from IFT difference between the bulk and the bottom of the cell, while enhancing the back feeding of the sludge. Therefore, the propensity of a cathode block to alter the acidity of the vertical bath film between the metal and the sidewall may then contribute to induce sludge back feeding. Cathode grades with high permeability may be more prone to sludge back feeding by IFT driven movement.

The wear of the carbon-aluminum interface may be faster for the cathode grades with a film that partially covers the cathode surface. A layer of aluminum carbide is observed with SEM-EDS inside the erosion pits. The erosion pits in the cathode surface may contribute to the voltage rise. In order to alleviate the problem of pit formation (i.e. erosion of cathode surface), other methods such as copper inserts can be used to lower the CVD, reduce the MHD forces and make current paths more uniform. The use of such inserts in combination with graphitic cathode grade was recently predicted to have an increased interest in a near future [Rivoaland, 2016b]. Furthermore, the use of such cathode grades with lower electrical and thermal conductivities may help to keep a better control over the heat balance, hence reduce sludge formation and its detrimental drawbacks.

### 5.3.8 References


X. Liao and H. A. Oye: Light Met. 1999, Proc. Int. Symp., 1999, pp. 621-27.

F. Allard, G. Soucy and L. Rivoaland: Metall. Mater. Trans. B, 2014, vol. 45B, pp. 2475-2485.

K. Grjotheim and H. Kvande, eds. Introduction to Aluminium Electrolysis - Understanding the Hall-Heroult Process, 2nd ed., Aluminium-Verlag, Düsseldorf, Germany, 1993.

Y. Song, J. Peng, Y. Di, Y. Wang and N. Feng: Can. Metall. Q., 2017, vol. 57, pp. Ahead of Print.

M. Sorlie and H. A. Oye: Cathodes in Aluminium Electrolysis, 3rd ed., Aluminium-Verlag, Düsseldorf, Germany, 2010.

T. Utigard and J. M. Toguri: Light Met. 1991, Proc. Int. Symp., 1991, pp. 273-81.

F. Allard, G. Soucy, L. Rivoaland and M. Désilets: Journal of Thermal Analysis and Calorimetry, 2014, vol. 119, pp. 1303-1314.

P. Y. Geay, B. J. Welch and P. Homsi: Light Met. 2001, Proc. Int. Symp., 2001, pp. 541-47.

M. Fallah Fini, G. Soucy, D. Martin, P. Pelletier, D. Lombard and L. Rivoaland: Bauxite, Alumina, Alum., Proc. Int. Symp. ICSOBA, 2017, 42, pp. 987-96.

T. Li, S. T. Johansen and A. Solheim: TMS Light Met., 2015, pp. 831-36.

T. Utigard: Light Met. 1999, Proc. Int. Symp., 1999, pp. 319-26.

X. Liao and H. A. Oye: Light Met. 1998, Proc. Int. Symp., 1998, pp. 667-74.

B. Novak, K. Tschöpe, A. P. Ratvik and T. Grande: Light Met. 2012, Proc. Int. Symp., 2012, pp. 1343-48.

A. Zoukel, P. Chartrand and G. Soucy: Light Met. 2009, Proc. Int. Symp., 2009, pp. 1123-28.

B. Novak, A. P. Ratvik, Z. Wang and T. Grande: Light Met. 2018, Proc. Int. Symp., 2018, pp. 1215-22.

M. A. Coulombe, G. Soucy, L. Rivoaland and L. Davis: Metall. Mater. Trans. B, 2016, vol. 47, pp. 1280-1295.

K. Kalgraf and K. Torklep: Light Met. 1998, Proc. Int. Symp., 1998, pp. 455-64.

Z. Wang, S. Nobakhtghalati, A. Store, A. Solheim, K. Tschöpe, A. P. Ratvik and T. Grande: Light Met. 2016, Proc. Int. Symp., 2016, pp. 895-902.

K. Tschöpe, A. Store, S. Rorvik, A. Solheim, E. Skybakmoen, T. Grande and A. P. Ratvik: Light Met. 2012, Proc. Int. Symp., 2012, pp. 1349-54.

K. Tschöpe, A. Store, E. Skybakmoen, A. Solheim, T. Grande and A. P. Ratvik: Light Met. 2013, Proc. Int. Symp., 2013, pp. 1251-56.

E. Skybakmoen, S. Roervik, A. Solheim, K. R. Holm, P. Tiefenbach and O. Ostrem: Light Met. 2011, Proc. Int. Symp., 2011, pp. 1059-66.

J.-M. Dreyfus and L. Joncourt, In Light Metals 1999, ed. C.E. Eckert (The Minerals, Metals and Materials Society (TMS),Warrendale,PA.: 1999), pp 199-206.

L. Rivoaland: Bauxite, Alumina, Alum., Proc. Int. Symp. ICSOBA, 2016, pp.

F. R. Feret: Light Met. 2008, Proc. Int. Symp., 2008, pp. 118-28.

F. Allard, M. A. Coulombe, G. Soucy and L. Rivoaland: Light Met. 2014, Proc. Int. Symp., 2014, pp. 1233-38.

J.-R. Landry, M. Fallah Fini, G. Soucy, M. Désilets, P. Pelletier, L. Rivoaland and D. Lombard: Light Met. 2018, Proc. Int. Symp., 2018, pp. 1229-33.

A. Yurkov: Refractories for Aluminium Electrolysis and the Cast House, 1st ed., Springer, Switzerland, 2015.

M. Brassard, M. Soucy, M. Désilets and D. Lombard: Can. Metall. Q., 2016, vol. 55, pp. 356-64.

M. Korenko: J. Chem. Eng. Data, 2008, vol. 53, pp. 794-97.

E. W. Dewing and P. Desclaux: Metall. Mater. Trans. B, 1977, vol. 4, pp. 555-61.

Z. Wang, E. Skybakmoen and T. Grande: Light Met. 2009, Proc. Int. Symp., 2009, pp. 353-58.

J. Thonstad, G. Felnner, G. M. Haarberg, J. Hives and H. Kvande: Aluminium Electrolysis - Fundamentals of the Hall-Héroult Process, 3rd ed., Aluminium-Verlag, Düsseldorf, Germany, 2001.

# CHAPITRE 6 CONCLUSION ET TRAVAUX FUTURS

## 6.1 Sommaire des travaux et contributions aux connaissances

Le procédé Hall-Héroult menant à la production d'aluminium est entravé par la formation de dépôts résistifs qui abaissent l'efficacité énergétique du procédé et réduisent la durée de vie des cellules. Dans le but de minimiser la formation de ces dépôts nocifs, il est nécessaire de cerner les facteurs régissant leur formation. Dans cette étude expérimentale, l'impact de la nuance de bloc cathodique sur la formation de boues résistive a été examiné.

Bien que l'objectif principal de ce projet de recherche était de comprendre l'impact de la nuance de cathode sur la formation des boues, les mécanismes de formation ont aussi été investigués. Les expériences d'électrolyse en laboratoire effectuées dans le cadre de ce projet ont permis de générer des dépôts de boues, de talus et de pieds de talus. La variabilité des dimensions de ces dépôts, observés avec les cinq nuances de blocs cathodiques, suggère que les propriétés physico-chimiques des blocs ont un impact sur la formation de ces dépôts. Sachant que le talus, le pied de talus et la boue se forment par refroidissement et par surchauffe de bain insuffisante (pour une acidité et une teneur en alumine donnée dans le bain), les pertes de chaleur de la cellule ont un impact sur l'étendue de leur formation. La chaleur générée par effet Joule est transférée par conduction dans le bloc cathodique, d'où l'importance de la conductivité thermique de la nuance de bloc. Dans cette étude expérimentale, le profil des boues semblait varier en raison des multiples mécanismes de transfert de chaleur ayant lieu durant l'électrolyse. Le profil variable des dépôts de boues avec les différentes nuances de cathode prouve la sensibilité des cellules aux variations sur le banc d'essais.

En raison de la grande taille et de la forme des cellules industrielles, de forts flux de chaleurs sont engendrés durant l'opération. La chaleur générée par effet Joule durant l'opération des cellules est partiellement utilisée pour garder le système à haute température et partiellement perdue. Avec un meilleur contrôle de l'uniformité des flux de chaleurs dans les parois, il serait plus facile de maintenir une épaisseur de talus protecteur plus uniforme à l'intérieur. De plus, la réduction de pertes de chaleurs subites et importantes permettrait aussi de garder la température

interne plus stable et uniforme. Un meilleur contrôle de la température interne aiderait au maintien d'une surchauffe adéquate du bain, ainsi la minimisation de la formation de boue.

Il a été démontré que les divers mécanismes de formation et dissolution des boues (tensions d'interface, MHD, etc.) s'entrecroisent tous durant l'opération des cellules d'électrolyse Hall-Héroult. La présence d'un gradient de CR entre un film de bain à l'interface carbone-aluminium et l'interface aluminium-électrolyte suggère un gradient de tensions d'interfaces entre la surface du bloc cathodique et le lit du bain. Un tel gradient induirait un mouvement du bain connectant la surface du bloc cathodique et le lit du bain. Dépendamment du sens du gradient de CR, le film de bain vertical connectant le dessus et le dessous de la nappe d'aluminium pourrait favoriser l'accumulation de dépôts à l'interface carbone-aluminium ou sa dissolution. De plus, les blocs cathodiques ayant une forte perméabilité aux flux de sodium accentueraient l'acidification du bain dans le film vertical, favorisant ainsi le transport de la boue vers le lit du bain. Une telle observation a été faite avec le bloc cathodique ayant la plus haute perméabilité à l'air. Cependant, le CR et la teneur en alumine des dépôts de boue ne semblent pas corrélées avec la nuance de bloc cathodique pour les conditions utilisées.

Dans ce projet de recherche, les cinq nuances de bloc cathodique utilisées ont démontré des courbes de voltage différentes. Il ne semblait pas que la hausse de voltage des cellules expérimentales soit directement liée à l'embourbement de l'interface carbone-aluminium. Cependant, une hausse nette de voltage a été observée avec les nuances de graphite imprégné (nuance E) et la nuance dont l'interface carbone-aluminium présentait des marques d'érosion (nuance C). Contrairement aux nuances C et E, le voltage des nuances A, B et D n'a pas affiché de hausse aussi drastique. La forte hausse de voltage de la nuance C suggère que les marques d'érosion pourraient avoir perturbé la trajectoire des lignes de courant au niveau de l'interface bloc cathodique-aluminium, expliquant la hausse de voltage observée. Cela suggère que la minimisation de l'érosion des blocs cathodiques soit importante pour ralentir la hausse de la CVD et aussi prolonger la durée de vie des cellules. Les fortes marques d'érosion ont été observées sur la nuance C qui possédait les conductivités électrique et thermique les plus hautes parmi les cinq nuances à l'étude. L'embourbement excessif des cellules peut être contré par une hausse de la surchauffe du bain alors que l'érosion des blocs cathodiques est un phénomène irréversible qui contribue aussi à la baisse de l'efficacité des cellules. De plus, la présence de

carbone dans le bain, venant des parties érodées du bloc cathodique, augmente la résistivité du bain, ce qui contribuerait aussi à une hausse du voltage total nécessaire pour produire l'aluminium et donc du prix de production.

La formation d'une couche de carbures d'aluminium fut aussi notée dans toutes les expériences de cette étude. Les mesures de l'épaisseur de cette couche de carbures d'aluminium, effectuées par microscopie électronique à balayage et analyse dispersive en énergie, suggèrent que son épaisseur augmente avec la porosité ouverte du bloc cathodique.

Le travail de minimisation des boues ne passerait pas seulement par l'optimisation des composantes du système, telles que le bloc cathodique, mais aussi par l'optimisation des conditions d'opération (acidité du bain, teneur en alumine, MHD). Les résultats reportés dans la revue de la littérature sur la formation des boues insinuent que les techniques d'alimentation d'alumine et les propriétés mêmes de l'alumine d'alimentation auraient aussi un impact sur la formation des boues. Indépendamment des matériaux cathodiques employés en industrie, il semblerait que la teneur en alumine du lit du bain (en vertu de l'acidité du bain), l'optimisation de la technique d'alimentation, la surchauffe du bain et la stabilisation de la nappe de métal par minimisation de la MHD soient les paramètres dominants à maîtriser afin de réduire la formation des boues.

## 6.2 Travaux futurs

Les usines d'électrolyse d'aluminium présentes actuellement dans le monde fonctionnent avec un courant continu à longueur d'année. Il est important pour les compagnies utilisant le procédé Hall-Héroult de maintenir autant que possible une opération sans interruption majeure des cellules pour maximiser la production. Il est économiquement non viable pour un producteur d'aluminium de fermer complètement des salles de cuves d'électrolyse pour effectuer des changements majeurs dans l'usine tels que le remplacement de toutes les nuances de blocs cathodiques par exemple. En raison des forts coûts associés à l'interruption de la production, les compagnies sont commises à ne pouvoir qu'apporter des modifications au procédé existant au lieu de le remplacer. La recherche actuelle en optimisation du procédé Hall-Héroult porte aussi sur des éléments plus facilement remplaçables ou modifiables que le bloc cathodique tels que les anodes précuites ou les techniques d'opération et d'alimentation d'alumine. Ces opérations

ne nécessitent pas le remplacement des blocs cathodiques. L'impact des différents facteurs affectant la formation des boues doit être quantifié pour peaufiner le contrôle du procédé. En raison du prix de l'électricité et du désir grandissant de protéger l'environnement, la recherche actuelle et future doit se tourner davantage sur la réduction des pertes d'efficacité de courant et des dommages causés à l'environnement. Dans ce courant d'idée, les anodes inertes et les systèmes de traitement des gaz d'échappement des cellules d'électrolyse semblent être des avenues permettant l'amélioration continue de ce procédé centenaire.

La plus courte durée de vie des cellules avec des blocs cathodiques graphitisés est liée à la faible résistance de ces types de nuance. L'érosion de la surface des blocs cathodiques peut être physique (par abrasion venant du mouvement MHD du métal) ou chimique (par formation et dissolution des carbures d'aluminium). Beaucoup d'efforts sont actuellement faits en recherche pour tenter de stabiliser la nappe d'aluminium et ainsi réduire l'abrasion physique de la surface des blocs cathodiques. Parmi les avenues de recherches actuelles, l'insertion de tiges de cuivre dans les blocs cathodiques permettrait d'uniformiser les lignes de courants dans le bloc cathodique et ainsi favoriser les courants verticaux, stabiliser la nappe de métal et réduire le taux d'érosion [Rivoaland, 2016b]. La recherche actuelle sur l'érosion chimique des blocs porte sur les mécanismes de formation et de dissolution des carbures d'aluminium à l'interface carbone-aluminium. En effet, la formation de carbures d'aluminium à l'interface carbone-aluminium et leur dissolution subséquente dans un film de bain provoquent la perte nette de carbone cathodique ainsi qu'une réduction de l'efficacité du procédé. La minimisation de la portée de ce phénomène d'érosion chimique permettrait de ralentir l'érosion des blocs cathodiques, particulièrement pour les nuances graphitisées. D'autre part, des brevets ont été proposés afin d'apporter des modifications majeures sur le procédé Hall-Héroult, tel que les cathodes mouillées et drainées [Pawlek, 2010a]. Celles-ci permettraient d'opérer avec seulement un film de bain dans l'ACD et aussi de recueillir l'aluminium formé dans un canal central, éliminant du même coup le phénomène de formation des boues. Dans ce cas, le diborure de titane semble attrayant comme matériau cathodique en raison de sa faible solubilité dans l'aluminium, sa résistance à la corrosion de l'électrolyte et sa bonne conductivité électrique. Cependant, il est difficile de remplacer un procédé centenaire comme le procédé Hall-Héroult sur lequel l'entièreté de l'industrie mondiale de la production primaire d'aluminium est basée. De tels nouveaux procédés, comme aussi celui de réduction carbothermique [Tabereaux et Peterson,

2014], ne sont pas encore industriellement matures et leur implantation pourrait encore prendre plusieurs décennies.

# RÉFÉRENCES


ABD EL ALL, S., GERLACH, J. & HENNIG, U. 1980. Interactions between powdered alumina and fluoride melts with regard to the properties of the reaction products. *Erzmetall,* 33**,** 504-9.

ALLARD, F., COULOMBE, M.-A., SOUCY, G. & RIVOALAND, L. 2014a. Cartography and chemical composition of the different deposits in the hall-heroult process. *Light Metals***,** 1233-1238.

ALLARD, F., COULOMBE, M. A., SOUCY, G. & RIVOALAND, L. 2014a. Cartography and Chemical Composition of the Different Deposits in the Hall-Heroult Process. *Light Met. 2014, Proc. Int. Symp.***,** 1233-1238.

ALLARD, F., SOUCY, G. & RIVOALAND, L. 2014b. Formation of Deposits on the Cathode Surface of Aluminium Electrolysis Cells. *Metall. Mater. Trans. B,* vol. 45B**,** 2475-2485.

ALLARD, F., SOUCY, G. & RIVOALAND, L. 2014c. Formation of deposits on the cathode surface of aluminum electrolysis cells. *Metallurgical and Materials Transactions B,* 45**,** 2475-2485.

ALLARD, F., SOUCY, G., RIVOALAND, L. & DÉSILETS, M. 2014b. Thermodynamic and thermochemical investigation of the deposits formed on the cathode surface of aluminum electrolysis cells. *Journal of Thermal Analysis and Calorimetry,* vol. 119**,** 1303-1314.

ALLARD, F., SOUCY, G., RIVOALAND, L. & DÉSILETS, M. 2015. Thermodynamic and thermochemical investigation of the deposits formed on the cathode surface of aluminum electrolysis cells. *Journal of Thermal Analysis and Calorimetry,* 119**,** 1303-1314.

ALUMINIUM, W. 2018. *Primary Aluminium Production* [Online]. Available: http://www.world-aluminium.org/statistics/primary-aluminium-production/#histogram [Accessed 2018].

ARCHER, A. M. 1983. Considerations in the selection of alumina for smelter operation. *Journal of Metals,* 35**,** 43-46.

ARCHER, A. M. 2013. Considerations in the selection of alumina for smelter operation. *In:* BEARNE, G., DUPUIS, M. & TARCY, G. (eds.) *Essential Readings in Light Metals.* Hoboken, NJ, USA: John Wiley & Sons, Inc.

BAGSHAW, A. N., KUSCHEL, G., TAYLOR, M. P., TRICKLEBANK, S. B. & WELCH, B. J. 1985. Effect of operating conditions in the dissolution of primary and secondary (reacted) alumina powders in electrolytes. *Light Metals***,** 649-659.

BAGSHAW, A. N. & WELCH, B. J. 2013. The Influence of alumina properties on Its dissolution in smelting electrolyte. *In:* DONALDSON, D. & RAAHAUGE, B. E. (eds.) *Essential Readings in Light Metals.* Hoboken, NJ, USA: John Wiley & Sons, Inc.

BARZI, Y. M. & ASSADI, M. Heat transfer and thermal balance analysis of an aluminum electrolysis cell side lines: A heat recovery capability and feasibility study. ASME International Mechanical Engineering Congress and Exposition, Proceedings (IMECE), 2013.

BRASSARD, M., SOUCY, M., DÉSILETS, M. & LOMBARD, D. 2016. Impact of Aluminium Pad and Operation Parameters on Graphitised & Graphitic Cathodes Expansion and Bath Penetration. *Can. Metall. Q.,* vol. 55**,** 356-364.

BRAY, E. L. 2018. *Aluminum Statistics and Information* [Online]. U.S. Geological Survey. Available: https://minerals.usgs.gov/minerals/pubs/commodity/aluminum/index.html#myb [Accessed 13-05-2018].

BUGNION, L. & FISCHER, J. C. 2016. Effect of carbon dust on the electrical resistivity of cryolite bath. *Light Metals***,** 587-591.

BURCHELL, T. D. 1999. *Carbon Materials for Advanced Technologies*, Pergamon.

CHAI, D., SHI, Z., ZHANG, Y., ZHANG, Y., HOU, G., WANG, Y., HU, Q. & FANG, B. 2018. The successful implementation of energy saving technology based on steady flow and heat preservation. *Minerals, Metals and Materials Series.*

CHARETTE, A. KOCAEFE, Y.S. 2012. *Le carbone dans l'industrie de l'aluminium*.

COULOMBE, M.-A., SOUCY, G., RIVOALAND, L. & DAVIES, L. 2016a. Factors leading to the formation of a resistive thin film at the bottom of aluminum electrolysis cells. *Metallurgical and Materials Transactions B.,* 47**,** 1280-1295.

COULOMBE, M. A., SOUCY, G., RIVOALAND, L. & DAVIS, L. 2016b. Factors Leading to the Formation of a Resistive Thin Film at the Bottom of Aluminum Electrolysis Cells. *Metall. Mater. Trans. B,* vol. 47**,** 1280-1295.

COURSOL, P., DUFOUR, G., COTÉ, J., CHARTRAND, P. & MACKEY, P. 2012. Application of thermodynamic models for better understanding and optimizing the hall-heroult process. *JOM,* 64**,** 1326-1333.

DANDO, N., WANG, X., SORENSEN, J. & XU, W. 2010. Impact of thermal pretreatment on alumina dissolution rate and HF evolution. *Light Metals***,** 541-546.

DASSYLVA-RAYMOND, V., KISS, L. I., PONCSAK, S., CHARTRAND, P., BILODEAU, J.-F. & GUÉRARD, S. 2014. Modeling the Behavior of Alumina Agglomerate in the Hall-Heroult Process. *TMS Annual Meeting.* San Diego, California.

DAVIDSON, P. A. & LINDSAY, R. I. 1998. Stability of interfacial waves in aluminium reduction cells. *Journal of Fluid Mechanics,* 362**,** 273-295.

DEWING, E. W. & DESCLAUX, P. 1977. The interfacial tension between aluminum and cryolite melts saturated with alumina. *Metall. Mater. Trans. B,* vol. 4**,** 555-561.

DONNET, J.-B. 2006. Carbon allotropes: a large family. *Actual. Chim.,* 295-296**,** 115-118.

DREYFUS, J.-M. & JONCOURT, L. 1999. Erosion Mechanisms in Smelters Equipped with Graphite Blocks. A Mathematical Modeling Approach. *In:* ECKERT, C. E., ed. Light Metals 1999, 1999. The Minerals,Metals and Materials Society (TMS),Warrendale,PA., 199-206.

EINARSRUD, K. E., SKYBAKMOEN, E. & SOLHEIM, A. 2014. On the influence of MHD driven convection on cathode wear. *TMS Annual Meeting.* San Diego, California.

FALLAH FINI, M., SOUCY, G., DÉSILETS, MARTIN, PELLETIER, P., LOMBARD, I. & RIVOALAND, L. Sludge formation in Hall-Héroult Process: an existing problem. Proceedings of ICSOBA Conference, 2017a. Hamburg, Germany: ICSOBA, 987-996.

FALLAH FINI, M., SOUCY, G., MARTIN, D., PELLETIER, P., LOMBARD, D. & RIVOALAND, L. 2017b. Sludge formation in hall héroult process: an existing problem. *Bauxite, Alumina, Alum., Proc. Int. Symp. ICSOBA,* 42**,** 987-996.

FERET, F. R. 2008. Breakthrough in analysis of electrolytic bath using Rietveld-XRD method. *Light Met. 2008, Proc. Int. Symp.***,** 118-128.

GASIK, M. M. & GASIK, M. I. 2003. Smelting of aluminum. *In:* TOTTEN, G. E. & MACKENZIE, D. S. (eds.) *Handbook of Aluminum.* NY, USA: Marcel Dekker.

GEAY, P.-Y., WELCH, B. J. & HOMSI, P. 2013. Sludge in operating aluminum smelting cells. *In:* BEARNE, G., DUPUIS, M. & TARCY, G. (eds.) *Essential Readings in Light Metals.* Hoboken, NJ, USA: John Wiley & Sons, Inc.

GEAY, P. Y., WELCH, B. J. & HOMSI, P. 2001. Sludge in operating aluminum smelting cells. *Light Met. 2001, Proc. Int. Symp.***,** 541-547.

GERLACH, J., HENNIG, U. & KERN, K. 1975. The dissolution of aluminum oxide in cryolite melts. *Metallurgical and Materials Transactions B,* 6**,** 83-86.

GERLACH, J. & WINKHAUS, G. 1985. Interactions of alumina with cryolite-based melts. *Light Metals***,** 301-313.

GRJOTHEIM, K. 2010. *Introduction to Aluminium Electrolysis: Understanding the Hall-Héroult Process*, Alu Media.

GRJOTHEIM, K., KROHN, C., MALINOVSKÝ, K., MATIAŠOVSKÝ, J. & THONSTAD, J. 1982. *Aluminium Electrolysis: Fundamentals of the Hall-Héroult Process,* Düsseldorf, Germany, Aluminium-Verlag.

GRJOTHEIM, K. & KVANDE, H. (eds.) 1993a. *Introduction to Aluminium Electrolysis - Understanding the Hall-Heroult Process,* Düsseldorf, Germany: Aluminium-Verlag.

GRJOTHEIM, K. & KVANDE, H. (eds.) 1993b. *Introduction to Aluminium Electrolysis: Understanding the Hall-Héroult Process,* Düsseldorf, Germany: Aluminium-Verlag GmbH.

GRJOTHEIM, K. & WELCH, B. J. 1989. Technological developments for aluminum smeltinq as the industry enters the 21st century. *JOM,* 41**,** 12-16.

GRJOTHEIM, K., WELCH, B. J. & TAYLOR, M. P. 1989. Relating operating strategy and performance in aluminium smelting cells - an overview. *Light Metals***,** 255-260.

HABASHI, F. 2003. Extractive metallurgy of aluminum. *In:* TOTTEN, G. E. & MACKENZIE, D. S. (eds.) *Handbook of Aluminum.* NY, USA: Marcel Dekker.

HAUPIN, W. 1997. Understanding boundary layers. *Light Metals***,** 319-323.

HERSTAD, O., KROHN, C. H., SOERLIE, M. & ØYE, H. A. 1983a. Precipitation of alumina and aluminum carbide during electrolysis of cryolite-alumina melts. *Light Metals***,** 347-56.

HERSTAD, O., KROHN, C. H., SOERLIE, M. & ØYE, H. A. 1983b. Precipitation of solid components during electrolysis of cryolite-alumina melts. *Aluminium,* 59**,** 200-6.

HOLM, J. L. 1962. Structural interpretation of the system cryolite + sodium aluminate. *Trans. Faraday Soc.,* 58**,** 1104-7.

HOVE, S. J. & KVANDE, H. 1982. Center-break alumina feeding and sludge control of prebaked cells. *Light Metals***,** 513-529.

ISAEVA, L. A., BRASLAVSKII, A. B. & POLYAKOV, P. V. 2009. Effect of the content of the α-phase and granulometric composition on the dissolution rate of alumina in cryolite-alumina melts. *Izvestiya VUZ. Tsvetnaya Metallurgiya***,** 35-40.

JAIN, R. K., TAYLOR, M. P., TRICKLEBANK, S. B. & WELCH, B. J. A study of the relationship between the properties of alumina. Its interaction with aluminium smelting electrolytes. Proceedings of the 1st International Symposium on Molten Salt Chemistry and Technology, 1983a. Kyoto, Japan: Electrochemical Society of Japan, 59-64.

JAIN, R. K., TRICKLEBANK, S. B., WELCH, B. J. & WILLIAMS, D. J. 1983b. Interaction of aluminas with aluminium smelting electrolytes. *Light Metals***,** 609-622.

JAMES, B. J., WELCH, B. J., HYLAND, M., METSON, J. B. & MORRISON, C. D. 1995a. Interfacial Processes and the Performance of Cathode Linings in Aluminum Smelters. *JOM,* 47**,** 22-25.

JAMES, B. J., WELCH, B. J., HYLAND, M. M., METSON, J. B. & MORRISON, C. D. 1995b. Interfacial processes and the performance of cathode linings in aluminum smelters. *JOM,* 47**,** 22-5.

KACHANOVSKAYA, I. S. & ARAKELYAN, O. I. 1976. Behavior of alumina in the deposits and crust of an aluminum electrolytic cell. *Tsvetnye Metally***,** 37-40.

KALGRAF, K. & TORKLEP, K. 1998a. Sediment transport and dissolution in Hall-Heroult Cells. *Light Metals***,** 455-464.

KALGRAF, K. & TORKLEP, K. 1998b. Sediment Transport and Dissolution in Hall-Heroult Cells. *Light Met. 1998, Proc. Int. Symp.***,** 455-464.

KELLER, R. 1984. Alumina dissolution and sludge formation. *Light Metals***,** 513-518.

KELLER, R. 2005a. Alumina dissolution and sludge formation revisited. *TMS Annual Meeting.* San Francisco, CA: Minerals, Metals & Materials Society.

KELLER, R. 2005b. Alumina dissolution and sludge formation revisited. *Light Metals***,** 147-150.

KELLER, R., BURGMAN, J. W. & SIDES, P. J. 1988. Electrochemical reactions in the Hall-Heroult cathode. *Light Metals***,** 629-31.

KHEIRI, M., GERLACH, J., HENNIG, U. & KAMMEL, R. 1987. Formation and behavior of crusts and bottom sludge in alumina reduction electrolysis. *Erzmetall,* 40**,** 127-131.

KOBBELTVEDT, O. 1997. *Dissolution Kinetics for Alumina in Cryolite Melts. Distribution of Alumina in the Electrolyte of Industrial Aluminium Cells.* PhD Thesis, Norwegian University of Science and Technology.

KOBBELTVEDT, O. & MOXNES, B. P. 2013. On the bath flow, alumina distribution and anode gas release in aluminium cells. *In:* BEARNE, G., DUPUIS, M. & TARCY, G. (eds.) *Essential Readings in Light Metals.* Hoboken, NJ, USA: John Wiley & Sons, Inc.

KOBBELTVEDT, O., ROLSETH, S. & THONSTAD, J. 1996. On the mechanisms of alumina dissolution with relevance to point feeding aluminium cells. *Light Metals***,** 421-427.

KORENKO, M. 2008. Interfacial Tension between Aluminum and Cryolite Alumina Melts. *J. Chem. Eng. Data,* vol. 53**,** 794-797.

KROSCHWITZ, J. I. 2004. Carbon. *Kirk-Othmer Encyclopedia of Chemical Technology.*

KUSCHEL, G. I. & WELCH, B. J. 2013. Further studies of alumina dissolution under conditions similar to cell operation. *In:* BEARNE, G., DUPUIS, M. & TARCY, G. (eds.) *Essential Readings in Light Metals.* Hoboken, NJ, USA: John Wiley & Sons, Inc.

KVANDE, H., CHEN, J. & HAUPIN, W. E. 1994. Minimizing energy consumption through optimizing alumina concentration in the bath of Hall-Heroult Cells. *Light Metals***,** 429-440.

LANDI, M. F., BACCHIEGA, R. & BATTAGLIA, A. 1968. Oriented recrystallization of alumina from cryolite baths for the production of aluminum by electrolysis of the separated ore. *La Metallurgia Italiana,* 60**,** 939-44.

LANDRY, J.-R., FALLAH FINI, M., SOUCY, G., DÉSILETS, M., PELLETIER, P., RIVOALAND, L. & LOMBARD, D. 2018a. Laboratory study of the impact of the cathode grade on the formation of deposits on the cathode surface in Hall-Héroult Cells. *Light Metals***,** 1229-1233.

LANDRY, J.-R., FALLAH FINI, M., SOUCY, G., DÉSILETS, M., PELLETIER, P., RIVOALAND, L. & LOMBARD, D. 2018b. Laboratory Study of the Impact of the Cathode Grade on the Formation of Deposits on the Cathode Surface in Hall-Héroult Cells. *Light Met. 2018, Proc. Int. Symp.***,** 1229-1233.

LARSEN, S. Y., XIAN-AN, L., GRAN, H., MADSHUS, S. & JOHANSEN, J. A. Development of high density graphitized cathode blocks for aluminium electrolysis cells. Light Metals 2010. The technical sessions presented by the TMS Aluminum Committee at the TMS 2010 Annual Meeting & Exhibition, 14-18 Feb. 2010, 2010 Warrendale, PA, USA. Metals & Materials Society (TMS), 835-40.

LAVOIE, P., TAYLOR, M. P. & METSON, J. B. 2016. A review of alumina feeding and dissolution factors in aluminum reduction cells. *Metallurgical and Materials Transactions B,* 47**,** 2690-2696.

LEITNER, M., LEITNER, T., SCHMON, A., AZIZ, K. & POTTLACHER, G. 2017. Thermophysical properties of liquid aluminum. *Metallurgical and Materials Transactions A,* 48**,** 3036-3045.

LI, T., JOHANSEN, S. T. & SOLHEIM, A. 2015. Detailed model of electrochemical cathode wear in Hall-Héroult cells. *Light Met. 2015, Proc. Int. Symp.***,** 831-836.

LIAO, X. & OYE, H. A. 1998. Physical and Chemical Wear of Carbon Cathode Materials. *Light Met. 1998, Proc. Int. Symp.***,** 667-674.

LIAO, X. & OYE, H. A. 1999. Carbon cathode corrosion by aluminum carbide formation in cryolitic melts. *Light Met. 1999, Proc. Int. Symp.*, 621-627.

LIAO, X. & ØYE, H. A. 2013. Carbon cathode corrosion by aluminium carbide formation in cryolitic melts. *In:* TOMSETT, A. & JOHNSON, J. (eds.) *Essential Readings in Light Metals.* Hoboken, NJ, USA: John Wiley & Sons, Inc.

LIU, X. Thermochemistry of electrolyte, sludge/ridge, ledge and cell cover. Proceedings of the 5th Australasian Aluminum Smelter Technology Workshop, 1995. Queenstown, New Zealand: Royal Australian Chemical Institute and University of South Wales, 619-627.

MEYER, A., BØRSET, O., SOMMERSETH, C., OSEN, K., ROSENKILDE, C. & KRISTIANSEN, L. Examination of drop in bath acidity due to change-over of alumina qualities in the sunndal aluminium smelter, Norway. Proceedings of the 9th International Alumina Quality Workshop, 2012 Perth, Australia. Sidney, Australia: AQW Inc., 316-321.

MIRCHI, A. A., CHEN, W. & TREMBLAY, M. 2003. Comparative characterization of graphitized and graphitic cathode blocks. *Light Met. (Warrendale, PA, U. S.)*, 617-624.

MOXNES, B., SOLHEIM, A., LIANE, M., SVINSÅS, E. & HALKJELSVIK, A. 2009. Improved cell operation by redistribution of the alumina feeding. *Light Metals*, 461-466.

MOXNES, B. P., AGA, B. E. & SKAAR, J. H. 1998. How to obtain open feeder holes by installing anodes with tracks. *Light Metals*, 247-255.

NOVAK, B., RATVIK, A. P., WANG, Z. & GRANDE, T. 2018. Formation of Aluminium Carbide in Hall-Héroult Electrolysis Cell Environments. *Light Met. 2018, Proc. Int. Symp.*, 1215-1222.

NOVAK, B., TSCHÖPE, K., RATVIK, A. P. & GRANDE, T. 2012. Fundamentals of aluminium carbide formation. *Light Met. 2012, Proc. Int. Symp.*, 1343-1348.

ØDEGÅRD, R., ROENNING, S., ROLSETH, S. & THONSTAD, J. 1985. Crust formation in aluminum cells. *JOM,* 37, 25-28.

ØDEGÅRD, R., ROENNING, S., ROLSETH, S. & THONSTAD, J. 2013a. On alumina phase transformation and crust formation in aluminum cells. *In:* BEARNE, G., DUPUIS, M. & TARCY, G. (eds.) *Essential Readings in Light Metals.* Hoboken, NJ, USA: John Wiley & Sons, Inc.

ØDEGÅRD, R., STERTEN, Å. & THONSTAD, J. 2013b. On the solubility of aluminium carbide in cryolitic melts - influence on cell performance. *In:* BEARNE, G., DUPUIS, M. & TARCY, G. (eds.) *Essential Readings in Light Metals.* Hoboken, NJ, USA: John Wiley and Sons Inc.

PAWLEK, R. P. 2010. Wettable Cathodes: An Update. 2010a. The Minerals, Metals & Materials Society, 377-382.

PAWLEK, R. P. 2010b. Wettable cathodes: an update. *Light Metals*, 377-382.

RENY, P. & WILKENING, S. 2000. Graphite Cathode Wear Study at Alouette. *In:* PETERSON, R. D., ed. Light Metals 2000, 3/2000 Nashville, Tennessee 2000. Warrendale, PA.: The Minerals, Metals and Materials Society, 399-404.

RIVOALAND, L. Development of a new type of cathode for aluminium electrolysis. Proceedings of ICSOBA Conference, 2016a. QC, Canada: ICSOBA-RioTinto-REGAL, 9.

RIVOALAND, L. 2016b. Development of a New Type of Cathode for Aluminium Electrolysis. *Bauxite, Alumina, Alum., Proc. Int. Symp. ICSOBA*.

ROBILLIARD, K. R. & ROLOFS, B. 2013. A demand feed strategy for aluminium electrolysis cells. *In:* BEARNE, G., DUPUIS, M. & TARCY, G. (eds.) *Essential Readings in Light Metals.* Hoboken, NJ, USA: John Wiley & Sons, Inc.

RYE, K. A., ROLSETH, S., THONSTAD, J. & ZHANLING, K. Behaviour of alumina on addition to cryolitic baths. Proceedings of the 2nd International Alumina Quality Workshop, 1990. Perth, Australia: AQW Inc., 24-37.

SCHNITTKER, A. & NAWROCKI, H. 2003. Performance of graphitized carbon cathode blocks. *Light Met. (Warrendale, PA, U. S.)***,** 641-645.

SCHUBERT SEVERO, D. & GUSBERTI, V. Heat exchanger for alumina preheating in aluminium reduction cells. Proceedings of ICSOBA Conference, 2017. Hamburg, Germany: ICSOBA, 1059-1069.

SELE, T. 1977. Instabilities of the metal surface in electrolytic alumina reduction cells. *Metallurgical Transactions B,* 8**,** 613-618.

SIEW, E. F., IRELAND-HAY, T., STEPHENS, G. T., CHEN, J. J. J. & TAYLOR, M. P. 2005. A study of the fundamentals of pothole formation. *TMS Annual Meeting.* San Francisco, California.

SINGH, R., DAS, K., MISHRA, A. K. & KALO, N. 2017a. An Approach for Estimation of Cathode Voltage Drop in an Aluminum Reduction Cell with an Inclined Carbon Block and a Copper Insert. *Trans. Indian Inst. Met.,* 70**,** 1795-1804.

SINGH, R., DAS, K., MISHRA, A. K. & KALO, N. 2017b. An approach for estimation of cathode voltage drop in an aluminum reduction cell with an inclined carbon block and a copper Insert. *Transactions of the Indian Institute of Metals,* 70**,** 1795-1804.

SKVBAKMOEN, E., ROERVIK, S., SOLHEIM, A., HOLM, K. R., TIEFENBACH, P. & OSTREM, O. 2011. Measurement of Cathode Surface Wear Profiles by Laser Scanning. *Light Met. 2011, Proc. Int. Symp.***,** 1059-1066.

SLEPPY, W. C. & COCHRAN, C. N. 2013. Bench scale electrolysis of alumina in sodium fluoride–aluminum fluoride melts below 900°C. *In:* BEARNE, G., DUPUIS, M. & TARCY, G. (eds.) *Essential Readings in Light Metals.* Hoboken, NJ, USA: John Wiley & Sons, Inc.

SOLHEIM, A. 2002. Crystallization of cryolite and alumina at the metal-bath interface in aluminium reduction cells. *Light Metals***,** 225-230.

SOLHEIM, A. 2014. A novel design criterion for alumina feeders in aluminium electrolysis cells. *Light Metals***,** 709-716.

SOLHEIM, A. 2018. Inert anodes—the blind alley to environmental friendliness? *Light Metals***,** 1253-1260.

SONG, Y., PENG, J., DI, Y., WANG, Y. & FENG, N. 2017a. Metal flow performance in aluminium electrolytic cells with different side-wall types. *Canadian Metallurgical Quarterly***,** 1-9.

SONG, Y., PENG, J., DI, Y., WANG, Y. & FENG, N. 2017b. Metal flow performance in aluminium electrolytic cells with different side-wall types. *Can. Metall. Q.,* vol. 57**,** Ahead of Print.

SONG, Y., PENG, J., DI, Y., WANG, Y. & FENG, N. 2017c. Performance of the Cathodes with Trapezoidal Protrusions in Aluminum Electrolysis Cells. *JOM,* 69**,** 2844-2850.

SONG, Y., PENG, J., DI, Y., WANG, Y., LI, B. & FENG, N. 2016. The impact of cathode material and shape on current density in an aluminum electrolysis cell. *JOM,* 68**,** 593-599.

SORLIE, M. & OYE, H. A. 2010. *Cathodes in Aluminium Electrolysis,* Düsseldorf, Germany, Aluminium-Verlag.

SØRLIE, M. & ØYE, H. A. 2010. *Cathodes in Aluminium Electrolysis,* Düsseldorf, Germany, Aluminium Verlag GmbH.

STAM, M. A., TAYLOR, M. P., CHEN, J. J. J., MULDER, A. & RODRIGO, R. 2008. Common behaviour and abnormalities in aluminium reduction cells. *Light metals***,** 309-314.

TABEREAUX, A. 2000. Prebake Cell Technology: A Global Review. *JOM,* 52**,** 23-29.

TABEREAUX, A. T. & PETERSON, R. D. 2014. Aluminum Production. *Treatise on Process Metallurgy.*

TARAPORE, E. D. 2013. The effect of some operating variables on flow in aluminum reduction cells. *In:* BEARNE, G., DUPUIS, M. & TARCY, G. (eds.) *Essential Readings in Light Metals.* Hoboken, NJ, USA: John Wiley & Sons, Inc.

TARCY, G. P., KVANDE, H. & TABEREAUX, A. 2011. Advancing the industrial aluminum process: 20th century breakthrough inventions and developments. *JOM,* 63**,** 101-108.

TAYLOR, M. P. Challenges in optimizing and controlling the electrolyte in aluminum smelters. Proceedings of the International Conference on Molten Slags, Fluxes and Salts, 1997. Warrendale, PA, USA: Iron and Steel Society of AIME, 659-674.

TAYLOR, M. P., LIU, X., FRASER, K. & WELCH, B. J. 1990. Dynamics and performance of reduction cell electrolytes. *Light Metals***,** 259-266.

TAYLOR, M. P. & WELCH, B. J. 2004. The future outlook and challenges for smelting aluminium. *Aluminium International Today,* 16**,** 20-24.

THONSTAD, J. 1977. Semicontinuous determination of the concentration of alumina in the electrolyte of aluminum cells. *Metallurgical Transactions B,* 8**,** 125-130.

THONSTAD, J., FELLNER, P., HAARBERG, G. M., HÍVEŠ, J., KVANDE, H. & STERTEN, Å. 2001a. *Aluminium Electrolysis: Fundamentals of the Hall-Héroult Process,* Düsseldorf, Germany, Aluminium-Verlag.

THONSTAD, J., FELNNER, G., HAARBERG, G. M., HIVES, J. & KVANDE, H. 2001b. *Aluminium Electrolysis - Fundamentals of the Hall-Héroult Process,* Düsseldorf, Germany, Aluminium-Verlag.

THONSTAD, J., JOHANSEN, P. & KRISTENSEN, E. W. 1980. Some properties of alumina sludge. *Light Metals*, 227-39.

THONSTAD, J., NORDMO, F. & PAULSEN, J. B. 1972. Dissolution of alumina in molten cryolite. *Metallurgical Transactions,* 3, 407-412.

THONSTAD, J., ROENNING, S. & ENTNER, P. 1982. Formation of bottom crusts in aluminum pots. a laboratory study. *Light Metals*, 485-497.

THONSTAD, J., SOLHEIM, A., ROLSETH, S. & SKAR, O. 2013. The dissolution of alumina in cryolite melts. *In:* BEARNE, G., DUPUIS, M. & TARCY, G. (eds.) *Essential Readings in Light Metals.* Hoboken, NJ, USA: John Wiley & Sons, Inc.

TORKLEP, K., KALGRAF, K. & NORDBO, T. 1997. Alumina distribution in point-fed Hall-Heroult Cells. *Light Metals*, 377-386.

TSCHÖPE, K., STORE, A., RORVIK, S., SOLHEIM, A., SKYBAKMOEN, E., GRANDE, T. & RATVIK, A. P. 2012. Investigation of the cathode wear mechanism in a laboratory test cell. *Light Met. 2012, Proc. Int. Symp.*, 1349-1354.

TSCHÖPE, K., STORE, A., SKYBAKMOEN, E., SOLHEIM, A., GRANDE, T. & RATVIK, A. P. 2013a. Critical reflections on laboratory wear tests for ranking commercial cathode materials in aluminium cells. *Light Met. 2013, Proc. Int. Symp.*, 1251-1256.

TSCHÖPE, K., STØRE, A., SKYBAKMOEN, E., SOLHEIM, A., GRANDE, T. & RATVIK, A. P. 2013b. Critical reflections on laboratory wear tests for ranking commercial cathode materials in aluminium cells. *TMS Annual Meeting.* Light Metals 2013 - At the TMS 2013 Annual Meeting and Exhibition ed. San Antonio, Texas.

UTIGARD, T. 1987. Mass transfer in Hall-Heroult Electrolysis induced by interfacial tension gradients. *Aluminium,* 63, 608-13.

UTIGARD, T. 1999a. Why "best" Pots Operate Between 955 and 970 °C. *Light Met. 1999, Proc. Int. Symp.*, 319-326.

UTIGARD, T., ROLSETHT, S., THONSTAD, J. & TOGURI, J. M. 1989. Interfacial phenomena in aluminum electrolysis. *In:* CLOSSET, B. (ed.) *Production and Electrolysis of Light Metals.* Oxford, UK: Pergamon.

UTIGARD, T. & TOGURI, J. M. 1985. Interfacial tension of aluminum in cryolite melts. *Metallurgical Transactions B,* 16, 333-338.

UTIGARD, T. & TOGURI, J. M. 1991a. Marangoni Flow in the Hall--Heroult Cell. *Light Met. 1991, Proc. Int. Symp.*, 273-281.

UTIGARD, T. & TOGURI, J. M. 1991b. Marangoni flow in the Hall-Heroult Cell. *Light Metals*, 273-81.

UTIGARD, T. A. 1993. An analysis of the effect of bath density variations on the behaviour of Hall-Heroult Cells. *Canadian Metallurgical Quarterly,* 32, 327-333.

UTIGARD, T. A. 1999b. Why best pots operate between 955 and 970 °C. *Light Metals*, 319-326.

VENERAKI, I. E., ROMANKO, K. S., URDA, N. N. & SEMENOV, V. S. 1973. Thermal conductivity of materials of aluminum electrolytic cells. *Energetika i Elektrifikatsiya*, 52-54.

VON KAENEL, R., BUGNION, L., VON KAENEL, L., SPINETTI, G. & PFEFFER, M. The use of copper in cathodes of aluminium reduction cells. Proceedings of ICSOBA Conference, 2017. Hamburg, Germany: ICSOBA, 879-889.

WALKER, D. I., UTIGARD, T. A. & TAYLOR, M. P. 1995. Alumina agglomerates in aluminum smelters. *Light Metals*, 425-434.

WALKER, M. L., PURDIE, J. M., WAI-POI, N. S., WELCH, B. J. & CHEN, J. J. J. 2013. Design considerations for selecting the number of point feeders in modern reduction cells. *In:* BEARNE, G., DUPUIS, M. & TARCY, G. (eds.) *Essential Readings in Light Metals.* Hoboken, NJ, USA: John Wiley & Sons, Inc.

WANG, L., TABEREAUX, A. T. & RICHARDS, N. E. 1994. Electrical conductivity of cryolitic melts containing aluminum carbide. *Light metals*, 177-185.

WANG, Q., LI, B., HE, Z. & FENG, N. 2014. Simulation of Magnetohydrodynamic Multiphase Flow Phenomena and Interface Fluctuation in Aluminum Electrolytic Cell with Innovative Cathode. *Metallurgical and Materials Transactions B,* 45, 272-294.

WANG, X. 2009. Alumina dissolution in aluminum smelting electrolyte. *Light Metals*, 383-388.

WANG, Z., NOBAKHTGHALATI, S., STORE, A., SOLHEIM, A., TSCHÖPE, K., RATVIK, A. P. & GRANDE, T. 2016. Cathode Wear in Electrowinning of Aluminum Investigated by a Laboratory Test Cell. *Light Met. 2016, Proc. Int. Symp.*, 895-902.

WANG, Z., SKYBAKMOEN, E. & GRANDE, T. 2009a. Spent Si3N4 bonded SiC sidelining materials in aluminium electrolysis cells. *Light Metals*, 353-358.

WANG, Z., SKYBAKMOEN, E. & GRANDE, T. 2009b. Spent Si3N4 bonded SiC sidelining materials in aluminium electrolysis cells. *Light Met. 2009, Proc. Int. Symp.*, 353-358.

WELCH, B. J. The role cell design and cell operating conditions can play in reducing problems from alumina. Proceedings of the 2nd International Alumina Quality Workshop, 1990. Perth, Australia: AQW Inc., 15-22.

WELCH, B. J. Sludge/muck in smelting cells. Proceedings of the 5th Australasian Aluminum Smelter Technology Workshop, 1995. Sidney, Australia: Royal Australian Chemical Institute and University of South Wales, 651–659.

WELCH, B. J. 2007. Gaining that extra 2 percent current efficiency. *In:* PETERSON, W. S. & MILLER, R. E. (eds.) *Hall-Héroult Centennial.* Hoboken, NJ, USA: John Wiley & Sons, Inc.

WELCH, B. J. & GRJOTHEIM, K. Alumina's and cell feeding technologies. Proceedings of the 1st International Alumina Quality Workshop, 1988. Gladstone, Australia: AQW Inc., 75-86.

WELCH, B. J. & KINERY, J. T. 2000. Advancing the hall heroult electrolytic process. *Light Metals*, 17-25.

WELCH, B. J. & KUSCHEL, G. I. 2007. Crust and alumina powder dissolution in aluminum smelting electrolytes. *JOM,* 59**,** 50-54.

WHITFIELD, D., SKYLLAS-KAZACOS, M., WELCH, B. & MCFADDEN, F. S. 2004. Aspects of alumina control in aluminium reduction cells. *TMS Annual Meeting.* Charlotte, North Carolina: Minerals, Metals & Materials Society.

WORLD-ALUMINIUM. 2017. *Primary aluminium smelting energy intensity* [Online]. The International Aluminium Institute. Available: http://www.world-aluminium.org/statistics/primary-aluminium-smelting-energy-intensity/#data [Accessed 18.04.2017].

YANG, Y., GAO, B., WANG, Z., SHI, Z. & HU, X. 2015. Study on the dissolution of alumina in cryolite electrolyte using the see-through cell. *Light Metals***,** 583-588.

YURKOV, A. 2015. *Refractories for Aluminium Electrolysis and the Cast House,* Switzerland, Springer.

ZHAN, S., LI, M., ZHOU, J., YANG, J. & ZHOU, Y. 2014. CFD simulation of dissolution process of alumina in an aluminum reduction cell with two-particle phase population balance model. *Applied Thermal Engineering,* 73**,** 805-818.

ZOUKEL, A., CHARTRAND, P. & SOUCY, G. 2009. Study of Aluminum Carbide Formation in Hall-Heroult Electrolytic Cells. *Light Met. 2009, Proc. Int. Symp.***,** 1123-1128.